How to escape from a tense situation: Bacterial mechanosensitive channels

Joost H.A. Folgering

Voor mijn familie

Cover: Thomas Huber (Jakobs Traum II, 1997)
Cover design: Gijs Noorlander and Joost Folgering

This Ph.D. study was carried out in the Biochemistry Department of the Groningen Biomolecular Sciences and Biotechnology Institute (GBB) of the University of Groningen and was financially supported by the Material Science Center (MSC*plus*)

ISBN 90-367-2293-4
ISSN 1570-1530
MSC Ph.D.-thesis series 2005-08

Printed and bound in the Netherlands by PrintPartners Ipskamp, Enschede

RIJKSUNIVERSITEIT GRONINGEN

How to escape a tense situation:

Bacterial mechanosensitive channels

Proefschrift

ter verkrijging van het doctoraat in de
Wiskunde en Natuurwetenschappen
aan de Rijksuniversiteit Groningen
op gezag van de
Rector Magnificus, dr. F. Zwarts,
in het openbaar te verdedigen op
vrijdag 9 september 2005
om 16:15 uur

door

Jozef Hendrik Arnold Folgering

geboren op 6 juli 1975
te Nijmegen

Promotor:	Prof. Dr. B. Poolman
Beoordelingscommissie:	Prof. Dr. A.E. Mark Prof. Dr. A.J.M. Driessen Prof. Dr. J.B.F.N. Engberts

Contents

Channel electrophysiology: history, current applications and future prospects

Joost H.A. Folgering and Bert Poolman

Abbreviations: BLM: Black-lipid Membrane; GUV: Giant Unilamellar Vesicle; MS: Mechanosensitive; GOF: Gain of Function; LOF: Loss of Function; MTSET: [2-(trimethylammonium)ethyl]methanethiosulfonate; TM: Trans Membrane helix

Electrophysiology is the science concerned with the flow of ions in biological tissues and, in particular, the electrical recording techniques that enable the measurement of this flow (1). Ion channels are present in the membranes that surround all biological cells. By conducting and controlling the flow of ions, these pore-forming proteins influence the voltage (100-150mV) across the membrane of cells and they play an important role in the generation of action potentials in nerve cells. If one realizes that in the human genome around 350 genes code for channel proteins (2), it can be appreciated, that as a field of research, electrophysiology is very important.

Thus far, around 40 hereditary channelopathies have been described and are currently the subject of intense research. These channelopathies can be divided into three main groups: muscular diseases (e.g., heart disease and muscular dystrophy), neuronal diseases (e.g., epilepsy and some forms of blindness) and internal diseases (e.g., cystic fibrosis and renal disorders); a more detailed description of hereditary channelopathies and the channels involved can be found in references 3 and 4. To fully appreciate current research in electrophysiology, two landmarks need to be discussed. The first is the development of the field of bioelectricity, the second the concept of the membrane bilayer. This introduction does not cover the complete field of electrophysiology, but indicates highlights that have directly or indirectly led to the work described in the following chapters.

History of bio-electricity

The first persons to study bio-electricity were Luigi Galvani and Alessandro Volta in the late 18th century. Galvani prepared frog legs, with their muscles and nerves exposed, and connected them to different sources of electricity (5, 6). The electrical stimuli resulted in twitching of the legs. These observations led to a discussion between Galvani and Volta on the nature of the stimulus that resulted in the activation of the leg muscles. Galvani thought the stimulation showed that a form of what he called "animal electricity" existed. We now understand the ”animal electricity” as ion-fluxes across cell membranes. However, as the twitching could also be observed when a purely physical stimulus was applied, Volta was sure that it was caused by the electricity stemming from the touching of two different substances (metal touching tissue, 7). A simple experiment, where two nerves of separately prepared legs from the same frog were brought into contact and resulted in

muscle contraction showed that Volta's interpretation was incorrect (8 and Fig. 1). However, because of Volta's success with electricity generated from contact between dissimilar objects (in the so called "voltaic pile"), the experiments of Galvani, and their consequences, went unnoticed at that time. (9, 10)

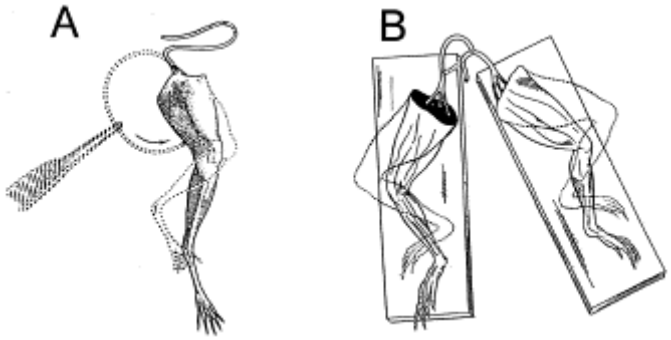

Figure 1: Galvani's experiment demonstrating muscle contraction without using dissimilar substances (metal and tissue). (A) When the surface of section of the nerve touches the muscle, the leg contracts. (B) When the surface of section of the right sciatic nerve touches the intact surface of the left sciatic nerve, both legs contract (modified from 6).

During the early part of the 19th century, Galvani's experiments were often repeated but not interpreted correctly. After identifying the organ responsible for electrical discharges in electrical fish, Carlo Matteucci had turned his attention to the potentials that are responsible for muscle contraction. In 1838, he first reported his findings on muscle contractions (11). He showed that in rest there was a potential difference between the damaged and the intact surface of a severed muscle (i.e., the inside and the outside of a muscle cell). This potential was large enough to create a measurable current (12). He was the first to demonstrate that it is possible to induce muscle contraction by means of an action potential, and he showed that this action potential is associated with the depolarization of the muscle resting potential (13, 14). However, it was Emil Heinrich du Bois-Reymond, under the guidance of Alexander von Humboldt, who finally interpreted the membrane potential experiments correctly and refined the methods to record muscle currents from frogs and even humans (15-17). The last person that needs to be mentioned from the early days of bio-electricity is Hermann von Helmholz, who was able to determine the propagation speed of an electrical signal along the nerve cell. He found that nerve signals had a speed of ”only” 10 - 100 meters per second. This is a lot slower than the speed of light, previously assumed to be the speed at which nerve impulses traveled (18, 19). The contribution of von Helmholz to the field of bio-electricity did not stop there; he also developed a number of instruments that made more accurate measurements of currents possible (9).

Membrane bilayers

The history of lipid bilayers starts half-way through the 19th century, when three botanists, Karl von Nägeli, Karl Cramer and Wilhelm Pfeffer, realized that when plant cells were submerged in hypotonic solutions they would expand, whereas in hypertonictonic solutions they would shrink (20, 21). This observation led them to conclude that the cells were surrounded with some sort of membranous envelope. At the end of the 19th century, Ernest Overton had classified over 500 chemical compounds for their solubility in oil and in water and their ability to diffuse over the cell membrane (22-25). From this work, he concluded that the postulated membrane consisted of lipoid material and was semi-permeable. Inspired by the work of du Bois-Reymond, Overton subsequently studied the effect of extracellular sodium ion concentrations on nerve excitation and found that sodium ions were exchanged for internal potassium ions upon excitation of muscle cells (26, 27). Another scientist who contributed to the initial ideas on biological membranes, before actual models were proposed, was Alexander Langmuir (28). He was the first to quantitatively investigate the self-assembly of mono- and bi-layers on air-water interfaces (27-31).

The first real membrane model was proposed by Evert Gorter and F. Grendel in Utrecht in 1925 (32). They observed that lipids extracted from a single human red blood cell could cover an area twice the size of the cell surface area in a monolayer formation experiment. This indicated that the organization of the lipids in the membrane had to be that of a lipid bilayer (Fig. 2A). After studying membranes with an electron microscope, Hugh Davson, James Danielli and James David Robertson realized that this model was incomplete, as they found particles (proteins) associated with the membrane bilayer. They proposed a membrane model with a bilayer lipid core and a layer of proteins on either side of this so called unit-membrane (27, 29-31, 33, 34 and Fig. 2B).

The unit-membrane model was replaced in the early 1970s by a model from the biochemists Jonathan Singer and Garth Nicolson, known as the fluid mosaic model (35). This model (Fig. 2C) retains the basic lipid bilayer structure, first proposed by Gorter and Grendel and modified by Danielli and Davson and Robertson. The proteins, however, are thought to be globular and to float within the lipid bilayer rather than just on the membrane surface as in the sandwich-type model (27, 29-31). Owing to modern molecular dynamics and spectroscopic techniques, it is now possible to describe lipid bilayers at an even more detailed level. Molecular dynamics and spectroscopic studies have shown that the lipid water interface is not a solid barrier, but that water can penetrate the bilayer, and crystallographic studies have shown that proteins do not necessarily form globular structures within the membrane (Fig. 2D).

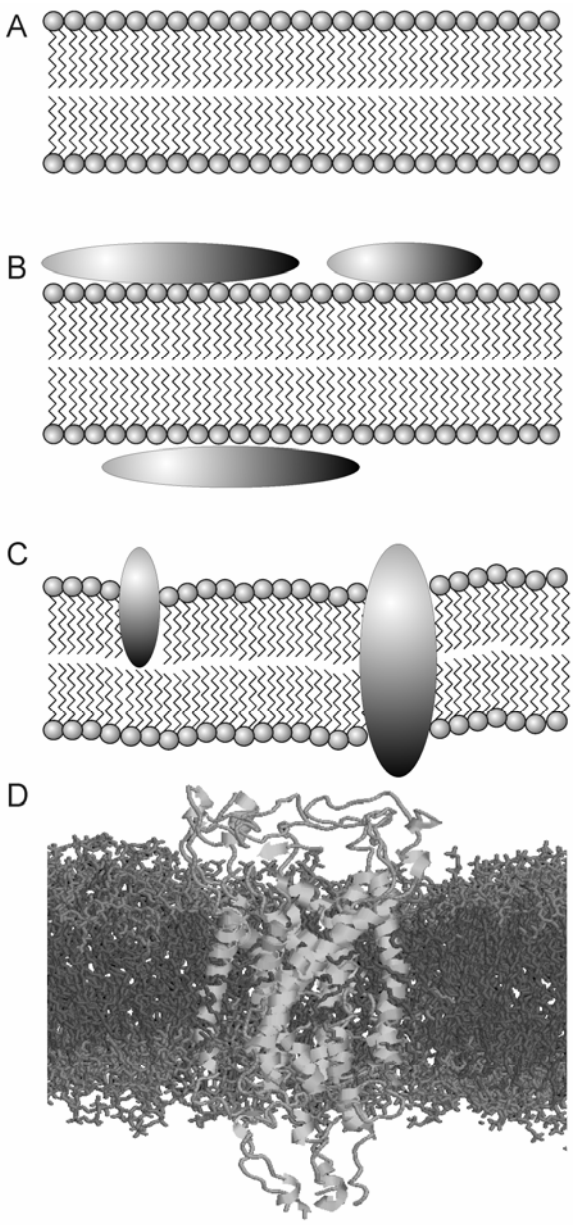

Figure 2: Four different membrane models as proposed by A) Gorter and Grendel; B) Davson, Danielli and Robertson; C) Singer and Nicolson; and D) a molecular dynamics simulation of a lipid bilayer. Clearly the components (lipids, proteins and water) are not present in an ordered form as proposed in the Singer and Nicolson model. A membrane protein (MscL) is depicted by the light grey α-helices and linker regions, part of the lipid headgroups are shown in darker grey, and the hydrophobic lipid acyl chains are shown in the darkest grey. The image was kindly provided by Alex H. de Vries.

Modern electrophysiology

In the 1930s, John Zachary Young discovered how to prepare squid giant neurons (36). The size of these axons made it very easy to apply external electrodes and to follow the depolarization of the membrane potential along the neurons. His work demonstrated that the membranes of the neurons became selectively permeable to sodium during depolarization. This was the first indication of the presence of ion-selective membrane channels.

Around the same time, Alan Hodgkin and Andrew Huxley succeeded in inserting electrodes into these giant neurons and so in measuring the membrane potential in rest and during excitation (37). An even greater break through came when they applied to these membranes a method devised by Kenneth Cole, which is now known as the voltage clamp (38). With this method, they could set a voltage across the neuronal membrane and then measure ion currents (9).

However, these ion currents were the result of fluxes through an ensemble of membrane channels. It took until the early 1960s before ion fluxes through single pores or channels were measured. By using a fine brush, Paul Müller and Donald Rudin painted planar lipid bilayer membranes over a small aperture in a septum between two chambers filled with buffer (39, 40 and Fig. 3). After formation of these so called black-lipid membranes (BLM, they have an optically black appearance under a microscope), channels could be inserted in two ways. Firstly, channels were solubilized from a membrane fraction and added to one of the chambers. Through diffusion the channels would reach the bilayer and insert, albeit with a very low efficiency. A second method involves the use of proteoliposomes, which can be prepared by for instance, by detergent-mediated reconstitution (41). Through fusion of these proteoliposomes with the stabilized BLM, the channel can be inserted. All current applications of the BLM involve the same basic technique, but are often refined to counteract the disadvantages of the first generation of the BLM set-up, that are: the small available bandwidth of sampling and filtering frequencies and the low signal to noise ratio (e.g. 42). Both these disadvantages are caused by the relatively large lipid area used in the system, which acts as a large antenna. Another disadvantage of the system is that the formed bilayer is usually stable for only 2-3h. The main advantages of BLMs are the ease with which buffer on either side of the membrane can be replaced and the fact that it can be used in combination with a large variety of lipids.

Finally, one remarkable recent application of BLMs needs to be mentioned. Generally ion pumps have a turnover-rate between 1 and $100s^{-1}$, whereas the ion flow through a channel is in the order of $10^5 – 10^6 s^{-1}$. This implies that one would need to reconstitute 10^4-10^5 of these pumps in a single membrane to measure a current equivalent to that of a single channel. However, if one uses the BLM membrane as a sensitive capacitive electrode, it is possible to sense changes in charges inside an adsorbed proteoliposome containing ion pumps. As the charge needs to be equal on both sides of the ”capacitive electrode”, an opposing charge needs to be added for any ion transported into the adsorbed proteoliposome. The new charge distribution can be measured by charging and discharging the capacitor. The additional number of ions present in the proteoliposome determines the change in the time-constant for discharge and can be calculated from the time-constant. As the time between two charge and discharge events is known, the turnover number of the transporter can be determined. An added advantage is that any required substrate (e.g., ATP) can be added to the inside of the

proteoliposomes before the vesicles are added to the chamber in the BLM set-up. This method has been applied by Ernst Bamberg and colleagues to bacteriorhodopsin and a number of ATP dependent ion pumps (Na^+/K^+-ATPase and H^+/K^+-ATPase) as reviewed in (43).

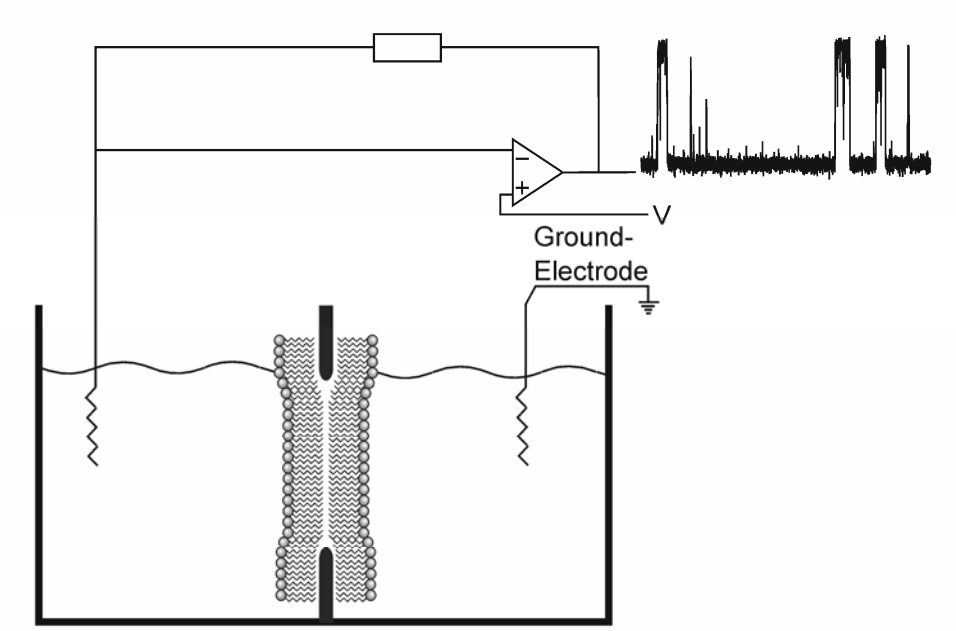

Figure 3: Set-up for Black-Lipid-Membrane measurements. Left and right of the membrane are buffer-filled chambers that are connected to an amplifier via submerged electrodes. After insertion of a channel into the membrane, currents can be measured following the application of a potential across the membrane.

Another approach to measure single channel ion currents was proposed by Erwin Neher and Bert Sakmann in 1976, that is, after many years of improving existing electrophysiological methods. By using blunt-tipped glass pipettes, gently pressed against a cell, and application of negative pressure inside the pipette (as suggested by Owen Hammill (44)), a part of the cell-membrane could be isolated (diameter ~ 1µm). This resulted in a very tight seal between pipette (containing one of the electrodes) and the membrane. The (giga-ohm) seal prevents leak currents to flow from the pipette electrode along the membrane to the bath electrode, and reduces the noise in the single channel measurements. This method, now called the patch-clamp, was first used to record activity of muscle acetylcholine receptors. In 1991 Neher and Sackmann were rewarded the Nobel Prize for physiology and medicine for the development of the patch-clamp technique.

Currently three forms of patch clamp are distinguished:

1) Whole cell recording: in which a single electrode is brought in contact with the cytoplasm of the cell to measure currents across the membrane of the whole cell. This technique is similar to voltage clamp, but can be applied to smaller and more fragile cells (Fig. 4B).

2) Cell attached recording: here the pipette is attached to the outside of a cell and channel activity in a patch of membrane is recorded. By formation of a giga-ohm seal, the patch is electrically isolated from the rest of the membrane; the behavior of channels trapped inside the pipette can be studied in relation to the native constituents of the living cell membrane and cytoplasm (Fig. 4C).
3) Excised patch recording: the pipette is again brought into contact with the outside of a cell, but now the isolated patch is pulled free from the cell, allowing the experimenter to exchange the cell plasma for buffer of desired composition (Fig. 4D).

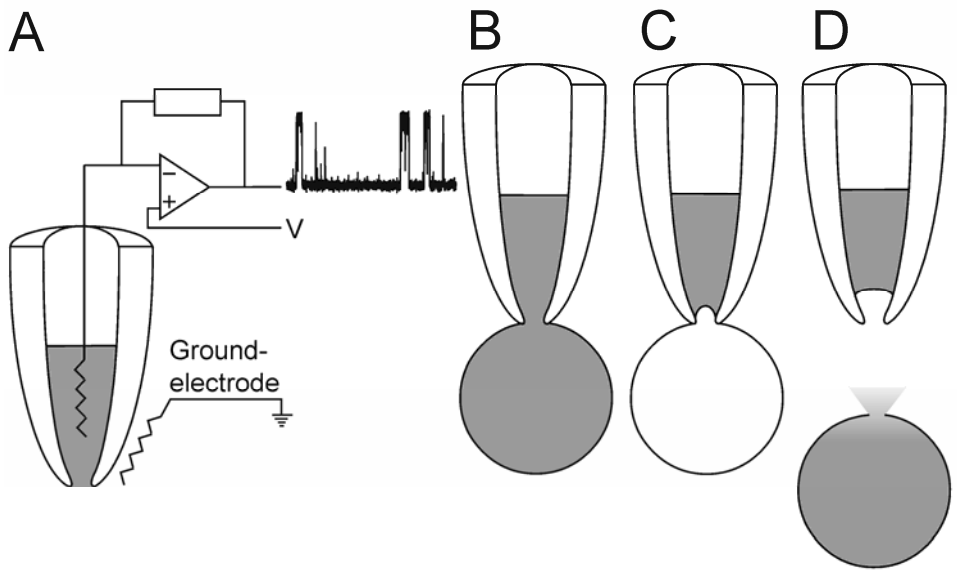

Figure 4: Patch clamp set-up and configurations: A) an electrode is brought in contact with a small amount of buffer inside the pipette. The signal generated by ion-currents, occurring in response to a set voltage, is amplified. A second electrode in the bath solution serves a reference or ground electrode. B) patch clamp in whole cell mode: the buffer inside the pipette is brought in contact with the cell cytoplasm. C) cell attached mode: the channel activity of a small number of channels in the patch is monitored, while the whole cell is still attached. D) excised patch mode: the channel activity of a small number of channels in the excised patch is monitored, solutions on both sides of the membrane can be exchanged to medium of desirable compositions. The disadvantage is that cellular components that may affect channel activity can no longer interact with the channel.

All three forms of patch-clamp can be applied to whole cells, provided their diameter is larger than the diameter of the pipette tip. Generally, bacteria with a diameter of 1-2µm are too small. However, a number of artificial systems have been developed. The first technique uses *Xenopus* (frog) oocytes, into which DNA is injected to enable overproduction and characterization of mutated or newly discovered channels in a eukaryotic system (45-47). For bacteria, it is possible to treat a growing cell culture with cephalexin, which prevents septation of the dividing cells. This causes the cells to grow into long snake-like structures. These snakes can subsequently be treated to form

giant spheroplasts, with diameters ranging from 10-20µm. The procedure for making the giant spheroplasts is described in more detail in (48). A third artificial system for patch-clamp measurements concerns Giant Unilamellar Vesicles (GUVs). For this the channel of interest is purified and reconstituted into liposomes, and the so formed proteoliposomes are then used to form GUVs (chapter 3). Alternatively, one could isolate native membranes from cells expressing the channel of interest, fuse the membranes with lipid vesicles (48), and convert the hybrid membranes into GUVs.

Future

One of the important recent advances in the understanding of channel function has come from the crystallization of a number of ion channels. The first channel to be crystallized was the KcsA channel from *Streptomyces lividans* by the MacKinnon group (49). This was followed in the same year by MscL from *Mycobacterium tuberculosis* by the Rees group (50). Since then the structures of a number of other channel proteins have been determined and without a doubt more will follow in the near future, enabling further insights in channel gating and selectivity. Combining the information retrieved from electrophysiology, crystallography, atomic force microscopy and spectroscopic techniques will increase our understanding of channel structure and function even more (4, 51). As for electrophysiology itself, part of the future developments may come from scaling-up of the existing techniques, so that multiple samples can be screened in parallel. For patch-clamp, the first requirement for a successful high-throughput system is automation of the formation of high resistance seals, which has been established in a number of cases. These systems are all based on a chip (or membrane) with very small (1-10µm) openings, made of glass, teflon or silicon polymers. The openings could be coated with lipid bilayers in which proteins were reconstituted (52-54). Alternatively, cells could be positioned on the apertures, and after high resistance seal formation, it was possible to apply suction and form the equivalent of the three patch configurations described in Fig. 4 (55-57). Recently, the Port-a-Patch© was introduced by Nanion Technologies GmbH, this is an automated electrophysiology workstation that enables patch clamp experiments on a single cell at a time. Patch clamp recordings in the whole cell configuration and single channel recordings can be performed with planar patch clamp chips, which are mounted in a workstation and to which samples can be applied in the form of a cell suspension. The process of seal formation is performed automatically, and recordings, under different conditions, are computer-controlled (58, 59). Also, the original patch-clamp set-up, using a glass pipette, has been adapted for high-throughput work, both *in situ* (multiple electrodes inserted into neuronal tissue for three-dimensional monitoring of signals; 60) and in model systems (drug screening in oocytes; 61, 62).

There are numerous examples, in which channels in supported bilayers may be used as biosensors. For instance, one could think of channels reacting to toxic compounds either as their natural ligand, or after they have

been rationally redesigned and modified to do so. Another potential application would be as light-sensitive or electrochemical devices that can store or generate energy (microelectronics). The biggest challenge at the moment for these applications is the stability of the supported bilayer, which is currently on the hour scale, but has to be longer for useful applications. (4, 27)

A medical application of channels may be found in the delivery of hydrophilic compounds (drugs) into human tissues. The compounds can be included in liposomes, which can be used as vehicles for the compound of interest to a target site in the human body. However, because of the hydrophilicity, the compound will not diffuse across the hydrophobic membrane. If a remotely switchable mechanosensitive (MS) channel (63 and chapter 4) would be incorporated into the liposome, the open channel may facilitate the outward diffusion of the compound. This concept is one of the current research topics within the BioMaDe Technology Foundation (64-66).

A case study: bacterial mechanosensitive channels

MS channels from bacteria have been the subject of research for over a decade now. The advances in patch clamp techniques enabled researchers to look at ion channel activity in bacteria. This resulted in the initial characterization of two types of so-called mechanosensitive channels in the cytoplamic membrane of *E. coli*. The channels were activated by a pressure decrease inside the patch pipette or the addition of amphipaths, indicating that it is the membrane tension (and not the pressure inside the patch pipette) that triggers channel activation (67, 68). In 1994, Sergei Sukharev, Paul Blount, Boris Martinac, Frederick Blattner and Ching Kung identified the protein and corresponding gene for one of the observed channel activities. This MS channel had a conductance of 2.5-4 nanoSiemens (at 200mM KCl bath solution), which was large compared to previously observed channels and resulted in the name MechanoSensitive Channel of Large conductance (MscL; 69). Based on its conductance the pore diameter of MscL was estimated to be around 40Å, which was confirmed by patch clamp measurements in the presence of poly-L-lysine molecules of different sizes that were screened for their ability to influence channel activity. MscL conductivity was reduced by poly-L-lysine molecules ranging in size from 27-42Å, but not by poly-L-lysine molecules smaller than 29Å (70). Soon after the initial discovery of MscL from *E. coli*, homologous channels were identified in over 40 eubacteria and around 10 have been characterized (71-73 and chapter 2). More recently, MS channels have also been identified in archaea (74). The proteins and corresponding genes of the MS channel activity of ~ 1nanoSiemens have also been identified and are named MscK (coded by *kefA*; 75, 76) and MscS (coded by *yggB*; 77, 78).

As shown in Fig. 5, the crystal structures of both MscL (50) and MscS (79) have been determined. The structure of MscL most likely represents a largely closed state of the channel, whereas the structure of MscS probably represents an open state of the channel. The clear pentameric organization of MscL has been confirmed in a number of studies (81-83 and chapter 5). The

availability of a crystal structure of the MscL channel made new directions of research possible, both experimentally and in *silico*. Using molecular dynamics, the response of MscL to membrane tension has been described (84-88). Unfortunately, there are no structures available of MscL in the open or intermediate conformations, so that the molecular dynamics models cannot be verified directly. However, an interesting mutant channel has recently been described that can be locked in the open state. This mutant, and the crystallization of MscL in the open conformation, may result in the elucidation of the channel gating mechanism (89).

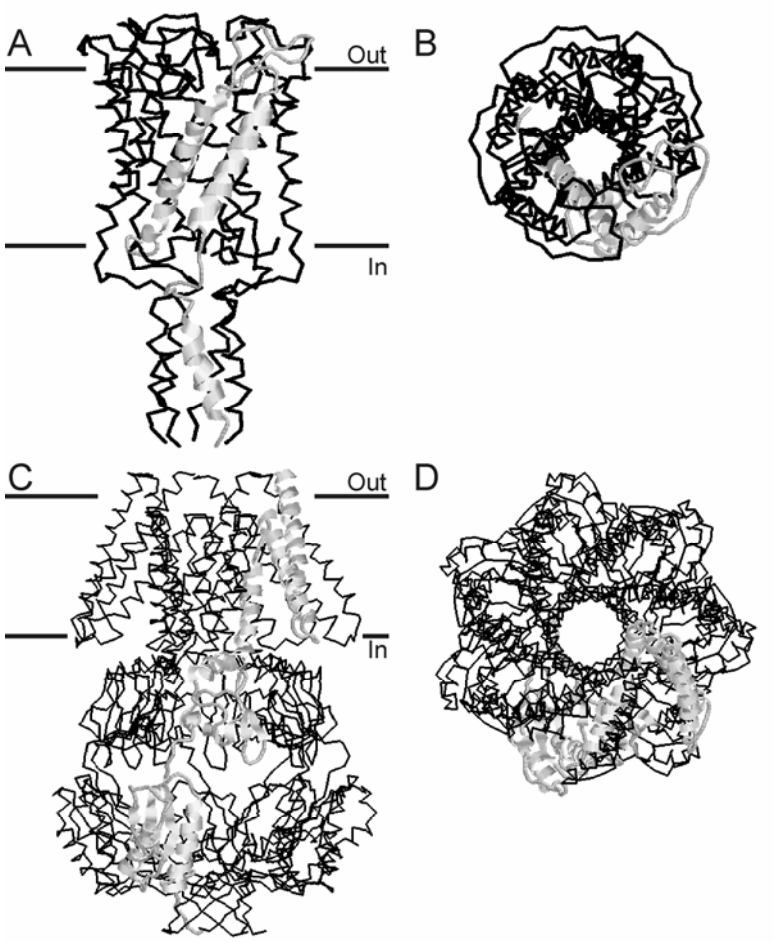

Figure 5: Crystal structures of MscL and MscS. A) side view and B) top view of MscL. The pentameric structure of MscL is clearly visible, as are the cytoplasmic helices. C) side view and D) top view of MscS channel. The heptameric structure of the protein is clearly visible. The large domain, formed by the intracellular helices, is thought to be the part of the protein that makes it size and charge selective. Structures from swiss-PDB (80).

The exact physiological function of the MS channels is not yet fully known. However, it is clear that they do play a role in cell survival upon osmotic downshift, i.e., when the cell environment suddenly changes from high to low osmolyte content (76, 90, 91 and chapter 2). Under these conditions, osmolytes may rapidly leave the cell via the MS channels and thereby prevent the cell from lysing. One of the still unanswered questions is:

why bacterial cells should have multiple ”osmotically regulated osmolyte-release valves” that differ relatively little in threshold tension and selectivity. The gating mechanism of MscL is only mechanosensitive, whereas MscS activity is also partly membrane-potential dependent (79, 92) and MscK appears to be regulated by external ionic environment (i.e., MscK is activated only in the presence of high concentrations of K^+, NH_4^+, Rb^+, or Cs^+; 74). This leaves the question, whether these latter two channels represent true MS osmolyte release valves, or have developed mechanosensitivity as an additional functionality, in which case MscL would be the only genuine MS channel. The remaining part of this introduction will focus on MscL, as this is the most intensively studied bacterial MS channel and is also the topic of the rest of this thesis.

To determine the parts of the MscL channel that are involved in tension sensing and the parts that form the channel constriction site (and are therefore involved in channel gating and size-exclusion ”selectivity”), a number of libraries with mutated *mscL* genes have been constructed and the mutant proteins have been studied (91, 93-95). These studies generally divide mutations into three groups: neutral mutations (i.e., mutants without altered tension sensitivity); Gain Of Function (GOF) mutations (i.e., channels that have a lower tension threshold for opening, or remain in the open conformation for long periods of time); and Loss Of Function (LOF) mutations (i.e., channels that have a higher tension threshold for opening, or remain in the open conformation for short periods of time).

One specific library was generated to elucidate the role of the α-amino acid positioned at the most constricted part of the channel: glycine 22 (95). If this residue was replaced by a hydrophilic (charged) residue the channel would generally become GOF, whereas more hydrophobic substitutions resulted in LOF phenotypes. A LOF channel is obtained when the glycine 22 is replaced by a cysteine, but this mutant becomes GOF upon labeling with the charged reagent [2-(trimethylammonium)ethyl]methanethiosulfonate (MTSET; 96). This was the first example of an engineered switchable channel. A very interesting modification to this switch is the replacement of MTSET with a label that changes charge when illuminated at a specific wavelength (63). A further cysteine library was scanned using MTSET, revealing that not only position 22 is very sensitive to charge modification, but also a number of other residues in the first transmembrane helix (TM 1). Interestingly, all these residues were found on the same face of the transmembrane α-helices that line the channel pore (97, 98). The corresponding residues were also modified to histidines. The five histidines of the subunits of the pentameric channel were found to form a metal binding site inside the pore, that is, when divalent cations (Ni^{2+}, Cd^{2+} and Zn^{2+}) were added to the patch clamp bath-solution, it became increasingly harder to open the modified channel. The only exception was MscL L19H, which became harder to open on the addition of Cd^{2+}, but easier to open in the presence of Ni^{2+}. This suggested that L19 rather than G22 may reside at the most constricted part of the pore. (99)

Apart from defining the constriction site of the channel, a number of studies have been undertaken to identify the sensing part of the protein. Initially, this was done by removing α-amino acids from both N- and C-terminal ends of the protein. This showed that fully functional channels could still be formed when three N-terminal α-amino acids or twenty-seven C-terminal α-amino acids were removed (100, 101). Databases have been searched to identify channel regions that were highly conserved. However, it has not been possible to directly link any of the conserved regions directly to the sensing mechanism of the protein (102, 103). An interesting series of experiments involved the separate expression of polypeptides for the N-terminal TM 1 and the C-terminal part of the wild-type subunit, including TM 2. This study showed that TM 1 alone was able to form channels, albeit with reduced conductance, that gated completely tension-independent. The TM 2 part alone was not able to form channels, but when it was co-expressed with the TM 1 polypeptide, channel activity was observed. This activity had a normal conductance, but a gain of function phenotype (it needed less tension to gate) compared to the wild-type MscL channel. This indicates that the actual tension sensing region is most likely located in TM 2. It also emphasized the importance of the interaction between the two helices and the communication through the connecting loop (103). An earlier study, in which the loop connecting the two transmembrane helices was digested with a protease (trypsin), had shown that this loop played an important role in the transduction of the tension signal. When the loop was digested, the channel was still tension-sensitive, but gated at a lower tension. The loop has been proposed to work like a spring that sets the sensitivity threshold of the channel (104). Recently, a number of mutations at the rim of the channel (end of TM 1) have been made, which resulted in channels with a marked decrease in mechanosensation (LOF; 105). Together, these data suggest that the connecting loop plays an important role in the communication between the sensing (TM 2) and gating modules (TM 1) of the MscL subunits.

Interaction between the sensing module of the protein (TM 2) and the surrounding lipids is also thought to be important for proper channel functioning. It is therefore not surprising that protein-lipid interactions have been the subject of a number of investigations, both in *silico* (106-109) and in *vitro*, using MscL reconstituted in proteoliposomes (110-112) and chapter 3). These studies showed the importance of lateral tension in the membrane (68), asymmetric bending, and membrane thinning (which was nicely demonstrated using a combination of electron spin resonance and lipids with different acyl chain lengths (112)) on the activation of the MscL channel. An overview of the role of membrane lipids in the regulation of osmotic downshift-activated MS channels (i.e., MscL and MscS) and osmotic upshift-activated transporters (i.e., BetP, OpuA and ProP) is available (113).

For a bacterial cell, it is important to have the appropriate number of channels present in the cell membrane. Too many channels may cause unwanted leakage of vital cytoplasmic components. Too few channels may lead to cell lyses under conditions of osmotic downshift. Regulation of the

expression of genes coding for MS channels is therefore important to the cell. A few papers have so far been published on this subject. The most rigorous study showed that expression of MS channels is up-regulated under the influence of *rpoS* during stationary growth phase. It also showed that in strains that lacked the MscL channel, the MscS channel was expressed to higher levels and *vice versa* (114). Interestingly, high external salt concentration did not have an effect on the level of mRNA for MscL or MscS in *L. lactis* (chapter 2).

A very promising recent development, in the light of the application of the channel in drug delivery, is the possibility to produce the channel in a cell free system. Using an enhanced *E. coli* cell lysate and mRNA coding for the MscL from *E. coli*, it was possible to produce channels in a detergent environment and reconstitute them into liposomes. These biologically produced channels showed normal channel activity in patch clamp (115). Chemically, the channel has been produced by linking synthetically-prepared polypeptides, using modified cysteines, and thereby forming functional channel subunits (116, 117). One final study worth mentioning, concerns the preparation of a series of TM 2 cysteine mutants that allowed the conversion of a lipid-soluble protein into a water soluble one by chemically linking amphipaths to the cysteines. This water soluble form has been investigated by circular dichroism, size exclusion chromatography and electron microscopy, which showed that the water soluble form resembled the lipid soluble form of the channel both in structure and in size. The electron micrographs obtained with MscL from *E. coli* showed a five-fold symmetry, indicating that it is structurally very similar to MscL from *M. tuberculosis* (83).

In conclusion: MscL is a versatile and flexible channel that, because of its relatively simple structural and functional properties, is easy to study. The channel is the paradigm of our understanding of the gating mechanism of MS channels, and it may be a good candidate for future applications in bio(nano)technology.

Outline of this thesis

Chapter 2: deals with the identification and characterization of the MS channels from *Lactococcus lactis*. It also shows that *Lactococcus lactis* uses MscL as the main mechanosensitive solute-release system to protect the cells under conditions of osmotic downshift.

Chapter 3: describes a new method for the formation of membrane protein-containing Giant Unilamellar Vesicles. The formed proteo-GUVs were applied in patch-clamp measurements to monitor channel activity and in fluorescence correlation spectroscopy experiments to monitor mobility of a number of model membrane proteins.

Chapter 4: describes the reversible activation of MscL via a light-sensitive lipid mimic. For these experiments MscL containing GUVs were prepared from bilayers composed of 80mol% 1,2-dioleoyl-*sn*-glycero-3-phosphocholine and 20mol% of di-(5-{[4-(4-butylphenyl)azo]-phenoxy}-pentyl)phosphate (4-Azo-5P). Light-

induced isomerization of the azobenzene moiety of 4-Azo-5P from *trans* to *cis* was used to activate MscL.

Chapter 5: shows the construction of covalent oligomers by gene fusion; up to six copies of the *mscL* gene were fused in tandem. Only the covalent pentamer opened at the same relative pressure (compared to the pressure required to open MscS) as the wild-type MscL channel. In a size exclusion chromatography, the wild-type channels and the covalent pentameric channel migrated similarly. Overall, the data strongly suggest that the pentameric MscL represents the functional state of the channel.

Chapter 6: presents a summary of the work carried out during the Ph.D. project, including some unpublished experiments, combined with future prospects. The chapter also contains information on the techniques that were used and developed for the work presented in this thesis.

Reference List

1. www.wikipedia.org
2. www.membranetranport.org
3. Lehmann-Horn, F. and Jurkat-Rott, K. (1999) *Physiol. Rev.* **79,** 1317-72
4. Lehmann-Horn, F. and Jurkat-Rott, K. (2003) *J. Neurol. Neurosurg. Psychiatry* **74,** 1466-75
5. Galvani, L. (1791) *Bon. Sci. Art. Inst. Acad. Comm.* **7,** 363-418
6. Galvani, L. (1841) (Ed. Gherardi, S.) Opere edite ed inedited del Professore Luigi Galvani pp. 59-125
7. Volta, A. (1918) Le opera di Allesandro Volta (edizione nazionale) vol I and II
8. Galvani, L. (1841) Opere edite ed inedited del Professore Luigi Galvani raccolte e pubblicate dall'Accademia delle Science dell'Instituto di Bologna
9. Picolini, M. (1998) *Brain Res. Bull.* **46,** 381-407
10. Sirol M. (1939) *Galvani et le galvanisme* Vigot Frères, Paris
11. Matteuci, C. (1938) Sur le courant électrique ou proper de la grénouille. *Bibl. Univ. Genève* **15,** 157-68
12. Matteuci, C. (1842) *Ann. Chim. Phys.* **6 (ser.3),** 301-39
13. Matteuci, C. (1844) Traité des phénomènes electro-physiologiques des animaux suive d'études anatomiques sur le systhème nerveux et sur l'organe électrique de la torpille par Paul Savi
14. Moruzzi. G. (1996) *Brain Res. Bull.* **40,** 69-91
15. du Bois-Reymond, E. (1848-1884) Untersuchungen über thierische elektricität vol I and II
16. Pearce, J.M. (2001) *J. Neurol. Neurosurg. Psychiatry* **71,** 620
17. Kettenmann, H. (1997) *Trends Neurosci.* **20,** 239-42
18. Helmholtz, H. (1850) *Arch. Anat. Physiol. Wiss. Med.* pp.71-3
19. Helmholtz, H. (1850) *C. R. Acad. Sci. (Paris)* **30,** 204-6
20. Nägeli, C. and Cramer, C. (1855) Pflanzenphysiologische Untersuchungen
21. Pfeffer, W.F.P. (1886) *Untersuch. Botan. Inst. Tübingen* **92,** 179-331
22. Overton, E. (1895) *Vierteljahrschr. Naturforsch. Ges. Zürich* **40,** 159-201
23. Overton, E. (1896) *Vierteljahrschr. Naturforsch. Ges. Zürich* **41,** 383-406
24. Overton, E. (1899) *Vierteljahrschr. Naturforsch. Ges. Zürich* **44,** 88-114
25. Overton, E. (1901) Studien über die Narkose, zugleich ein beitrag zur allgemeinen Pharmakologie
26. Overton, E. (1902) *Pflügers Arch.* **92,** 346-86
27. de Weer, P. (2000) *Annu. Rev. Physiol.* **62,** 919-926
28. Langmuir, I. (1917) *J. Am. Chem. Soc.* **39,** 1848-1906
29. Tien, H.T. and Ottova A.L. (2001) *J. Memb. Sci.* **189,** 83-117
30. Singer, S.J. (2004) *Annu Rev Physiol.* **66,** 1-27
31. Singer, S.J. (1990) *Annu Rev Cell Biol.* **6,** 247-96

32. Gorter, E. and Grendel, F. (1925) *J. Exp. Med.* **41,** 439-43
33. Danielli, J.F. and Davson, H. (1935) *J. Cell. Comp. Physiol.* **275,** 495-508
34. Robertson, J.D. (1957) *J. Physiol.* **140,** 58-9
35. Singer, S.J. and Nicolson, G.L. (1972) *Science* **175,** 720-31
36. Young, J.Z. (1936) *Cold Spring Harbour Symp. Quant. Biol.* **4,** 1-6
37. Hodgkin, A.L. and Huxley, A.F. (1939) *Nature* **144,** 710-1
38. Cole, K.S. (1949) *Arch. Sci. Physiol.* **3,** 253-8
39. Mueller, D., Rudin, O., Tien, H.T. and Wescott, W.C. (1963) *J. Phys. Chem.* **67,** 534-5
40. Andreoli, T.E. (1974) *Methods Enzymol.* **32(Part B),** 513-39
41. Rigaud, J-L. and Lévy, D. (2003) *Methods Enzymol.* **372,** 65-86
42. Wonderlin, W.F., Finkel, A. and French, R.J. (1990) *Biophys J.* **58,** 289-97
43. Bamberg, E., Butt, H.-J. and Fendler, K. (1993) *Quart. Rev. Biophys.* **26,** 1-25
44. Hamill, O.P., Marty, A., Neher, E., Sakmann, B. and Sigworth, F.J. (1981) *Pflugers Arch.* **391,** 85-100
45. Neher, E. and Sakmann, B. (1992) *Sci. Am.* **266,** 44-51
46. Sakmann, B. (1992) *Science* **256,** 503-12
47. Sherman-Gold, R. (1993) (Ed. Axon instruments Inc.) The axon guide
48. Blount, P., Sukharev, S.I., Moe, P.C., Martinac, B. and Kung, C. (1999) *Methods Enzymol.* **294,** 458-82
49. Doyle, D.A., Morais-Cabral, J., Pfuetzner, R.A., Kuo, A., Gulbis, J.M., Cohen, S.L., Chait, B.T. and MacKinnon, R. (1998) *Science* **280,** 69-77.
50. Chang, G., Spencer, R.H., Lee, A.T., Barclay, M.T. and Rees, D.C. (1998) *Science* **282,** 2220-6
51. Ellis, C. and Smith, A. (2004) *Nature Rev. Drug Disc.* **3,** 238-78
52. Fertig, N., Meyer, C., Blick, R.H., Trautmann, C. and Behrends, J.C. (2001) *Phys. Rev. E* **64,** 1-4
53. Mayer, M., Kriebel, J.K., Tosteson, M.T. and Whitesides, G.M. (2003) *Biophys. J.* **85,** 2684-95
54. Peterman, M.C., Ziebarth, M., Braha, O., Baylay, H., Fishman, H.A. and Bloom, D.M. *Biomedical Microdevices* **4,** 231-6
55. Klemic, K.G., Klemic, J.F., Reed, M.A. and Sigworth, F.J. (2002) *Biosens. Bioelectron.* **17,** 597-604
56. Fertig, N., Blick, R.H. and Behrends, J.C. (2002) *Biophys. J.* **82,** 3056-62
57. Fertig, N., George, M., Klau, M., Meyer, C., Tilke, A., Sobotta, C., Blick, R.H. and Behrends, J.C. (2003) *Receptors Channels*. **9,** 29-40
58. www.nanion.de
59. Bruggemann, A., George, M., Klau, M., Beckler, M., Steindl, J., Behrends, J.C. and Fertig, N. (2003) *Assay. Drug Dev. Technol.* **1,** 665-73
60. Buzsaki, G. (2004) *Nat. Neurosci.* **7,** 446-51

61. Asmild, M., Oswald, N., Krzywkowski, K.M., Friis, S., Jacobsen, R.B., Reuter, D., Taboryski, R., Kutchinsky, J., Vestergaard, R.K., Schroder, R.L., Sorensen, C.B., Bech, M., Korsgaard, M.P. and Willumsen, N.J. (2003) *Receptors Channels* **9,** 49-58
62. Willumsen, N.J., Bech, M., Olesen, S.P., Jensen, B.S., Korsgaard, M.P. and Christophersen, P. (2003) *Receptors Channels* **9,** 3-12.
63. Koçer, A., Walko, M., Meijberg, W. and Feringa, B.L. (2005) *Science* in press
64. www.biomade.nl/channel.htm
65. Vermeulen E. (2004) *Natuurwetenschap en Techniek* **10,** 64-5
66. van Nieuwstadt, M. (2005) *NRC Handelsblad* **5 February,** 45
67. Sukharev, S.I., Martinac, B., Arshavsky, V.Y. and Kung, C. (1993) *Biophys. J.* **65,** 177-83
68. Martinac, B., Adler, J. and Kung, C. (1990) *Nature* **348,** 261-3
69. Sukharev, S.I., Blount, P., Martinac, B., Blattner, F.R. and Kung, C. (1994) *Nature* **368,** 265-8
70. Cruickshank, C.C., Minchin, R.F., Le Dain, A.C. and Martinac, B. (1997) *Biophys. J.* **73,** 1925-31
71. Moe, P.C., Blount, P. and Kung, C. (1998) *Mol. Microbiol.* **28,** 583-92
72. Maurer, J.A., Elmore, D.E., Lester, H.A. and Dougherty, D.A. (2000) *J. Biol. Chem.* **275,** 22238-44
73. Nottebrock, D., Meyer, U., Kramer, R. and Morbach, S. (2003) *FEMS Microbiol. Lett.* **218,** 305-9
74. Kloda, A. and Martinac, B. (2001) *Biophys. J.* **80,** 229-40.
75. Li, Y., Moe, P.C., Chandrasekaran, S., Booth, I.R. and Blount, P. (2002) *EMBO J.* **21,** 5323-30
76. McLaggan, D., Jones, M.A., Gouesbet, G., Levina, N., Lindey, S., Epstein, W. and Booth, I.R. (2002) *Mol. Microbiol.* **43,** 521-36
77. Levina, N., Totemeyer, S., Stokes, N.R., Louis, P., Jones, M.A. and Booth, I.R. (1999) *EMBO J.* 18, 1730-7
78. Miller, S., Bartlett, W., Chandrasekaran, S., Simpson, S., Edwards, M. and Booth, I.R. (2003) *EMBO J.* **22,** 36-46
79. Bass, R.B., Strop, P., Barclay, M. and Rees, D.C. (2002) *Science* **298,** 1582-7
80. Berman, H.M., Westbrook, J., Feng, Z., Gilliland, G., Bhat, T.N., Weissig, H., Shindyalov, I.N. and Bourne, P.E. (2000) *Nucleic Acids Research* **28,** 235-42
81. Blount, P., Sukharev, S.I., Moe, P.C., Schroeder, M.J., Guy, H.R. and Kung, C. (1996) *EMBO J.* **15,** 4798-805
82. Sukharev, S.I., Schroeder, M.J. and McCaslin, D.R. (1999) *J. Membr. Biol.* **171,** 183-93
83. Becker, C.F., Strop, P., Bass, R.B., Hansen, K.C., Locher, K.P., Ren, G., Yeager, M., Rees, D.C. and Kochendoerfer, G.G. (2004) *J. Mol. Biol.* **343,** 747-58
84. Sukharev, S., Betanzos, M., Chiang, C.S. and Guy, H.R. (2001) *Nature* **409,** 720-4

85. Gullingsrud, J., Kosztin, D. and Schulten, K. (2001) *Biophys. J.* **80,** 2074-81
86. Bilston, L.E. and Mylvaganam, K. (2002) *FEBS Lett.* **512,** 185-90
87. Perozo, E., Cortes, D.M., Sompornpisut, P., Kloda, A. and Martinac, B. (2002) *Nature* **418,** 942-8
88. Colombo, G., Marrink, S.J. and Mark, A.E. (2003) *Biophys. J.* 2003 **84,** 2331-7
89. Shapovalov, G., Bass, R., Rees, D.C. and Lester, H.A. (2003) *Biophys. J.* **84,** 2357-65
90. Nakamaru, Y., Takahashi, Y., Unemoto, T. and Nakamura, T. (1999) *FEBS Lett.* **444,** 170-2
91. Blount, P., Schroeder, M.J. and Kung, C. (1997) *J. Biol. Chem.* 1997 **272,** 32150-7
92. Akitake, B., Anishkin, A. and Sukharev, S. (2005) *J. Gen. Physiol.* **125,** 143-54
93. Blount, P., Sukharev, S.I., Schroeder, M.J., Nagle, S.K. and Kung, C. (1996) *Proc. Natl. Acad. Sci. USA* **93,** 11652-7
94. Maurer, J.A. and Dougherty, D.A. (2003) *J. Biol. Chem.* **278,** 21076-82
95. Yoshimura, K., Batiza, A., Schroeder, M., Blount, P. and Kung, C. (1999) *Biophys. J.* **77,** 1960-72
96. Yoshimura, K., Batiza, A. and Kung, C. (2001) *Biophys. J.* **80,** 2198-206
97. Levin, G. and Blount, P. (2004) *Biophys. J.* **86,** 2862-70
98. Bartlett, J.L., Levin, G. and Blount, P. (2004) *Proc. Natl. Acad. Sci. USA* **101,** 10161-5
99. Iscla, I., Levin, G., Wray, R., Reynolds, R. and Blount, P. (2004) *Biophys. J.* **87,** 3172-80
100. Hase, C.C., Le Dain, A.C. and Martinac, B. (1997) *J. Membr. Biol.* **157,** 17-25
101. Moe, P.C., Blount, P. and Kung, C. (1998) *Mol. Microbiol.* **28,** 583-92
102. Kumanovics, A., Levin, G. and Blount, P. (2002) *FASEB. J.* **16,** 1623-9
103. Park, K.H., Berrier, C., Martinac, B. and Ghazi, A. (2004) *Biophys. J.* **86,** 2129-36
104. Ajouz, B., Berrier, C., Besnard, M., Martinac, B. and Ghazi, A. (2000) *J. Biol. Chem.* **275,** 1015-22
105. Yoshimura, K., Nomura, T. and Sokabe, M. (2004) *Biophys. J.* **86,** 2113-20
106. Wiggins, P.A. and Phillips, R. (2005) *Biophys. J.* **88,** 880-902
107. Gullingsrud, J. and Schulten, K. (2004) *Biophys. J.* **86,** 3496-509
108. Elmore, D.E. and Dougherty, D.A. (2003) *Biophys. J.* **85,** 1512-24
109. Colombo, G., Marrink, S.J. and Mark, A.E. (2003) *Biophys. J.* **84,** 2331-7
110. Powl, A.M., East, J.M. and Lee, A.G. (2003) *Biochemistry* **42,** 14306-17
111. Moe, P.C. and Blount, P. (2002) *Conference proceedings: Biophysical Chemistry: Membranes and Proteins* (Ed: Templer, R.H. and Leatherbarrow, R.) 199-207

112. Perozo, E., Kloda, A., Cortes, D.M. and Martinac, B. (2002) *Nat. Struct. Biol.* **9,** 696-703
113. Poolman, B., Spitzer, J.J. and Wood, J.M. (2004) *Biochim. Biophys. Acta* **1666,** 88-104
114. Stokes, N.R., Murray, H.D., Subramaniam, C., Gourse, R.L., Louis, P., Bartlett, W., Miller, S. and Booth, I.R. (2003) *Proc. Natl. Acad. Sci. USA* **100,** 15959-64
115. Berrier, C., Park, K.H., Abes, S., Bibonne, A., Betton, J.M. and Ghazi, A. (2004) *Biochemistry* **43,** 12585-91
116. Becker, C.F., Clayton, D., Shapovalov, G., Lester, H.A. AND Kochendoerfer, G.G. (2004) *Bioconjug. Chem.* **15,** 1118-24
117. Clayton, D., Shapovalov, G., Maurer, J.A., Dougherty, D.A., Lester, H.A. and Kochendoerfer, G.G. (2004) *Proc. Natl. Acad. Sci. USA* **101,** 4764-9

Lactococcus lactis uses MscL as its principal mechanosensitive channel

Joost H.A. Folgering, Paul C. Moe, Gea K. Schuurman-Wolters, Paul Blount and Bert Poolman

This chapter was published: (2005) *J. Biol. Chem.* **280,** 8784-92

Abbreviations: GUV: Giant Unilamellar Vesicle; MTSET: [2-(trimethylammonium)ethyl] methanethiosulfonate; ITO: Indium-Tin-Oxide; NTA: Nitrilo-Triacetic Acid; CFU: Colony Forming Units; GOF: Gain-Of-Function; MS: Mechano-Sensitive; CDM: Chemically Defined Medium; RT-PCR: Reverse Transcription - Polymerase Chain Reaction

Abstract

The functions of the mechanosensitive channels from *Lactococcus lactis* were determined by biochemical, physiological and electrophysiological methods. Patch-clamp studies showed that the genes *yncB* and *mscL* encode MscS and MscL-like channels, respectively, when expressed in *E. coli* or if the gene products were purified and reconstituted in proteoliposomes. However, unless *yncB* was expressed in *trans*, membranes derived from wild-type of *Lactococcus lactis* displayed only MscL activity. Membranes prepared from a *mscL* disruption mutant did not show any mechanosensitive channel activity, irrespective of whether the cells had been grown on low or high osmolarity medium. In osmotic downshift assays, wild-type cells survived and retained 20% of the glycine betaine internalized under external high salt conditions. On the other hand, the *mscL* disruption mutant retained 40% of internalized glycine betaine and was significantly compromised in its survival upon osmotic downshifts. The data strongly suggest that *Lactococcus lactis* uses MscL as the main mechanosensitive solute-release system to protect the cells under conditions of osmotic downshift.

Introduction

Mechanosensitive channels play an important role in prokaryotic cell volume regulation (1). In small, single-cell, organisms this regulation can mean the difference between life and death under extreme osmotic downshift conditions. By diffusion over the semi-permeable cell membrane and/or aquaporins embedded in the membrane, water can enter and leave the cell until equilibrium is established between internal and external osmolality. This allows microorganisms to adapt to changes in external osmolyte concentrations. When the external osmolyte concentrations increase (hyper-osmotic stress), water will leak out of the cell, causing loss of turgor and ultimately the cell may plasmolyse. Bacteria respond to this hyperosmotic stress by rapid uptake of ions (K^+) and/or compatible solutes or increasing the intracellular osmolyte concentration through synthesis of compatible solutes. The increase in internal compatible solute concentration compensates for the

high external osmolality allowing water to diffuse back and the cell to regain its original volume and turgor (2-4).

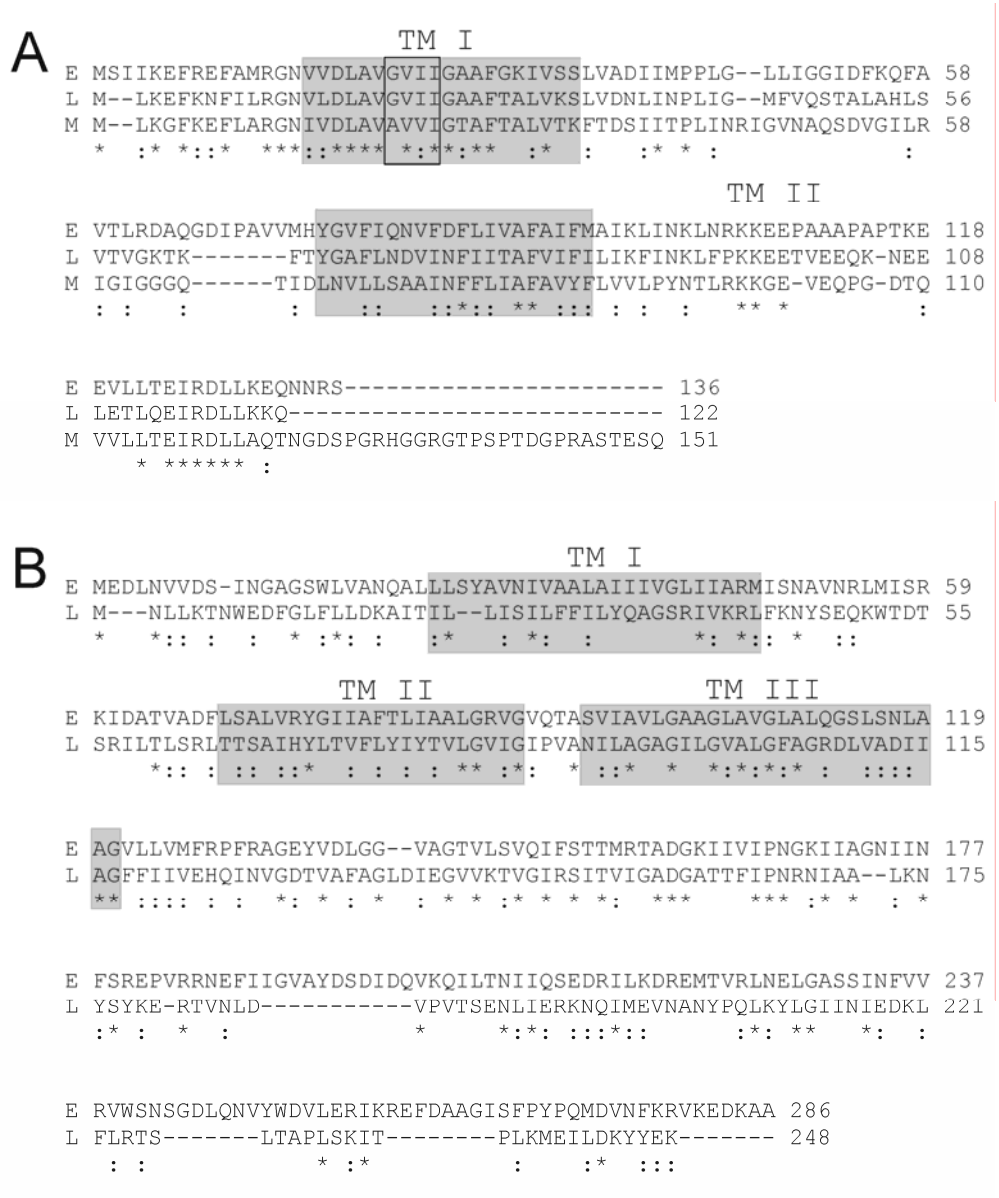

Figure 1: (A) Alignment of MscL from *E. coli* (E), *L. lactis* (L) and *M. tuberculosis* (M). The boxed α-amino acids in panel A correspond to the positions of the cysteine mutants. (B) Alignment of MscS from *E. coli* (E) and *L. lactis* (L). The homology between the proteins is indicated as follows: (*) fully conserved residues, (:) close conservative substitutions. The transmembrane segments are shaded grey.

Conversely, when the external osmolyte concentration suddenly decreases, water will diffuse into the cell causing it to swell and, in extreme conditions, lyse. This is where the mechanosensitive channels are thought to play a role by opening in response to the increased membrane tension effected by the rapid increase in cell volume. The best-known example of a channel in this role is the Mechanosensitive Channel of Large conductance

from *E. coli* ($MscL^{Ec}$), but homologues are present in most eubacteria (5-7). MscL opens near the lytic tension limit of the bacterial membrane. A second mechanosensitive channel, that of small conductance, MscS, has been characterized in only a few organisms (8, 9). MscS opens at lower membrane tensions and has a smaller conductance than MscL, making it useful for fine-regulation of internal compatible solute concentration. Crystal structures of MscL and MscS are available (10, 11). The electrophysiological characteristics of MscS from *E. coli* (12) and of a number of MscL homologues (5) have been described. So far their physiological roles in osmoprotection are not fully understood.

Previously we have established the mechanism of the osmotic regulation of the upshift activated glycine betaine transporter OpuA from *Lactococcus lactis* (13, 14). Although the physicochemical properties of the membrane and lipid-protein interactions also play a critical role in the osmotic activation of OpuA, the mechanism is entirely different from that underlying the gating of MS channels. We have shown that increasing internal ionic strength, a consequence of osmotic upshift, activates OpuA by altering the electrostatic interactions between anionic lipids and charged residues at the cytoplasmatic face of the protein (15). For a better understanding of the total osmoregulatory response of *L. Lactis,* we present here the electrophysiological and biochemical characterization of *L. lactis* MscL ($MscL^{Ll}$; 45.4% identity with $MscL^{Ec}$; Fig 1A) and YncB (hereafter referred to as $MscS^{Ll}$; 24.0% identity with MscS from *E. coli*; Fig 1B) and show that $MscL^{Ll}$ is critical for protection of *L. lactis* against osmotic downshifts. In fact, the majority of glycine betaine, accumulated upon upshift activation of OpuA, seems to exit the cell via $MscL^{Ll}$ upon subsequent osmotic downshift. We also examined the expression of the *opuA, mscL* and *yncB* genes during cell growth under low and high salt conditions.

Table 1: Bacterial strains and their relevant genotypes

Strain	Relevant genotype	Reference
E. coli		
PB104	*E. coli* AW405, Δ*mscL::Cm*^{res} *recA*$^{-}$	16
MJF465	*E. coli* Frag1, Δ*mscL::Cm*^{res}, Δ*yggB*, Δ*kefA::kan*^{res}	12
JM110	*dam*$^{-}$*, dcm*$^{-}$	17
L. lactis		
IL1403	Plasmid free strain	18
MG1363	Plasmid free strain	19
NZ9000	MG1363 pepN*::nisR nisK*	20
JIM7049	IL1403 *his::nisR nisK*	21
JIM7049ΔMscL	IL1403 *his::nisR nisK*; *MscL::Em*^{res}	This work
LI108	*RepA*$^{+}$ MG1363, carrying multiple copies of pWVO1 *repA* in the chromosome, *Cm*$^{res+}$	22

Table 2: List of plasmids used in this study and their characteristics

Plasmid	Relevant characteristics	Reference
pBlueScript	β-galactosidase α-complementation; *Xba*I, XhoI in multiple cloning site; Amp^{res}	23
pB10b	pBR322 *ori*; *lacUV5* promoter; *Xba*I, *Xho*I in multiple cloning site; Amp^{res}	16
pBAD	pBR322 *ori;* P_{BAD} promoter; *Nco*I, *Hind*III in multiple cloning site; Amp^{res}	24
pB10bmscL^{LI}	pB10b with *L.lactis mscL* inserted in *Xba*I, *Xho*I	This work
pB10bmscL^{LI}6H	pB10b with *L. lactis mscL*, and sequence coding for a C-terminal 6-histidine tag, inserted in *Xba*I, *Xho*I	This work
pB10bmscL^{LI}6H G20C	pB10BMscLLl6H G20C	This work
pB10bmscL^{LI}6H V21C	pB10BMscLLl6H V21C	This work
pB10bmscL^{LI}6H I22C	pB10BMscLLl6H G22C	This work
pB10bmscL^{LI}6H I23C	pB10BMscLLl6H V23C	This work
pBADyncB10H	pBAD with *L. lactis yncB*, and sequence coding for a C-terminal 10-histidine tag, inserted; in *Nco*I, *Hind*III	This work
pET324	pBR322 *ori*; *lacUV5* promoter; *Nco*I, *Hind*III in multiple cloning site; Amp^{res}	25
pET324yncB10H	pET324 with *L. lactis yncB*, and sequence coding for a C-terminal 10 histidine tag inserted; in *Nco*I, *Hind*III	This work
pNZ8020	pSH71 replicon; *nisA* promoter; *Xba*I *Xho*I in multiple cloning site; Cm^{res}	20
pNZ8020mscL^{LI}6H	pNZ8020 with *L. lactis mscL*, and sequence coding for a C-terminal 6-histidine tag; inserted in *Xba*I, *Xho*I	This work
pNZ8048	pSH71 replicon; *nisA* promoter, *Nco*I, *Hind*III in multiple cloning site; Cm^{res}	26
pNZ8048yncB10H	pNZ8048 with *L. lactis yncB*, and sequence coding for a C-terminal 10-histidine tag; inserted in *Nco*I, *Hind*III	This work
pOri280	pWV01-derivative; $repA^{-}$,replicates only in strains that carry *repA* in *trans*; Em^{res}	22
pOri280ΔMscL^{LI}	pOri280 with an internal fragment of $mscL^{LI}$ inserted in *Xba*I, *BamH*I; Em^{res}	This work

Materials and Methods

Strains, plasmids and growth conditions

Experiments were performed using the strains listed in Table 1 and plasmids listed in Table 2. *Escherichia coli* strains were grown in Luria broth, with 100µg/ml ampicillin when required. *Lactococcus lactis* cells were grown in M17 broth (Difco) or chemically defined medium (27) supplemented with 25mM glucose and 365mM KCl for high salt conditions (1050mOsmol/kg).

Chloramphenicol (5μg/ml) or erythromycin (5μg/ml) was added when the cells were transformed with plasmids. For growth on solid medium 1.5% (w/v) agar was added to the broth.

Cloning of *mscL* and *yncB*

The primers that were used for the amplification of *mscL* and *yncB* are listed in Table 3. As the *yncB* gene product is homologous to MscS from *E. coli*, and functions similarly, the YcnB protein is referred to as $MscS^{Ll}$. The superscripts Ll and Ec will be used to denote genes or proteins from *L. lactis* and *E. coli*, respectively. For PCR amplifications, Expand High-Fidelity DNA polymerase (Roche) was used and reactions were performed according to the manufacturer's instructions. Chromosomal DNA of *L. lactis* IL1403 was used as template, the annealing temperature was 50°C for $mscL^{Ll}$ and 53°C for *yncB*, and the elongation times were 30 and 60 sec, respectively. For the histidine-tagged version of $MscL^{Ll}$, a two step PCR was performed using primers LL.SD.5' and LL.SD.4H3' (see Table 3) to introduce a 4-histidine tag, and then a second step was used to engineer another two histidines, a stop codon and a restriction site for cloning.

Table 3: Primers used in this study

Name	Sequence
FW WT $MscL^{Ll}$	5'-TCTAGATCTAGATATTATATAGGATTTATGTTAA
REV WT $MscL^{Ll}$	5'-GAGCTCGAGCTCGGGCTAGAGGGAGTTTGGTTAGC
LL.SD.5'	5'-TCTAGATCTAGAAGGAGGAGCCATGGTAAAGGAATTTAAAAAC
LL.SD.4H3'	5'-GTGATGGTGATGTTGTTTTTTCAATAAATCGCGAATTTC
LL.SD.6H3'	5'-CTCGAGCTCGAGTTAGTGATGGTGATGGTGATGTTGTTTTTTCAATA
yncB FW	5'-ATATATCCATGGACTTATTAAAAACAAACTGGGAA
yncB REV	5'-ATATATAAGCTTAATGGTGATGGTGATGGTGTTTTTCATAATATTTA TCTAAAATCTCC
G20C	5'-GGGAACGTATTGGACTTAGCCGTTTGTGTTATCATCGGGGCAG
V21C	5'-GGGAACGTATTGGACTTAGCCGTTGGGTGTATCATCGGGGCAG
I22C	5'-GGGAACGTATTGGACTTAGCCGTTTGTGTTTGTATCGGGGCAG
I23C	5'-GGGAACGTATTGGACTTAGCCGTTGGGGTTATCTGTGGGGCAG
DIS FW	5'-CTGGCGTCTAGAGGGAACGTATTGGACTTAGCCG
DIS REV	5'-CCGGCCGGATCCAAGAATGAAAATAACAAAGGC
RT-YncB fw	5'-CTCTATCAAGCCGGCTCTCG
RT-YncB rev	5'-GAGGGCAGCAATATTTCGATTAGG
RT-MscL fw	5'-GGGAACGTATTGGACTTAGCCG
RT-MscL rev	5'-CGCGAATTTCTTGGAGAGTTTCC
RT-Opu fw	5'-CGCGCAGAGAAGGCCTTAG
RT-Opu rev	5'-CAGCCATTAGAGAGCTGACC

The $mscL^{Ll}$ and $mscL^{Ll}6H$ genes were first sub-cloned in pBluescript, isolated from *E. coli* JM110, using the *Xho*I-*Xba*I restriction sites. This construct was used to transform JM110, and after plasmid isolation, the genes were excised from the pBluescript vector and ligated into pNZ8020 and pB10b again using the *Xho*I-*Xba*I restriction sites. The resulting plasmids

pNZ8020mscL^{LI}6H and pB10bmscL^{LI} were then used to transform *L. lactis* JIM7049 and *E. coli* PB104, respectively. *YncB10H* was ligated directly after PCR into the vectors pNZ8048, pET324 and pBAD and used to transform *L. lactis* IL1403 and *E. coli* JM465, respectively. Finally, all constructs were midi-prepped (Qiagen) and the DNA sequence was analyzed to confirm fidelity.

Construction of single cysteine mutants and a *L. lactis mscL* disruption strain

The primers used for the construction of the mutants of MscL^{LI} are listed in Table 3. The cysteine mutants were constructed using pB10bmscL^{LI}6H as template. First, LL.SD.6H3' was combined with the primer for the specific mutant to create a megaprimer, which in a second amplification step was combined with LL.SD.5' to obtain the complete *mscL* sequence with the desired cysteine modification. All other conditions were as described above for the cloning of MscL6H.

For the construction of the *L. lactis* JIM7049 *mscL* disruption strain, an internal gene fragment, from codon 12 to codon 86, was amplified. From earlier studies with truncation mutants of *E. coli* MscL, it could be predicted that a disruption with this gene fragment should lead to complete inactivation of MscL (28). The amplification was performed using the same conditions as described above for amplification of *mscL6H*. The internal gene fragment was ligated in pOri280, using the *Xba*I and *Bam*HI restriction sites. The vector was hosted in *L. lactis* LI108 for propagation of the plasmid and, after confirmation of the DNA sequence, the plasmid was introduced into *L. lactis* JIM7049. The cells were grown on M17-glucose solid medium, supplemented with erythromycin (5µg/ml) to select for colonies that harboured the plasmid DNA integrated into the chromosome (22). The *mscL* disruption strain is designated JIM7049ΔMscL.

Transcriptional analysis

Cells were grown to mid-exponential phase of growth on CDM and diluted 1:1 to CDM without NaCl or CDM plus 0.5M NaCl (final concentration), and harvested 10 minutes after dilution. RNA was extracted as described (29) at concentrations of 4-5µg/µl. The RNA was used as template for the AMV reverse transcriptase, using the 1st strand cDNA synthesis kit for RT-PCR (Roche Applied Science, Indianapolis), according to the manufacturer's instructions and in the presence of the supplied random hexanucleotide primers. The obtained cDNA was subsequently used as template in a PCR reaction with Taq polymerase using the RT-MscL, RT-MscS and RT-OpuA forward (fw) and reverse (rev) primers listed in Table 3. The primers were designed to amplify internal gene fragments of 316 (bp 34 - 349 of *mscL*), 418 (bp 94 - 513 of *yncB*) and 502 (bp 430 - 931 of *opuAA*) basepairs.

For PCR amplification, the annealing temperature was 50°C and the elongation time was 60sec. The products were analyzed on a 1.5% agarose gel after 15 and 25 cycles. As a control, the PCR was also performed on chromosomal DNA of *L. lactis*; as a negative control the RNA samples were treated in exactly the same manner, except that the AMV reverse transcriptase was omitted in the reaction with RNA as template.

Preparation of MS channel-containing membranes for patch clamp analysis

Hybrid proteo-GUVs. L. lactis NZ9000 containing pNZ8020mscL^{LI}6H was grown in M17-glucose medium to an OD_{600} of 0.8, after which *mscL* expression was induced for three hours with a 1:1000 dilution of the supernatant of a culture from the nisinA producing *L. lactis* NZ9700 strain (20). Inside-out membrane vesicles were prepared by lysing the bacteria (20mg/ml protein) with a high-pressure homogenizer (Kindler type NN2002; single passage at 10,000psi), following (partial) digestion of the cell wall with 10mg/ml lysozyme for 30min at 30°C. After removing unlysed cells and cell wall debris by centrifugation at 20,000xg, the membrane vesicles were washed once by centrifugation at 150,000xg and then resuspended in 50mM KPi, pH 6.5. Aliquots of 0.5ml were frozen in liquid nitrogen and stored at -80°C. The membrane vesicles were mixed with liposomes (2:25 w/w total membrane protein/lipid ratio), centrifuged at 270,000xg and resuspended in 5% ethylene glycol and dehydrated on a glass slide. To obtain fused proteo-GUVs rehydration was performed by placing rehydration buffer (200mM KCl, 0.1mM EDTA, 0.01mM $CaCl_2$ plus 5mM HEPES, pH 7.2) on top of the dried membranes to obtain a final lipid concentration of 100mg/ml as described (30). Alternatively, after drying on glass slides coated with indium tin oxide (ITO), hybrid proteo-GUVs were obtained by rehydration in a flow chamber with 300µl of 10mM KCl, 2mM $MgCl_2$, 0.25mM HEPES, pH 7.2 plus 320mM sucrose (the sucrose was added to make the rehydration medium equiosmolar to the buffer for patch-clamp analysis). The flow chamber was closed with a second ITO-coated glass slide. A voltage of 1.2V at 10Hz was applied for at least 3h through electrodes sealed on the glass plates. The resulting giant unilamellar vesicles (GUVs), 5-50µm in diameter, were used in patch clamp experiments (31).

Proteo-GUVs. Membrane vesicles, containing overexpressed channel protein (MscL^{LI} or MscS^{LI}), were solubilized in 50mM KPi, 35mM imidazole, 300mM NaCl, pH 7.0 plus 3% octyl-β-D-glucoside (Anatrace) at 4°C for 20 min and under continuous stirring of the suspension. The solubilized proteins and remaining membrane material were separated by ultracentrifugation at 270,000xg for 20min at 4°C. The supernatant was then loaded onto Ni-NTA affinity resin pre-equilibrated with solubilization buffer. The column was washed with 20-30 volumes of solubilization buffer containing 0.5% Triton X-100, after which the proteins were eluted with 50mM KPi, 300mM NaCl, pH 7.0 plus 0.2% Triton X-100 with a step gradient of imidazole. The purified proteins were mixed with Triton X-100-destabilized preformed liposomes (10mg/mL of lipid); the lipid mixtures were composed of dioleoyl 18:1 (Δ9 cis) phospholipids, that are, DOPC, DOPE and/or DOPS, typically at protein-to-lipid ratios of 1 to 2,000-20,000 (mol monomeric channel protein per mol lipid), and reconstitutions were performed as described (32). The proteoliposomes were converted to proteo-GUVs by dehydration and rehydration in the presence or absence of an electrical field, as described under ”*Hybrid proteo-GUVs*”.

Spheroplasts. For determination of pressure ratios, relative to $MscS^{Ec}$, of $MscL^{LI}$ and the individual cysteine mutants, giant spheroplasts were prepared from *E. coli* PB104 containing pB10bmscL^{LI}6H or its derivatives. For other channel characteristics giant spheroplasts were prepared from *E. coli* MJF465 containing pB10bmscL^{LI}, pB10bmscL^{LI}6H or pET324yncB10H. All spheroplasts were prepared as described (30).

Patch clamp experiments

Experiments were performed as described previously (30). After preparation, an aliquot of proteo-GUVs or 1-5µl of a spheroplast sample was transferred to a sample chamber containing a ground electrode and 300µl of patch clamp buffer: 5mM HEPES, pH 7.2, 200mM KCl plus 40mM $MgCl_2$ for proteo-GUVs; 5mM HEPES, pH 7.2, 200mM KCl, 90mM $MgCl_2$, plus 10mM $CaCl_2$ for spheroplasts. Channel activity was recorded using an Axopatch 200A amplifier together with a digital converter and Axoscope software (Axon Instruments, Foster City, USA). Data were acquired at a sampling rate of 33kHz and filtered at 10kHz. The presented traces were additionally filtered to decrease electronic noise, using Clampfit 8.0 software (Axon Instruments, Foster City, USA) with the lowpass Boxcar filter at smoothing point 7. Offline analysis was performed using PClamp 6.0 software (Axon Instruments, Foster City, USA).

Glycine betaine efflux

Glycine betaine efflux was performed as described (13) with some modifications. Cells were grown overnight to late log phase in high osmolality medium (1050mOsmol/kg) and washed 3 times in their original volume with an equimosmolar buffer (50mM KPi, 500mM KCl, pH 6.5). The cells were then resuspended to a protein concentration of ~10mg/ml and stored on ice. For uptake of glycine betaine, the cells were diluted 10-fold in 50mM KPi, pH 6.5, 500mM KCl, supplemented with 10mM glucose and 1.88mM of [^{14}C]-glycine betaine. After 40 minutes of uptake at 30°C, aliquots of the cells were subjected to no dilution or 3, 5, 10, 20, 50 and 100-fold dilution into 50mM KPi, pH 6.5. This resulted in final osmolalities of 1050, 420, 295, 200, 155, 125 and 115mOsmol/kg, respectively. Samples were taken in five-fold, to determine the steady state internal glycine betaine concentrations prior to the osmotic downshift (final internal glycine betaine content) and at different time intervals (at 1 [in duplicate], 5, 10 and 30 minutes) after each of the downshifts. At least three independent uptake and downshift experiments were performed on three independent cultures of *L. lactis* IL1403 and JIM7049∆MscL. The steady state levels of internalized glycine betaine after uptake were ~900nmol/mg protein for both strains. Release is plotted as a percentage of retained glycine betaine.

Analysis of cell viability

Survival of *E. coli* MJF465, carrying pB10bmscL^{LI}6H, pET324yncB10H or empty plasmid controls, under osmotic downshift conditions, was analyzed as described (12). Because *E. coli* MJF465 is not able to use arabinose as an energy source and glucose represses the expression of the arabinose inducible-system, the IPTG-inducible construct pET324yncB10H was used

here. The cysteine mutants were screened for survival with, and without, MTSET as described (33). For survival under osmotic downshift conditions of *L. lactis* IL1403 or JIM7049ΔMscL, cells were grown overnight in chemically defined medium (27), supplemented with 25mM glucose and 5µg/ml erythromycin (where applicable) and diluted 1:100 to the same medium supplemented with 365mM KCl (1050mOsmol/kg). Cells were allowed to grow to OD_{600} of ~0.8 and then diluted 100-fold into 50mM KPi, pH 6.5 plus 500mM KCl (1050mOsmol/kg) or into 50mM KPi, pH 6.5 (final osmolality of 115mOsmol/kg). Prior to plating onto agar containing media, the cells were diluted serially with sterile equimosmolar buffers, all prewarmed to 30°C. To determine cell viability, 20µl samples were spotted onto equimosmolar CDM agar plates, and incubated for 36h at 30°C before the number of colony forming units (CFU) was determined.

Metabolic activity after osmotic downshift

Because *L. lactis* grows in chains, the number of CFU is not necessarily a quantitive indicator of the survival of cells after downshift. Therefore, metabolic activity based on the production of acid by *L. lactis* during fermentation of glucose was also determined. The method was adapted from (34). In brief: cells were cultured, washed and osmotically-stressed as described above for the glycine betaine efflux assay, but with 5mM KPi, pH 6.5 plus 65mM KCl (105mOsmol/kg) instead of 50mM KPi buffer (105mOsmol/kg) to reduce the buffering capacity. Acidification rates per mg total protein in the presence of 10mM glucose were determined for all samples and compared with the acidification rates of the unshocked sample (100% value).

Miscellaneous

Protein biochemistry. Purified proteins were analyzed on 15% acrylamide SDS-PAGE (35). Protein concentration was determined by Amido-black 10B staining as described (36). MscL was also identified and analysed for potential modifications or proteolysis products by MALDI-TOF mass spectrometry as described (37). The $MscL^-$ phenotype of *L. lactis* JIM7049ΔMscL was checked by preparation of cell membranes, and subsequent SDS-PAGE analysis. The presence or absence of $MscL^{LI}$ was determined by immuno-detection using specific rabbit serum with polyclonal antibodies raised against $MscL^{LI}$ (at a titer of 1:30,000) and the Western-light chemiluminescence detection kit (Tropix Inc., Bedford, MA.).

Determination of osmolality. Osmolalities of media and buffers were measured by freezing point depression with an Osmostat 030 (Gonotec, Berlin).

Results

Cloning, Expression and Purification

Cloning and expression of $mscL^{LI}$ and $yncB^{LI}$ was achieved both in *E. coli* (not shown) and *L. lactis* (Fig. 2A). For amplification of $MscL^{LI}$ and $MscS^{LI}$ in *L. lactis* the nisin-inducible expression system was used (38). In *E. coli* the *lacUV5* promoter system was used for amplification of $MscL^{LI}$ and the

arabinose-inducible system for amplification of MscS (24). MscL^{LI}-6H and MscS^{LI}-10H were purified by Ni-NTA chromatography. Based on the yield of purified protein, both channels were found to be amplified in *L. lactis* to levels between 5 and 10% and in *E. coli* between 2 and 5% of total membrane protein.

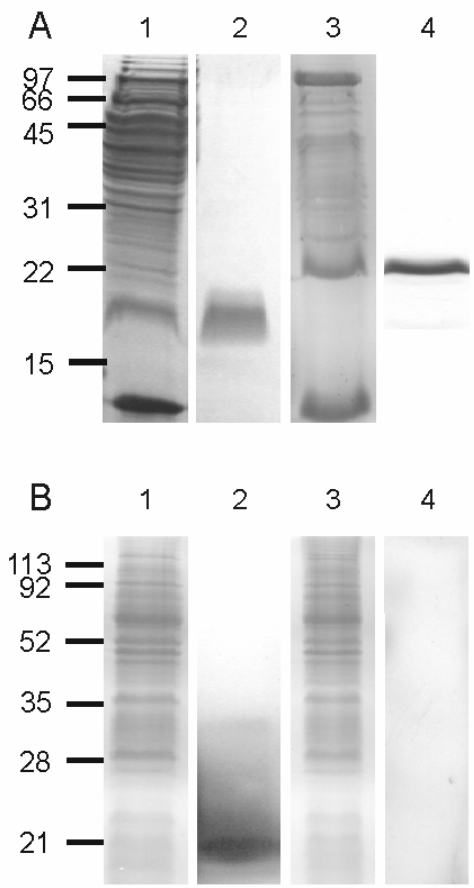

Figure 2: Overexpression, purification and immunodetection of MscL^{LI} and MscS^{LI}. (A) Coomassie brilliant blue-stained gel; lane 1: JIM7049, pNZ8020mscL^{LI}6H membrane vesicles, lane 2 purified MscL^{LI}, lane 3: JIM7049, pNZ8048yncB10H membrane vesicles, and lane 4: purified MscS^{LI}. SDS-PAGE analysis of purified MscL^{LI} showed. a remarkably broad band, which could not be refined by boiling of the samples prior to SDS-PAGE analysis. Mass-spectrometry analysis showed the MscL^{LI} band in the gel contained only full length MscL^{LI}. (B) lane 1: coomassie brilliant blue-stained gel of IL1403 membranes, lane 2: immunoblot of IL1403 membranes, using MscL^{LI}-specific antibodies, lane 3: coomassie brilliant blue-stained gel of JIM7049ΔMscL^{LI} membranes, and lane 4: immunoblot of JIM7049ΔMscL^{LI} membranes, using MscL^{LI} specific antibodies.

As can be seen in Fig. 2A and B, MscL^{LI} protein amplified in and purified from *L. lactis* NZ9000 migrated over a wide range in SDS-PAGE and gave rise to a 'fuzzy' appearance. To establish the nature of the differently migrating species, various fractions from the gel were analyzed by MALDI-TOF mass spectrometry. Four distinct slices of the gel were digested with CNBr and trypsin and the resulting peptide fragments were identified. The

fragments of the protein, after cleavage, accounted for 70% of the total protein (data not shown) including both the N and C termini, indicating that the heterogeneity observed on the gel was not due to proteolytic degradation of the amplified protein. We suggest that the broad and fuzzy band reflects incomplete unfolding of the protein in the presence of SDS, or a very strong association between individual subunits, which is only dissociated during SDS-PAGE analysis.

In vivo complementation of *E. coli MJF465* (MscL$^-$ / MscS$^-$)

For initial characterization of MscL^{LI} and MscS^{LI}, the corresponding genes were expressed in *E. coli* MJF465 (MscL$^-$/MscS$^-$), using plasmids pB10bmscL^{LI}6H and pET324yncB10H. This allowed a comparison of the ability of the *L. lactis* and *E. coli* channels to rescue the osmotic-fragile phenotype of *E. coli* MJF465 (12). Clearly both MscL^{LI} and MscS^{LI} were able to rescue MJF465 in osmotic downshift experiments (Table 4), albeit not as well as the endogenous *E. coli* channels.

Table 4: Survival of *E. coli*

Strain	Plasmid	Stress	Survival % (s.e.m.)	
MJF465	pB10b / pET324	osmotic downshift	0.6	(0.3)
MJF465	pB10bmscL^{Ec}6H	osmotic downshift	90.0	(4.5)
MJF465	pB10bmscL^{LI}6H	osmotic downshift	35.3	(3.2)
MJF465	p*yggb*2	osmotic downshift	78.0	(4.0)*
MJF465	pET324yncB10H	osmotic downshift	27.1	(1.9)
PB104	pB10bmscL^{LI}6H	–	100.0	(def)
PB104	pB10bmscL^{LI}6H	MTSET	100.0	(2.8)
PB104	pB10bmscL^{LI}6H G20C	MTSET	0.1	(0.1)
PB104	pB10bmscL^{LI}6H V21C	MTSET	1.0	(3.0)
PB104	pB10bmscL^{LI}6H I22C	MTSET	100.0	(1.7)
PB104	pB10bmscL^{LI}6H I23C	MTSET	100.0	(2.2)

* after (12)

Survival upon osmotic downshift of *E. coli* MJF465 (MscL$^-$ / MscS$^-$) carrying plasmids for MscL^{Ec} (pB10bmscL^{Ec}6H), MscL^{LI} (pB10bmscL^{LI}6H), MscS^{Ec} (p*yggb*2), MscS^{LI} (pET324yncB10H) or empty plasmid controls (pB10B, pET324). Survival upon modification with MTSET (1mM, final concentration) of *E. coli* PB104 (MscL$^-$) carrying pB10bmscL^{LI}6H or one of the derived cysteine mutants pB10bmscL^{LI}6H G20C, pB10bmscL^{LI}6H V21C, pB10bmscL^{LI}6H I22C or pB10bmscL^{LI}6H I23C. 100% survival was set for unchallenged cells. For all values, n≥3.

It has been demonstrated that MscL^{Ec} can be activated by MTSET modification of a cysteine introduced at position 22 (33, 39, 40). The equivalent residue, G20, in MscL^{LI} and its flanking residues (V21, I22 and I23; boxed region in Fig. 1) were replaced by cysteines and the phenotype of the

mutants, upon labeling with MTSET, was determined (Table 4). The cysteine positions that showed a clear GOF phenotype as a result of increased channel activity after reaction with MTSET under iso-osmotic conditions, G20C and V21C (equivalent to positions G22C and V23C in $MscL^{Ec}$), were further characterized in patch clamp experiments.

Electrophysiological characterisation

$MscS^{LI}$ in E. coli. Channel activity of an excised patch from *E. coli* MJF465 expressing $MscS^{LI}$10H (from pBADyncB10H) is shown in Fig. 3A. The slope of the current-voltage relationship in Fig. 4A indicates that $MscS^{LI}$ allows a conductance of 0.87 ±0.07nS. The fact that the data in Fig. 4A could be fit to a straight line reveals that the channel shows no rectification between −50mV and 50mV. Open dwell-times of one to several hundreds of ms were observed and the channel appeared to desensitize when pressure was maintained for longer periods of time (n=5). Overall, the channel characteristics of $MscS^{LI}$ are analogous to those previously described for MscS from *E. coli* (12).

$MscL^{LI}$ in E. coli. Channel activity of an excised patch from *E. coli* MJF465, expressing $MscL^{LI}$6H (from pB10bmscL6H) is shown in Fig. 3B. The current-voltage relationship for $MscL^{LI}$ (Fig. 4A) shows that $MscL^{LI}$ has a conductance of 2.00 ±0.25nS. Also, $MscL^{LI}$ did not show rectification between −50mV and 50mV. Two short but distinct dwell times were observed in 34 independent recordings (both from lipid fusions and spheroplasts; Fig. 4B). One dwell time could be determined at 3.6 ±0.29ms (mean and s.e.m.), the second was shorter than 1ms and could not be determined more accurately given the experimental parameters. These dwell times are comparable to the dwell times of MscL from *Staphylococcus aureus* and are shorter than the dwell times observed for MscL from *E. coli* (5). The pressure at which $MscL^{LI}$ fully opened for the first time was determined and compared to the pressure at which $MscS^{Ec}$ opened in giant spheroplasts from *E. coli* PB104. The pressure ratio of $MscL^{LI}$ / $MscS^{Ec}$, that is, the pressure at which MscL first opens fully relative to the pressure at which $MscS^{Ec}$ opens in giant spheroplasts of *E. coli* PB104, was 1.81 ±0.09 (n = 20). This means that there might be a small difference in the pressure sensitivity of $MscL^{LI}$ compared to $MscL^{Ec}$, which was found to have a $MscL^{Ec}$ / $MscS^{Ec}$ pressure ratio of 1.64 ±0.08 (41). The open probability of $MscL^{LI}$ was determined by the average current (measured at a given pressure) divided by the current if all channels in the patch were open. The open probability was plotted against the pressure-ratio MscL / $MscS^{Ec}$ and fitted to a Boltzmann distribution (Fig. 4C). Both $MscL^{Ec}$ and $MscL^{LI}$ show initial openings around the same relative pressure. However, further opening of $MscL^{LI}$ required a higher energy input than opening of $MscL^{Ec}$ as reflected by the different slopes of the sigmoidals (42). Finally, $MscL^{LI}$ appeared to have distinct substates at 0.26, 0.53 and 0.75 of full conductance (Fig. 4D), which compares to 0.22, 0.45, 0.70 and 0.93 of full opening for $MscL^{Ec}$ (43).

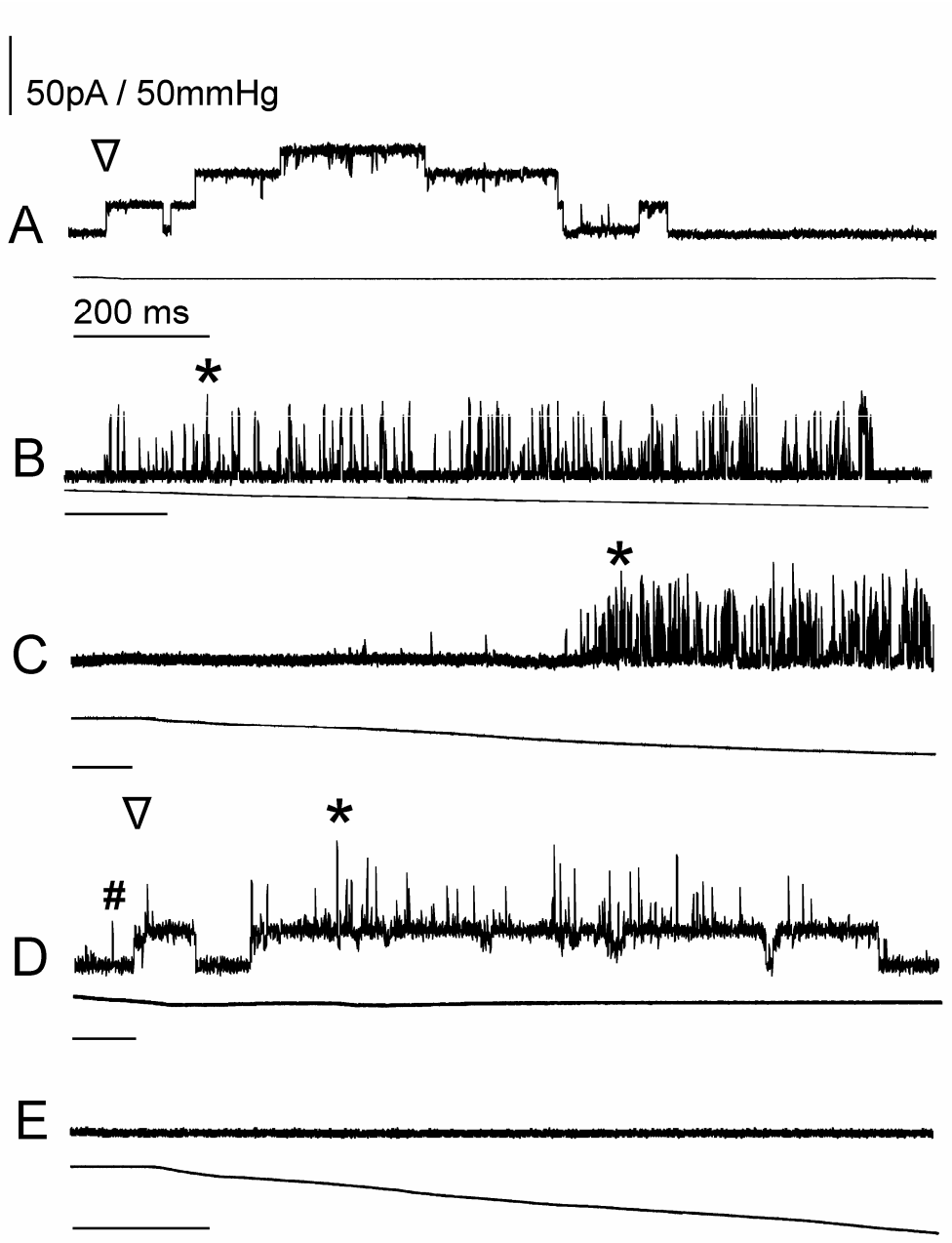

Figure 3: Typical electrophysiological recordings at 20mV (pipette) of patches excised from: (A) MJF465 spheroplasts expressing pBADyncB10H; (B) MJF465, pB10bmscL^{LI}6H spheroplasts; (C) IL1403 membranes fused with liposomes; (D) JIM7049, pNZ8048yncB10H membranes fused with liposomes; and (E) JIM7049ΔMscL^{LI} membranes fused with liposomes. Top traces show current (bar corresponds to 50pA for all traces), bottom traces show applied suction pressure (bar corresponds to 150mmHg for all traces). Horizontal bars below traces indicate 2s for each trace. All traces start at 0mmHg pressure and 0pA current and were filtered in Clampfit 8.0 software (Axon Instruments, Foster City, USA) with the lowpass Boxcar filter at smoothing point 7. ∇, first openings of MscS^{LI}, *, first full openings of MscL^{LI} #, partial opening MscL^{LI}.

MscS^{LI} and MscL^{LI} in L. lactis. Channel activity in a patch excised from a hybrid proteo-GUV, prepared from *L. lactis* IL1403, is shown in Fig. 3C. MscL^{LI}, but no MscS^{LI} activity was observed in 30 independent patches. MscS^{LI} activity was however observed in patches excised from hybrid proteo-GUVs from *L. lactis* JIM7049, over-expressing MscS^{LI} (from pNZ8048yncB10H) as shown in Fig. 3D, indicating that the *yncB* gene product can be functional, but is possibly not expressed in wild-type *L. lactis*. The observation that MscS^{LI} is apparently not functional in wild-type *L. lactis* is underscored by the observation that no MS channel activity whatsoever was observed in patches of JIM7049ΔMscL membranes fused with liposomes (n=10 with cells grown under low salt conditions; n=11 with cells grown under high salt conditions, Fig. 3E). Even if the native *L. lactis* JIM7049ΔMscL membrane to liposome ratio was increased 10-fold from 2:25 to 20:25 w/w (n=5, data not shown) MS channel activity was not observed. Recordings of channel activity of patches excised from proteoGUVs from *L. lactis* JIM7049 pNZ8048yncB10H, membranes expressing MscS^{LI} were used to determine the pressure ratio for full openings of MscL^{LI} relative to MscS^{LI}. This value was 1.48 ±0.05 (n=14), but substate channel activity of MscL^{LI} could be observed before the first opening of MscS^{LI} (e.g. # in Fig. 3D).

Cysteine mutants of MscL^{LI} in E. coli. The cysteine mutants that had a GOF phenotype in response to MTSET labeling were analyzed with respect to the pressure ratio MscL^{LI} / MscS^{Ec}, using *E. coli* PB104 expressing the channel from pB10bmscL^{LI}6H (G20C) or pB10bmscL^{LI}6H (V21C). Both G20C and G21C had a high pressure ratio of 2.6 ±0.3 (n=8) and 3.7 ±0.2 (n=4), respectively, in the absence of MTSET, but their activity became pressure independent upon addition of MTSET (data not shown).

Expression of *mscL*, *yncB* and *OpuAA*

As electrophysiological characterization of *L. lactis* IL1403 and JIM7049ΔMscL membranes, fused with liposomes, showed no MscS^{LI} activity (Fig 3C), it seemed possible that *yncB* was not transcribed in these cells. RT-PCR was performed on RNA extracted from *L. lactis* IL1403 cells grown in CDM or CDM plus 0.5M NaCl and the resulting amplified DNA fragments were analyzed on gel (Fig. 5). After 15 PCR cycles, it is clearly visible that the transcription of o*puAA* (the first gene of the *opuA* operon) was increased in the cells grown at high salt (compare lane A3 with B3 in Fig. 5A), which is in agreement with a higher glycine betaine uptake capacity under these conditions (13). RT-PCR DNA corresponding to *mscL* and *yncB* fragments were visible after 22 PCR cycles. Both *mscL* and *yncB* are transcribed in wild-type *L. lactis* IL1403 cells, albeit to a low level compared to the *opuAA* gene of the *opuA* operon; the expression of the *mscL* and *yncB* was not significantly influenced by the osmolality of the medium (compare lane A1 with B1 and A2 with B2 in Fig. 5B). The negative controls showed that the extracted RNA was not contaminated with significant amounts of DNA as no product was obtained when reverse transcriptase was omitted from the reaction mixture (Fig. 5B; lanes A^{-} and B^{-}); the lanes marked C1, C2 and C3

correspond to PCR products of *mscL*^{LI}, *yncB* and *OpuAA*, respectively, using chromosomal DNA as template.

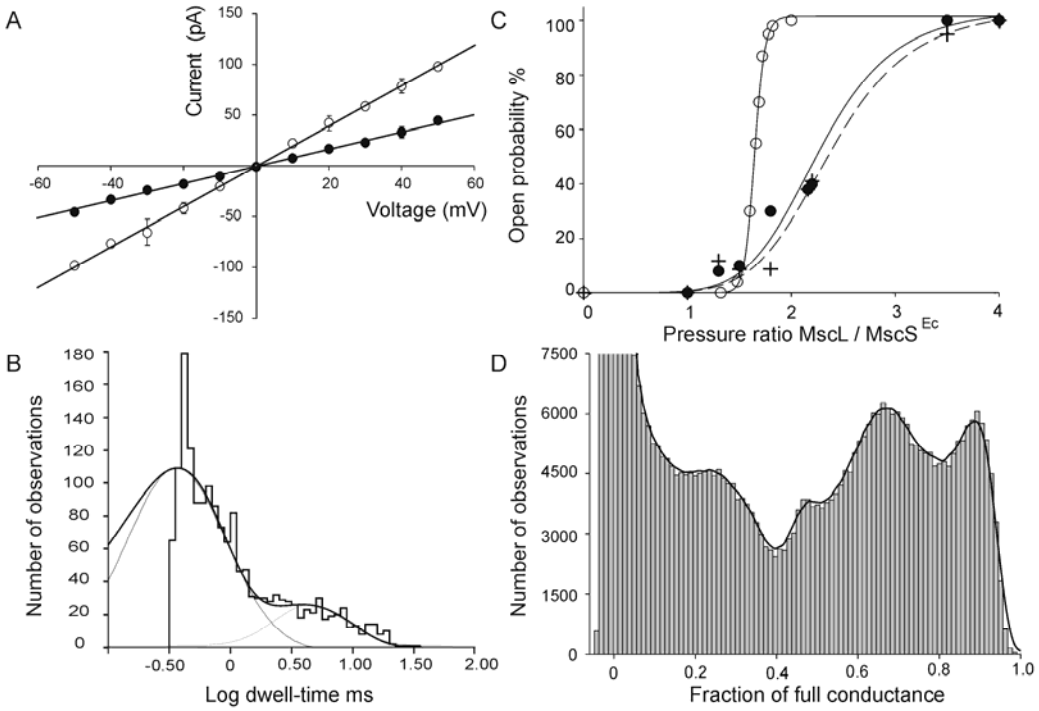

Figure 4: Characteristics of MscL^{LI} and MscS^{LI} (A) Current-Voltage relationship for MscL^{LI} (○) and MscS^{LI} (●), each based on three independent excised spheroplast patches. (B) Dwell time analysis of a single MscL^{LI} trace obtained at -20mV with a two-component fit; fitted dwell times for this recording were 0.35 and 3.94ms. (C) Open probability at -20mV of MscL^{LI} as a function of applied pressure: solid line; **●,** based on mean current measurements, dashed line; **+** based on Popen analysis in Pstat software (,Axon Instruments, Foster City, USA) and solid line; ○**:** open probability of MscL^{Ec} (based on data from 28). In all cases the open probabilities relative to the pressure required to open MscS^{Ec} are shown. Data for MscL^{LI} was collected from 3 independent spheroplast patches with 1 – 3 channels per patch, in which MscL^{LI} activity was saturated. (D) Relative conductive substates of MscL^{LI} (compared to full opening) at -20mV determined by using an all-points histogram based on data from 5 independent patches. Data were normalized and the number of events per conductance substate was determined, from which the most frequently visited and therefore most stable substates were obtained.

Physiological characterization of JIM7049ΔMscL

Plasmid pOri280ΔMscL^{LI} is not replicated in *L. lactis* JIM7049 unless it integrates into the chromosome, which preferentially takes place at the homologous position of the chromosomal *mscL* gene. By selecting for clones that grew in the presence of erythromycin, a disruption strain of *mscL* was obtained. MscL^{LI} could not be detected by Western blot analysis in membranes of these cells, using antibodies raised against MscL^{LI} (Fig. 2B).

To determine the role of MscL^{LI} under conditions of hypo-osmotic stress, *L. lactis* IL1403 and JIM7049ΔMscL^{LI} cells were grown on CDM supplemented with 365mM KCl. After washing in 50mM KPi plus 500mM KCl, pH 7.0, the cells were incubated with [^{14}C]-glycine betaine for 40 minutes to allow internalization of the compatible solute and thereby compensate for the high external osmolality. A steady state level of uptake was attained, corresponding to an internal concentration of about 900nmol glycine betaine / mg total protein. The cells were then diluted into various hypotonic media and the fate of the internal glycine betaine content was determined. In Fig. 6A the internal concentrations are expressed as a percentage of the internal glycine betaine before osmotic downshift. The *L. lactis* IL1403 cells released ~80% of their glycine betaine when diluted 5-fold or more. The release of glycine betaine from *L. lactis* JIM7049ΔMscL was significantly lower; around 40% of the glycine betaine was retained by the cells. Taken as a whole, the data suggest that at least a fraction of the internalized glycine betaine is released via MscL^{LI}.

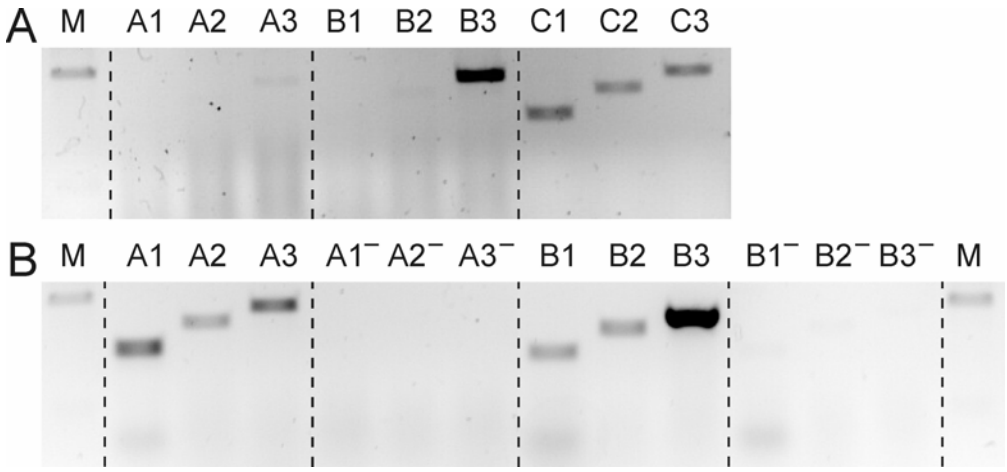

Figure 5: Analysis of RT-PCR products after (A) 15 cycles and (B) 22 cycles of amplification. Lanes A and B show RT-PCR products from RNA extracted from cells grown on CDM and CDM plus 0.5M NaCl, respectively, and lane C shows products from PCR on chromosomal DNA (positive control). Lanes A$^-$ and B$^-$ correspond to experiments with RNA samples not treated with AMV reverse transcriptase. For each condition (A, A$^-$, B, B$^-$ and C), lane 1 represents the presence or absence of a fragment from *mscL^{LI}*; lane 2 represents the presence or absence of a fragment from *yncB* and lane 3 represents the presence or absence of a fragment from *opuAA*. Lanes marked with M show the 500 base-pair band of the lambda marker.

Next, cell survival was examined using protocols developed for *E. coli*. Under osmotic downshift conditions, 98 ±6% (n=3) of wild-type CFU survived and 80 ±5% (n=3) of the disruption strain. Because *L. lactis* grows in chains of mostly 2 or 4 cells, this could mean that in reality between 33 and 55% of the cells survive; to obtain a CFU from a chain of cocci it is sufficient if only a single cell is viable, see also Discussion section.

To obtain a quantitative measure of the consequences of an osmotic downshift on the metabolic activity of *L. lactis* IL1403 and JIM7049ΔMscL, the capacity to ferment glucose was determined before and after osmotic downshift. Cells were grown in high salt medium and pre-loaded with glycine betaine and subjected to osmotic downshifts as described above. For *L. lactis* IL1403, only the metabolic activity after 100-fold dilution was determined, as even under this extreme downshift condition 100% of glucose metabolism was retained. In contrast, the rate of acidification of the buffer around *L. lactis* JIM7049ΔMscL decreased with the fold dilution (Fig. 6B). The decrease in metabolic activity is quantitatively similar to the release of glycine betaine from JIM7049ΔMscL, suggesting that the release of glycine betaine in the disruption mutant might be caused by loss of cell integrity rather than efflux through the $MscL^{LI}$ channel.

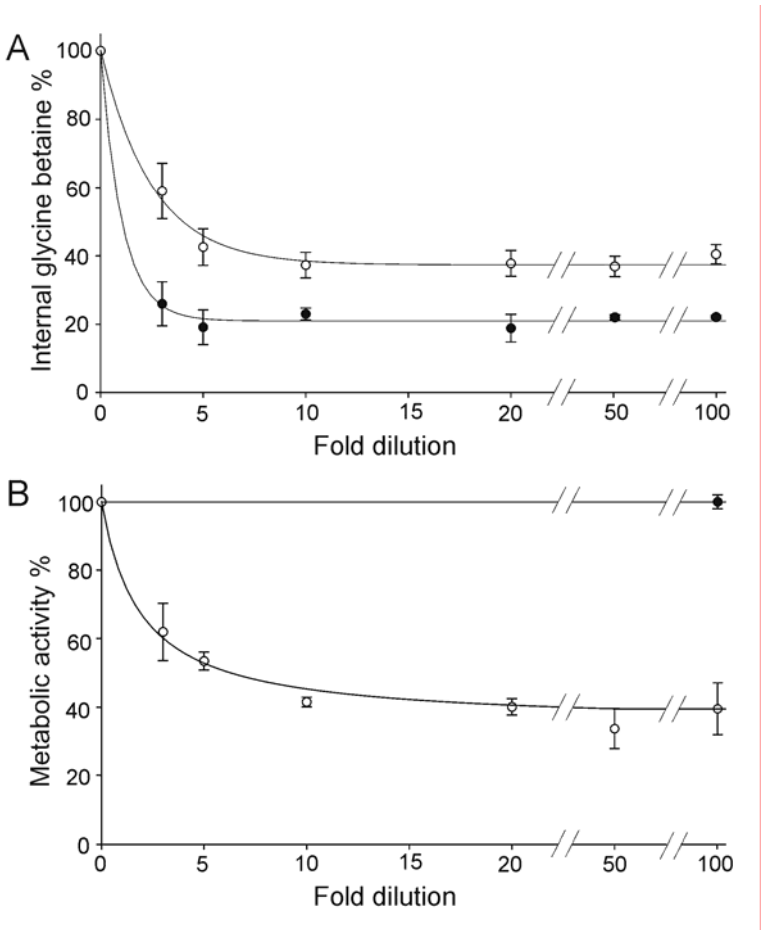

Figure 6: Glycine betaine efflux and metabolic activity of *L. lactis* IL1403 and JIM7049ΔMscL upon osmotic downshift. (A) Release of [^{14}C]-glycine betaine from IL1403 (●) and JIM7049ΔMscL (○) cells; 100% values correspond to ~900nmol/mg of total protein. (B) Glucose fermentation activity of *L. lactis* IL1403 (●) and JIM7049ΔMscL (○). Undiluted and 3, 5, 10, 20, 50 and 100-fold dilutions resulted in final osmolalities of 1050, 420, 295, 200, 155, 125 and 115mOsmol/kg, respectively. Values at "0-fold" dilution correspond to the values of the undiluted samples and were set to 100%. Metabolic activity at 100% corresponds to a pH change of 0.41 per hour per mg of total protein.

Discussion

MS channels of *L. lactis*

MscL and MscS from *L. lactis* form functional mechanosensitive channels when expressed in *E. coli* or *L. lactis*. Both channels provided *E. coli* MJF465 ($MscS^-$ / $MscL^-$) with protection against osmotic downshift as demonstrated in plate assays, and both channels were functional in patch-clamp experiments using membrane patches from *E. coli* spheroplasts, membrane patches from hybrid proteo-GUVs prepared from *L. lactis* membrane vesicles or membrane patches from proteo-GUVs prepared from purified and membrane-reconstituted protein. Importantly, in wild-type *L. lactis* only $MscL^{LI}$ seems to be functional, and this MS channel appears critical for survival of the organism under conditions of hypo-osmotic stress.

The unitary conductances of $MscS^{LI}$ and $MscL^{LI}$ were 0.87nS and 2.0nS, respectively, which are within the range previously reported for MscS and MscL from other organisms (8, 9, 39). Open dwell times for $MscL^{LI}$6H were short compared to $MscL^{Ec}$ and most other MscL homologues studied to date, giving rise to a ”flickery” appearance in channel recordings. The activation thresholds of both *L. lactis* channels were comparable to those of the *E. coli* homologues as were the channel substates observed for $MscL^{LI}$ (43). We also showed that $MscL^{LI}$ could be activated by modifying cysteine residues with MTSET (G20C or V21C) at the constriction site of the pore, demonstrating that MscL from *L. lactis* functions very much like MscL from *E. coli*.

Survival and metabolic activity after osmotic downshift

Cell survival of *E. coli* MJF465 after osmotic downshift conditions was determined after heterologous expression of $MscS^{LI}$ and $MscL^{LI}$. The experiments showed that both channels were able to partially rescue the $MscL^-$ / $MscS^-$ phenotype of the MJF465 strain. It can therefore be concluded that, in *E. coli,* both proteins form functional MS channels. In *L. lactis* it was harder to determine the effect of an osmotic downshift on cell survival because the cells grow in chains. The number of CFU of the disruption strain JIM7049ΔMscL decreased by 20% when the cells were subjected to an osmotic downshift. If a binomial distribution of cell death in a chain of 4 cells is assumed then the distribution of live and dead cells would be $L^4 + 4L^3D + 6L^2D^2 + 4LD^3 + D^4$ (where L stand for the fraction of live and D for the fraction of dead cells). As D^4, *i.e.*, all cells in one chain are dead, is the only case that gives rise to a decrease in the number of CFU, the fraction of dead cells can be calculated as the fourth root of the fractional decrease in CFU. In this case the fraction of dead cells is $(0.20)^{1/4} = 0.67$, implying that only 33% of the cells survived the osmotic downshift. Assuming a chain length of two cells and a normal distribution, the survival would be 55%. With the most cells growing in chains of 2 and 4, the observed decrease in cell viability of 20% thus corresponds to an actual decrease in viability of 45-67%

The glucose fermentation capacity of *L. lactis* JIM7049ΔMscL decreased by 60% after osmotic downshift. Since the IL1403 wild-type strain (which normally expressed $MscL^{LI}$) was not affected by the osmotic downshift,

a fraction of the JIM7049ΔMscL may have lysed, as a consequence of the inability to rapidly release osmolytes upon osmotic downshift. Strikingly, the decrease in glucose fermentation capacity of 60% compares well to the actual decrease in cell viability of 45-67%.

MscS activity is not detectable in wild-type *L. lactis*

Based on the following observations *L. lactis* IL1403 does not seem to possess detectable levels of functional MscS, even though the *yncB* gene is transcribed. Firstly, $MscS^{LI}$ activity was not observed in patches excised from hybrid proteo-GUVs of IL1403, which displayed MscL activity. Secondly, $MscS^{LI}$ activity was not observed in patches excised from hybrid proteo-GUVs of JIM7049ΔMscL, which lacked any MS activity even when prepared from cells grown under different osmotic conditions. Finally, efflux of glycine betaine upon osmotic downshift was significantly decreased in JIM7049ΔMscL. The residual 60% of efflux can be explained by cell lysis, as could be inferred from the decrease in CFU in the drop plate assay and the decrease in metabolic activity upon osmotic downshift. In contrast to *L. lactis*, an *E. coli* knockout strain released the same amount of glycine betaine as the wild-type *E. coli* upon osmotic downshift (44), suggesting that in *E. coli* another MS channel compensates for the absence of MscL or that in the wild-type strain MscL is not activated under the conditions used.

However, when *yncB* was expressed in *E. coli* MJF465 (using pBADyncB10H) or in *L. lactis* JIM7049 (using pNZ8048yncB10H) MS channel activity was observed. RT-PCR showed that the *yncB* gene is transcribed to levels comparable to *mscL* but much lower than *opuAA*. Moreover, and contrary to the *opuA* genes, the expression of *mscL* and *yncB* genes in *L. lactis* IL1403 does not seem to be influenced by the osmolality of the medium. In *E. coli* the expression of *mscL* and *mscS* is growth phase dependent and the transcription level of both genes increases when the osmolality of the medium increases (45). In analogy with MscS from *E. coli* one could argue that MscS from *L. lactis* is post-translationally inactivated; for instance, the open probability of MscS from *E. coli* is decreased by lowering of the pH and long exposures to membrane tension (12). Evidence for inactivation by prolonged exposure to membrane tension of $MscS^{LI}$ can be observed in Fig. 3A (*yncB* expressed in *E. coli*), and it is possible that MscS in *L. lactis* IL1403 is kept in an inactive state, for which we have not been able to find the activation trigger. In contrast to wild-type *L. lactis*, overexpression of *yncB* in *L. lactis* yielded channel activity, suggesting that, when excess MscS channel is produced, a population of the molecules escapes the inhibition mechanism.

What are the consequences of inactive MscS for *L. lactis*? It is possible that MscS is less critical for *L. lactis* than for *E. coli*. Substate activity of $MscL^{LI}$ can be observed at pressures at which $MscS^{LI}$ is not yet observed. The presence of substates, together with the short dwell times of $MscL^{LI}$, may be sufficient for *L. lactis* to fine-regulate the internal osmolyte concentration without requiring a MscS-like activity.

In conclusion: MscS and MscL of *L. lactis* are genuine mechanosensitive channel proteins with properties similar to those described

for MscS and MscL from *E. coli*. We show, however, that $MscL^{LI}$ is the primary, if not the only, mechanosensitive channel used by *L. lactis* under the conditions studied, through which a major portion of compatible solutes such as glycine betaine is released upon osmotic downshift.

Acknowledgements

We would like to thank MSC^{plus} for financial support, the Netherlands Organization for Scientific Research (NWO) for a travel grant (R88-247), Armağan Koçer (BioMaDe Technology Foundation) and the Neurobiophysics group of the University of Groningen for technical support with the electrophysiology experiments, and Sytse Henstra for assistance with the RT-PCR experiments. PB and PCM are supported by Grants GM61028 and DK60818 from the National Institutes of Health, Grant I-1420 of the Welch Foundation, and Grant F49620-01-1-0503 of the Air Force Office of Scientific Review. Strain MJF465 was kindly supplied by Prof. I.R.Booth, University of Aberdeen, UK.

Reference List

1. Hamill,O.P. and Martinac,B. (2001) *Physiol Rev.* **81,** 685-740
2. Wood,J.M., Bremer,E., Csonka,L.N., Kraemer,R., Poolman,B., van der,H.T., and Smith,L.T. (2001) *Comp. Biochem. Physiol. A Mol. Integr. Physiol.* **130,** 437-60.
3. Morbach,S. and Kramer,R. (2002) *Chembiochem.* **3,** 384-97
4. Poolman,B., Blount,P., Folgering,J.H.A., Friesen,R.H., Moe,P.C., and van der Heide,T. (2002) *Mol. Microbiol.* **44,** 889-902
5. Moe,P.C., Blount,P., and Kung,C. (1998) *Mol. Microbiol.* **28,** 583-92.
6. Maurer,J.A., Elmore,D.E., Lester,H.A., and Dougherty,D.A. (2000) *J. Biol. Chem.* **275,** 22238-44
7. Sukharev, S. I., Blount, P., Martinac, B., Blattner, F. R., and Kung, C. (1994) *Nature* **368,** 265-8
8. Sukharev,S.I., Martinac,B., Arshavsky,V.Y., and Kung,C. (1993) *Biophys. J.* **65,** 177-83
9. Ruffert, S., Berrier, C., Kramer, R., and Ghazi, A. (1999) *J. Bacteriol.* **181,** 1673-6
10. Chang,G., Spencer,R.H., Lee,A.T., Barclay,M.T., and Rees,D.C. (1998) *Science* **282,** 2220-6
11. Bass,R.B., Strop,P., Barclay,M., and Rees,D.C. (2002) *Science* **298,** 1582-7
12. Levina,N., Totemeyer,S., Stokes,N.R., Louis,P., Jones,M.A., and Booth,I.R. (1999) *EMBO J.* **18,** 1730-7
13. van der Heide,T. and Poolman,B. (2000) *J. Bacteriol.* **182,** 203-6
14. van der Heide,T., Stuart,M.C., and Poolman,B. (2001) *EMBO J.* **20,** 7022-32.
15. Poolman,B., Spitzer,J.J., and Wood,J.M. (2004) *Biochim. Biophys. Acta* **1666,** 88-104
16. Ou,X., Blount,P., Hoffman,R.J., and Kung,C. (1998) *Proc. Natl. Acad. Sci. USA* **95,** 11471-5
17. Yanisch-Perron,C., Vieira,J., and Messing,J. (1985) *Gene* **33,** 103-9
18. Chopin,A., Chopin,M.C., Moillo-Batt,A., and Langella,P. (1984) *Plasmid* **11,** 260-3
19. Gasson,M.J. (1983) *J. Bacteriol.* **154,** 1-9
20. de Ruyter,P.G., Kuipers,O.P., and de Vos,W.M. (1996) *Appl. Environ. Microbiol.* **62,** 3662-7
21. Drouault,S., Corthier,G., Ehrlich,S.D., and Renault,P. (2000) *Appl. Environ. Microbiol.* **66,** 588-98
22. Leenhouts,K., Buist,G., Bolhuis,A., ten Berge,A., Kiel,J., Mierau,I., Dabrowska,M., Venema,G., and Kok,J. (1996) *Mol. Gen. Genet.* **253,** 217-24
23. Alting-Mees,M.A. and Short,J.M. (1989) *Nucleic Acids Res.* **17,** 9494
24. Guzman,L.M., Belin,D., Carson,M.J., and Beckwith,J. (1995) *J. Bacteriol.* **177,** 4121-30

25. van der Does,C., den Blaauwen,T., de Wit,J.G., Manting,E.H., Groot,N.A., Fekkes,P., and Driessen,A.J. (1996) *Mol. Microbiol.* **22,** 619-29
26. Kuipers,O.P., de Ruyter,P.G.G.A., Kleerebezem,M., and de Vos,W.M. (1998) *Journal Of Biotechnology* **64,** 15-21
27. Poolman,B. and Konings,W.N. (1988) *J. Bacteriol.* **170,** 700-7.
28. Blount,P., Sukharev,S.I., Schroeder,M.J., Nagle,S.K., and Kung,C. (1996) *Proc. Natl. Acad. Sci. USA* **93,** 11652-7
29. Hamoen,L.W., Smits,W.K., de,J.A., Holsappel,S., and Kuipers,O.P. (2002) *Nucleic Acids Res.* **30,** 5517-28
30. Blount,P., Sukharev,S.I., Moe,P.C., Martinac,B., and Kung,C. (1999) *Methods Enzymol.* **294,** 458-82
31. Folgering,J.H.A., Kuiper,J.M., de Vries,A.H., Engberts,J.B.F.N., and Poolman,B. (2004) *Langmuir* **20,** 6985-7
32. Knol,J., Sjollema,K., and Poolman,B. (1998) *Biochemistry* **37,** 16410-5
33. Batiza,A.F., Kuo,M.M., Yoshimura,K., and Kung,C. (2002) *Proc. Natl. Acad. Sci. USA* **99,** 5643-8
34. Pearce,L.E. (1969) *N. Z. J. Dairy Sci. Technol.* **4,** 246-7
35. Laemmli,U.K. (1970) *Nature* **227,** 680-5
36. Schaffner,W. and Weissmann,C. (1973) *Anal. Biochem.* **56,** 502-14
37. van Montfort,B.A., Doeven,M.K., Canas,B., Veenhoff,L.M., Poolman,B., and Robillard,G.T. (2002) *Biochim. Biophys. Acta* **1555,** 111-5
38. Kunji,E.R., Slotboom,D.J., and Poolman,B. (2003) *Biochim. Biophys. Acta* **1610,** 97-108
39. Yoshimura,K., Batiza,A., and Kung,C. (2001) *Biophys. J.* **80,** 2198-206
40. Bartlett,J.L., Levin,G., and Blount,P. (2004) *Proc. Natl. Acad. Sci. U. S. A* **101,** 10161-5
41. Yoshimura,K., Batiza,A., Schroeder,M., Blount,P., and Kung,C. (1999) *Biophys. J.* **77,** 1960-72
42. Sukharev,S.I., Sigurdson,W.J., Kung,C., and Sachs,F. (1999) *J. Gen. Physiol.* **113,** 525-40
43. Chiang,C.S., Anishkin,A., and Sukharev,S. (2004) *Biophys. J.* **86,** 2846-61.
44. Ajouz, B., Berrier, C., Garrigues, A., Besnard, M., and Ghazi, A. (1998) *J. Biol. Chem.* **273,** 26670-4
45. Stokes,N.R., Murray,H.D., Subramaniam,C., Gourse,R.L., Louis,P., Bartlett,W., Miller,S., and Booth,I.R. (2003) *Proc. Natl. Acad. Sci. USA* **100,** 15959-64

Membrane proteins reconstituted in Giant Unilamellar Vesicles for electrophysiology and mobility studies

Joost H.A. Folgering[#], Mark K. Doeven[#], Nicoletta Kahya, Victor Krasnikov, Eric R. Geertsma, Geert van den Bogaart and Bert Poolman

[#] These authors have contributed equally to this chapter; An extended version of this chapter was published: (2005) *Biophys. J.* **88,** 1134-42

Abbreviations: ABC, ATP-binding cassette; AC, alternating current; DDM, *n*-dodecyl-β-D-maltoside; DOPC, 1,2-dioleoyl-*sn*-glycero-3-phosphatidylcholine; DOPE, L-α-dioleoyl phosphatidylethanolamine; DOPG, 1,2-dioleolyl-*sn*-glycerol-3-[phospho-*rac*-(1-glycerol)]; DOPS, 1,2-dioleoyl-*sn*-glycero-3-phosphatidylserine; FCS, Fluorescence Correlation Spectroscopy; GUV, Giant Unilamellar Vesicle; LUV, Large Unilamellar Vesicle; NTA, nitrilotriacetic acid; CSSA, cross sectional surface area

Abstract

Giant Unilamellar Vesicles (GUVs) have been widely used for studies on lipid mobility, membrane dynamics and lipid domain (raft) formation, using single molecule techniques like Fluorescence Correlation Spectroscopy (FCS). Reports on membrane protein dynamics in this type of model membranes are by far less advanced due to the difficulty of incorporating proteins into GUVs in a functional state. Here, a method is described for the formation of membrane protein-containing GUVs in the presence of co-solvents to prevent protein inactivation during the dehydration step of the GUV formation process. A mechanosensitive channel protein (MscL), a membrane-anchored oligopeptide binding protein (OppA) and an ion-linked transporter protein (LacS) were purified to homogeneity and reconstituted into large unilamellar vesicles (LUVs) of ~ 200nm diameter. These LUVs were dried and converted into giant unilamellar vesicles (GUVs) of 5-50μm diameter by rehydration in the presence of a alternating electrical field. The presence of sucrose during the dehydration phase proved to be essential in maintaining activity of LacS and OppA. The proteo-GUVs were successfully applied in patch-clamp measurements to monitor channel activity and in fluorescence correlation spectroscopy experiments to monitor dynamics of the molecules.

Introduction

Biological membranes are complex matrices mainly composed of lipids and proteins that separate the contents of cells or specialized compartments from the external surroundings. Giant Unilamellar Vesicles (GUVs; diameter 5-50μm) have proven to be useful model systems for biological membranes to study lipid dynamics (1), lipid domain (raft) formation (2, 3), elastic properties of membranes (4, 5), and lipid-DNA interactions (6). The dynamics of individual lipid molecules and their interactions can be probed by fluorescence

correlation spectroscopy (FCS) (1, 6), whereas knowledge of the overall structure and phase separation can be obtained by confocal imaging (2-5). Information on the dynamics of proteins in membranes, their partitioning into specific lipid domains, and protein-protein interactions can also be obtained by FCS and confocal microscopy (7)

Membrane proteins with channel activity can be studied in GUVs or membrane patches derived thereof by patch clamp analysis (8, 9). Both FCS and patch clamp measurements offer the advantage that dynamics, complex interactions and function can be studied at the single molecule level rather than the ensemble average, which opens new opportunities for detailed kinetic analysis of the systems.

A limiting factor in these measurements has been the functional incorporation of membrane proteins into GUVs. To overcome this problem, a number of specific techniques have been developed, two of which will be discussed here. Large membrane blisters, suitable for electrophysiological measurements, can be formed by subjecting proteoliposomes (LUVs) to a cycle of dehydration and rehydration, followed by incubation with relatively high concentrations of $MgCl_2$ (9). The addition of $MgCl_2$ collapses the fused multilamellar proteoliposomes and induces the formation of membrane blisters (10). However, the success rate is dependent on the lipid composition and the membrane blisters formed are not suitable for FCS. A previously reported peptide-induced fusion method for proteo-GUV formation (7) has the disadvantage that one is restricted in the choice of lipid composition. Moreover, the technique is relatively laborious and time consuming.

The mechanism of formation and properties of GUVs have been studied since the 1980's (11, 12). GUVs can be prepared by drying lipids dissolved in organic solvent (chloroform or chloroform/methanol mixtures) followed by addition of distilled water. Water penetrates the dried lamellar structures and GUVs are formed spontaneously due to membrane fusion processes. Formation appears to be optimal if a fraction of anionic lipids is incorporated (phosphatidylglycerol or phosphatidylserine) or can be promoted by the addition of divalent cations (Ca^{2+} or Mg^{2+}) when only neutral lipids are used (13). In addition, AC electrical fields have been reported to facilitate, but also to impede the formation process (11, 14).

We have incorporated polytopic membrane proteins into GUVs by (partial) dehydration of LUVs, containing (purified) membrane proteins, followed by rehydration in the presence of an AC electrical field (4). This method was applied to the mechanosensitive channel of large conductance MscL from *Escherichia coli* and *Lactococcus lactis* (15), the lipid-anchored oligopeptide-binding protein OppA from *L. lactis* and the secondary lactose transport protein LacS from *Streptococcus thermophilus*. Advantage was taken of the stabilizing properties of co-solvents on membranes and proteins to prevent the membrane proteins from irreversibly inactivating during the dehydration of the LUVs.

Materials and Methods

Cysteine mutagenesis

Cysteine mutants of MscL from *Escherichia coli* (K55C), OppA from *Lactococcus lactis*, (I602C) and LacS from *Streptococcus thermophilus* (C320A / A635C) were prepared by standard molecular biology techniques. Each protein contains a C-terminal His_6-tag that was used for purification by Ni^{2+}-affinity chromatography.

OppA I602C was made by replacing the 368 basepair *BamHI-XbaI* fragment of plasmid pAMP42 (16) with a synthetic double-stranded oligonucleotide linker (5'-GATCC**TGT**ATTGAGGGTCGTCATCATCACCACCA TCACTGACGCGTCTGCAGT-3' annealed to 5'-CTAGACTGCAGACGCGTC AGTGATGGTGGTGATGATGACGACCCTCAAT**ACA**G-3') containing three extra basepairs coding for cysteine (letters in bold). The linker also contained a *PstI* site (underlined) outside the coding region to facilitate restriction analysis after ligation. Next, the insert of pAMP42 (*oppDFBC*) was replaced with a 1802 basepair *NcoI-BamHI* fragment of pAMP31 (17) containing the *oppA* gene. LacS C320A / A635C was constructed by changing the codon specifying alanine 635 in pSKE8his(C320A) (18) into a cysteine codon, using the Quikchange mutagenesis kit (Stratagene). The plasmid coding for MscL K55C was a gift from L. Dijkink from the BioMaDe Technology Foundation.

Protein production, purification and labeling

OppA was produced in *Lactococcus lactis* NZ9000, using the nisin expression system (19, 20). Production of MscL K55C was done in *Escherichia coli* PB104 (21), using the pB10b expression vector (22). LacS C320A / A635C was produced by *Escherichia coli* HB101, using the pSKE8his expression vector (18). Membrane vesicles were prepared by rupturing the cells with a high-pressure homogenizer (Kindler Maschinen AG, Zürich, Switzerland) and solubilized by 3% octyl-β-glucoside (MscL) or 0.5% DDM (OppA and LacS), and the proteins were purified by nickel affinity chromatography essentially as described previously (15, 23, 24). Solubilization buffers were 50mM KPi, pH 8.0, 200mM KCl, 10% (w/v) glycerol, 10mM imidazole (OppA), 50mM KPi, pH 8.0, 100mM NaCl, 10% (w/v) glycerol, 15mM imidazole (LacS), and 50mM KPi, pH 7.0, 300mM NaCl, 35mM imidazole (MscL).

After 15' centrifugation at 280,000xg, the solubilized material was incubated with Ni^{2+}-NTA resin (1mL resin per 20mg total membrane protein) for 1.5 hours at 4°C while rotating. Subsequently, the resin was drained and washed with 10 column volumes of solubilization buffer containing 0.2% Triton X-100 (MscL) or 0.05% DDM (OppA and LacS). The Ni^{2+}-NTA resins with OppA and LacS were washed with another 10 column volumes of the same buffer with 25mM imidazole. After the initial washing steps, the proteins used for FCS were labeled with a ~ 30 times excess Alexa Fluor 488 C5 maleimide (Molecular Probes) for 2 hours up to overnight at 4°C, while bound to the Ni^{2+}-NTA resin. Labeling was done in solubilization buffer without imidazole supplemented with 0.2% Triton X-100 (MscL) or 0.05% DDM (OppA and LacS). After labeling the column was washed with 20 column volumes of the

same buffer, and the proteins were eluted in the same buffer, pH 7.0, supplemented with 400, 300 or 200mM imidazole for MscL, OppA and LacS, respectively. The fluorophore concentration was estimated from the absorbance at 495nm (extinction coefficient of 72,000$M^{-1}cm^{-1}$). The degree of labeling was then determined using the Alexa Fluor 488 and the protein concentration (see below under "miscellaneous").

Functional reconstitution of membrane proteins into LUVs

Purified proteins were inserted into Triton X-100 destabilized lipsomes as described (23), with some modifications: Firstly, mixtures of dioleoyl 18:1 (Δ9 cis) phospholipids (T_m values of around -18°C), that is, DOPC, DOPE and/or DOPS (Avanti Polar Lipids Inc.) were used, typically at protein-to-lipid ratios of 1 to 1,000-100,000 (mol functional unit per mol lipid). Secondly, reconstitutions were performed in 50mM KPi, pH 7.0, before dehydration of the proteoliposomes, they were transferred to a buffer containing 50mM NH_4HCO_3, pH 8.0. Activity of the proteins was determined by measuring channel activity (MscL; 15), peptide-binding (OppA; 24) and lactose transport (LacS; 23) as described previously.

Formation of proteo-GUVs

LUVs containing Alexa Fluor 488-labeled membrane protein at given protein-to-lipid ratio in 50mM NH_4HCO_3, pH 8.0, were subjected to rapid freezing (liquid nitrogen) and slow thawing (at room temperature in a polystyrene block) in the presence or absence of 5% ethylene-glycol (MscL) or indicated amounts of sucrose (OppA and LacS). Subsequently, 10µL of 20mg/mL lipids were dried overnight under vacuum at 4°C on Indium Tin Oxide (ITO) coated coverslips (custom-coated by GeSim, Dresden, Germany). Ethylene glycol or sucrose was added at given amounts to stabilize the proteins during dehydration. Rehydration was done by addition of 0.5mL of 10mM KPi, pH 7.0, optionally 10mM $MgCl_2$ was also present.

Alternatively, when the proteo-LUVs were prepared from neutral lipids only, or when the sample was prepared for patch clamp, rehydration was performed by electroformation as schematically shown in Fig. 1A. For factors, such as lipid compositions of the membrane and the buffer compositions that influence the rate of GUV formation see ref. 25.

Electroformation was performed in a flow chamber, built from two coverslips coated with indium tin oxide and separated by a 1.75mm thick o-ring with a diameter of 15mm. One of the coverslips contained the dried proteo-LUVs. For rehydration of proteo-LUVs prepared from neutral lipids only, 0.4mL of 10mM KPi, pH 7.0, was added to the chamber. For patch clamp measurements with MscL, the sample had to be rehydrated in a chamber filled with 0.4mL 0.25mM K-Hepes, pH 7.2, 10mM KCl, 2mM $MgCl_2$ plus 320mM sucrose. This buffer is equimosmolar to the medium used for patch clamp, and after formation of proteo-GUVs the concentration of sucrose on the inside and outside of the vesicles is the same. The high internal sucrose concentration prevents collapsing of the proteo-GUVs upon transfer to the high osmolarity medium required for patch clamp.

After the flow chamber was closed, an AC electrical field was applied (10Hz, 1.2V) through electrodes sealed on the glass coverslides; electroformation was done at room temperature. For the formation of proteo-GUVs for patch clamp, the high sucrose concentration hampered the vesicle formation, therefore, and the electrical field had to be applied for at least 3h to obtain a good yield of proteo-GUVs. In all cases GUV formation was monitored by fluorescence or differential interference contrast microscopy as shown in Fig. 1B. The resulting GUVs, 5-50µm in diameter, were used in the activity assays described above and for FCS measurements as described below.

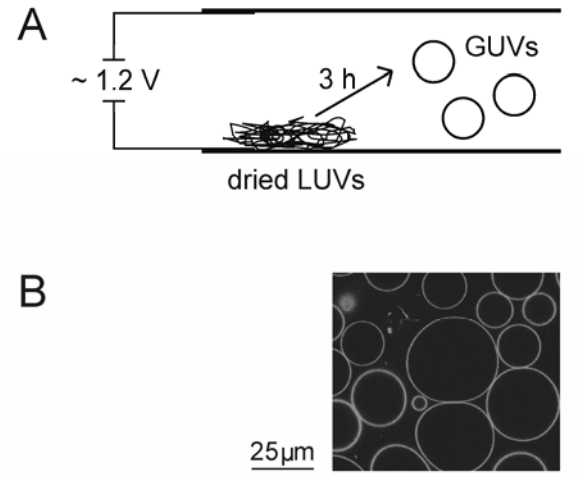

Figure 1: Electroformation and imaging of proteo-GUVs. (A) Schematic representation of the rehydration chamber used for GUV formation. Proteo-LUVs are dried onto an ITO-coated coverslip, which together with a second coated coverslip form the top and bottom of the chamber. An AC field (~ 1.2V, 10Hz) was applied to the chamber via the attached electrodes. After three hours, the GUV electroformation was generally complete (B) Confocal image of GUVs with Alexa Fluor 488-labeled MscL-K55C.

Confocal imaging and FCS measurements

FCS measurements were carried out on a laser scanning confocal microscope (LSCM). The LSCM is based on an inverted microscope Axiovert S 100 TV (Zeiss) in combination with a galvanometer optical scanner (model 6860, Cambridge Technology). The laser beam (488nm, argon ion laser, Innova 99, Coherent) was focused by a Zeiss C-Apochromat infinity-corrected 1.2 NA 63× water immersion objective for excitation of the Alexa Fluor 488 fluorophore. The fluorescence was collected through the same objective, separated by a dichroic beam splitter (61003bs, Chroma Technology) and directed through an emission filter (HQ 535/50, Chroma Technology) and a pinhole (diameter of 30µm) onto an avalanche photodiode (SPCM-AQR-14, EG&G). The fluorescence signal was digitized and autocorrelation curves were calculated on a PC using a multiple τ algorithm. The setup was calibrated by measuring the known diffusion coefficient of Alexa Fluor 488 in water (Molecular probes; D = 300µm^2/s). Autocorrelation curves were fitted

with a one-component two-dimensional diffusion model (26) using Origin software (OriginLab Corporation, Northampton, MA).

Miscellaneous

Mutations were confirmed by restriction analysis and DNA sequencing. MscL concentrations were determined according to the method of Lowry *et al.* (27), using bovine serum albumin as a standard. The concentrations of purified OppA and LacS were determined spectrophotometrically by measuring the absorption at 280nm and using extinction coefficients of 1.605 and 0.926$(mg/mL)^{-1}cm^{-1}$, respectively.

Results

Production, purification and fluorescent labeling of membrane proteins

The model membrane proteins used in this study are the mechanosensitive channel of large conductance MscL from *Escherichia coli*, the oligopeptide-binding protein OppA of the oligopeptide ABC transporter from *Lactococcus lactis*, and the secondary lactose transport protein LacS from *Streptococcus thermophilus*. In order to selectively label the proteins with fluorescent probes for detection by confocal imaging and FCS measurements, single-cysteine mutants were constructed. MscL from *E. coli* has no native cysteines. OppA contains an N-terminal cysteine residue that is lipid-modified and is thus not available for labeling with Alexa Fluor 488 C5 maleimide. The native cysteine of LacS at position 320 is located in the middle of a transmembrane helix and not accessible or unreactive for labeling. Therefore, this cysteine was replaced by an alanine. The position of the newly introduced cysteines was either in an extracellular loop (MscL-K55C), or near the C-terminus of the protein (OppA-I602C and LacS-A635C).

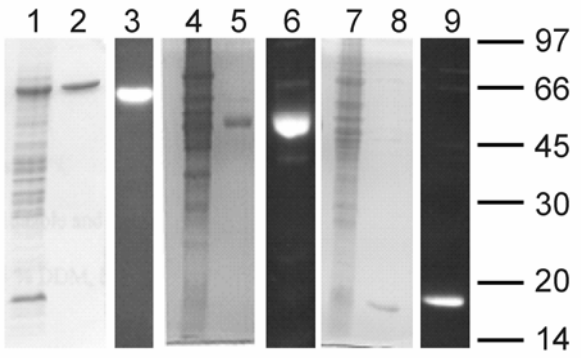

Figure 2: SDS-PAGE analysis of overexpressed, purified and Alexa Fluor 488- labeled membrane proteins. Membrane vesicles containing overexpressed cysteine mutants are shown in lanes 1, 4 and 7. Purified proteins labeled with Alexa Fluor 488 C5 maleimide (Molecular Probes) stained with coomassie brilliant blue (lanes 2, 5, and 8) and visualized with a UV lamp (lanes 3, 6 and 9) are shown. Mutants used were OppA I602C (lanes 1-3), LacS C320A / A635C (lanes 4-6) and MscL K55C (lanes 7-9).

The cysteines were labeled with Alexa Fluor 488 C5 maleimide, after which excess label was removed by washing of the proteins bound to nickel affinity resin. Fig. 2 shows SDS-PAGE analysis of membrane vesicles

containing the overexpressed cysteine mutants, the purified proteins, and the proteins labeled with Alexa Fluor 488. The labeling efficiency was 80-100% for each of the proteins.

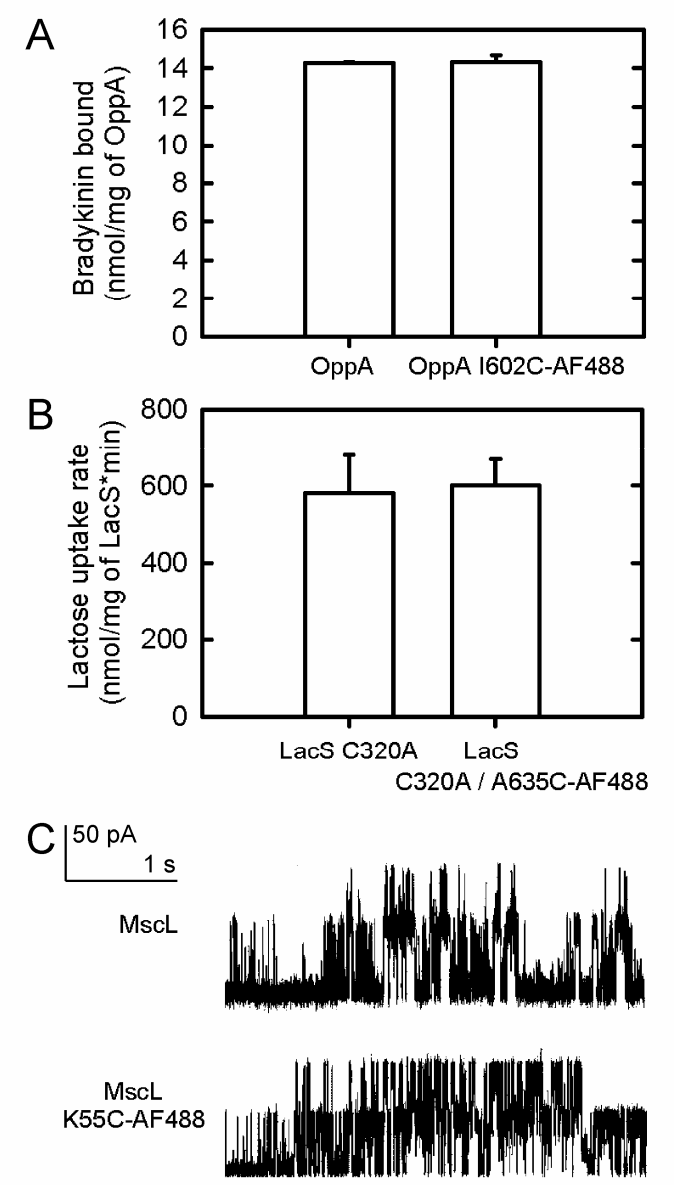

Figure 3: Activity of labeled membrane proteins. (A) Peptide binding by wild-type OppA and Alexa Fluor 488-labeled OppA I602C AF488. The concentration of [3H]-bradykinin was 3µM. (B) Lactose counterflow via LacS C320A and LacS C320A / A635C labeled with Alexa Fluor 488. The internal lactose and external [14C]-lactose concentrations were 10mM and 100µM, respectively. (C) Channel activity of wild-type MscL (upper trace) and MscL K55C labeled with Alexa

Membrane reconstitution and activity measurements

The Alexa Fluor 488 labeled proteins were reconstituted into Triton X-100 destabilized LUVs (23). After reconstitution, the functional integrity of the Alexa Fluor 488-labeled proteins was assessed in LUVs (for OppA and LacS) and in GUVs (for MscL) by the various activity assays (Fig. 3). The obtained

proteo-LUVs were converted to proteo-GUVs as described under ”Materials and Methods”.

To monitor the ion-conducting activity of single MscL molecules after GUV formation, suction through a patch-clamp electrode was used to form a giga-ohm seal between the GUV membrane and the electrode. Excised membrane patches were successfully obtained for the following lipid mixtures: DOPC:DOPE (at 1:1, 3:1, 7:1 and 1:0 mol/mol) and DOPC:DOPS (at 1:1, 3:1, 7:1 and 1:0 mol/mol). Channel currents of unlabeled (top panel) and Alexa 488-labeled K55C (bottom panel) are shown in Fig. 3C. Both traces show single and multiple channel openings.

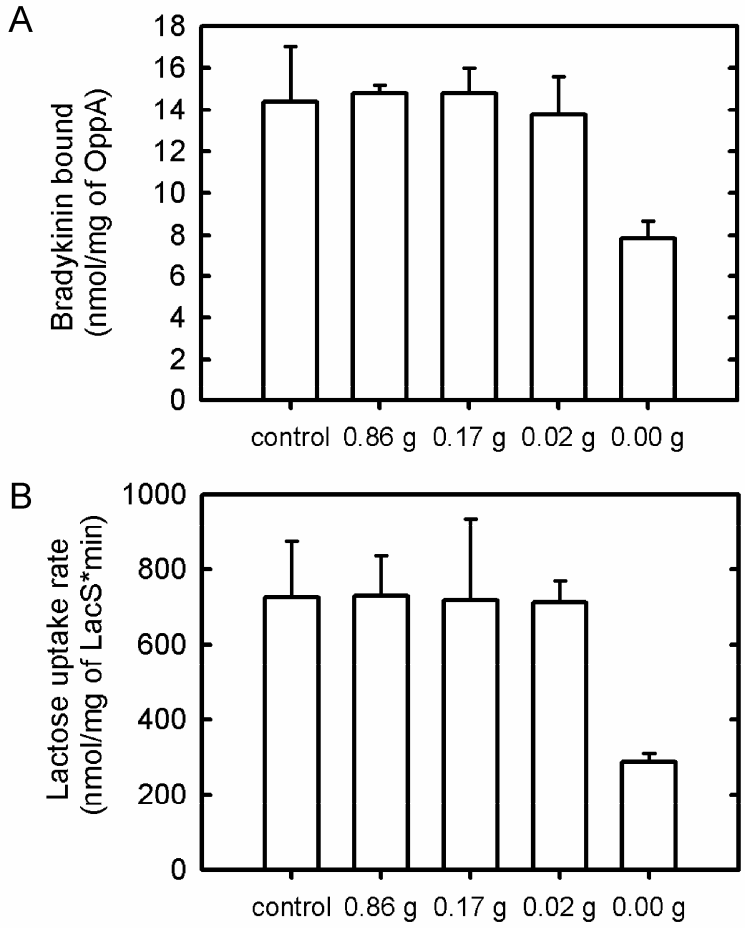

Fluor 488 (lower trace). Patch-clamp measurements were done in 5mM Hepes, pH 7.2, 200mM KCl, 40mM $MgCl_2$, and at +20mV pipette voltage. The unit conductance of a single MscL channel was about 2.5nS as indicated by the 50pA scale bar. Protein to lipid ratio’s were 1:50 (w/w). Proteins were inserted into DOPC:DOPS 3:1 (w/w) lipid mixtures.

Figure 4: Sucrose stabilizes membrane proteins during dehydration. (A) Peptide binding by OppA and (B) lactose counterflow by LacS C320A were measured after dehydration of the membranes in the presence of 0 – 0.86g sucrose / g lipids and rehydration in 10mM KPi, pH 7.0. “Control” samples were not dried and rehydrated. For further details see legend to figure 3.

In a bilayer membrane patch with a diameter of 1µm, there are about 2.6×10^6 lipids, using $0.6nm^2$ for the average area of a lipid molecule (28). At a channel to lipid ratio of 1 to 20,000 mol / mol, an average patch should contain 125 channels per patch. The number of channels observed in the electrophysiological recordings was between 5 and 20 (n=44) and comparable to the number of channels recorded in patches derived from membrane blisters prepared by the conventional method (9). With multiple channels in a patch, it is difficult to observe all the channels, because the seal often breaks before pressures needed for full saturation are reached. The main advantage of using GUVs, compared with the conventional method, relates to a much higher success rate in forming unilamellar membranes suitable for giga-ohm seal formation with a wide range of lipid compositions.

In the absence of sucrose, the activity of OppA and LacS was severly affected upon GUV formation by de- and rehydration (Fig. 4 A and B). Protein activity could be preserved by adding sucrose during drying of OppA- and LacS-containing LUVs, and as little as 20mg sucrose/g of lipid was sufficient for full recovery of activity. Notice that during drying the sucrose concentration increases from 1 to an estimated several hundreds of mM. Overall, it seems that the functional properties of the transport and channel molecules are not affected by the procedure to make the GUVs, provided care is taken to protect the proteins during the drying of the proteoliposomes.

Confocal imaging and lateral mobility of membrane proteins in GUVs

Confocal imaging of the proteo-GUVs confirmed that the proteins were incorporated homogeneously (Fig. 1B and 5A (OppA), B (MscL) and C (LacS)). The mobility of MscL, OppA, and LacS in GUVs was determined by FCS measurements. Confocal images were made of proteo-GUVs containing fluorescent labeled protein, and the focal volume was focused on the pole of the GUVs. Representative autocorrelation curves for each of the three proteins studied are shown in Fig. 5D; the experimental data could be fitted reasonably well with a one-component two-dimensional diffusion model. Occasionally, the membranes appeared to move or fluctuate during the autocorrelation measurements, the fluctuations were observed as a decay or systematic deviation in the count-rate. Autocorrelation curves affected by membrane undulations were not taken into account when analyzing the data. Undulations seemingly appeared more frequently with very large GUVs (> 30µm) and less when smaller GUVs (< 30µm) were used. The measured diffusion coefficients (D) are summarized in Table 1. The mobility of the integral membrane proteins MscL and LacS was ~ 2-3 fold lower than the mobility of the lipid-anchored OppA, with LacS being the slowest.

Table 1: Diffusion coefficients for membrane proteins in GUVs

Protein	Diffusion coefficient[1] ($10^{-8}cm^2/s$)
MscL K55C-AF488	3.9 ± 0.3
OppA I602C-AF488	7.5 ± 0.9
LacS C320A / A635C AF488	3.0 ± 0.3

[1]Diffusion coefficients represent the average of at least five measurements and the SD values are given. FCS setup was calibrated with Alexa Fluor 488.

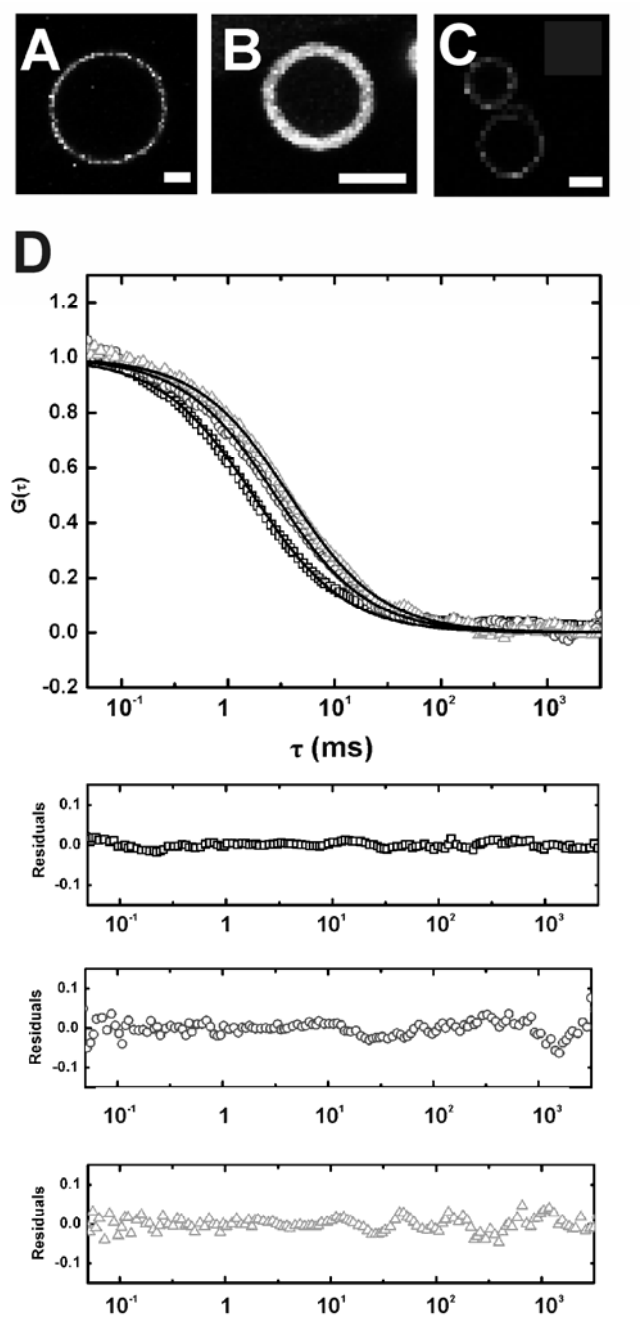

Figure 5: Confocal imaging and diffusion measurements of membrane proteins in GUVs. Confocal images of proteo-GUVs containing functional Alexa Fluor 488-labeled OppA I602C (A), MscL K55C (B), or LacS C320A / A635C (C). Scale bars are 10µm. GUVs were prepared in the presence of 0.02 (A), 0 (B), or 0.17 (C) g sucrose/g lipids. The protein to lipid ratio was 1:500 (w/w) and the lipid composition was DOPC:DOPS 3:1 (w/w). Differences in brightness of the GUVs are caused by the different amounts of labels attached to the proteins. Pentameric MscL, for example, has five labels attached per active unit, whereas OppA and lacS have one and two, respectively. (D) Autocorrelation curves for OppA I602C (□), MscL K55C (○), and LacS C320A / A635C (Δ) in GUVs. Curves were fit with a one-component two-dimensional diffusion model (solid lines), using Origin software (OriginLab Corporation, Northampton, MA); the residuals of the fits are shown in the panels below the figure.

Discussion

A method for direct incorporation of membrane proteins into GUVs without losing protein activity is described. After purification detergent-solubilized integral membrane proteins were inserted into liposomes that were subsequently dried and rehydrated in the absence or presence of an AC electrical field. Functional integrity of the proteins was conserved by drying the proteoliposomes in the presence of ethylene-glycol or sucrose. The distribution, lateral mobility and activity of representative membrane proteins from distinct families were analyzed in GUVs by confocal imaging, FCS, patch-clamp and other biochemical techniques.

Functional reconstitution of MscL, OppA and LacS

Previously, Rigaud and colleagues attempted to circumvent the problem of losing protein activity during drying of proteo-LUVs, by performing partial dehydration under controlled humidity (29). However, of the two proteins studied, the light-driven proton pump bacteriorhodopsin and the Ca^{2+}-ATPase, only the former completely survived the GUV formation process. The Ca^{2+}-ATPase had lost 30% of its biological activity. By adding 20mg sucrose/g of lipid we were able to retain 100% of OppA and LacS biological activity during the GUV formation process. Similar to bacteriorhodopsin (29), MscL proved less susceptible to inactivation by dehydration as no noticeable effect (positive or negative) of the addition of sucrose was observed. As described in more detail in ref. 25, too high a sucrose concentration prevented GUV formation, most likely by inhibition of membrane fusion in the dehydration step.

Saccharides (such as sucrose and trehalose) are known to stabilize the folded state of proteins in solution via a mechanism termed preferential exclusion (30, 31). At high solute concentration the sugar is excluded from the protein surface and the native state is thermodynamically favored over the unfolded state of the protein. The stabilization of soluble proteins during freezing is thought to occur via a similar mechanism. However, stabilization of soluble proteins by disaccharides during air-drying is thought to occur via direct interaction (hydrogen bonding) of the sugar with polar groups of the protein (31).

In addition, disaccharides are known to stabilize membranes during freezing or drying (32-35). When (proteo)liposomes prepared from unsaturated lipids are dried the transition temperature (T_M) increases by 70-80^oC (36). This means that the lipids go from a liquid crystalline to a gel phase and this causes lateral phase separation and may cause protein aggregation. Sucrose prevents this lateral phase separation and presumably protein aggregation by maintaining the membrane in the liquid crystalline phase; the sugars lower the T_M during drying by about 70^oC (36). The sugar molecules do this by replacing the evaporating water by hydrogen-bonding to the lipid headgroups, thereby maintaining the spacing between the headgroups and preventing the membrane from going from the liquid-crystalline to the gel phase. The interactions of sucrose with the proteins and the maintenance of

the liquid-crystalline phase of the membrane are most probably the determining factors for the stabilization of the OppA and LacS proteins.

Confocal imaging and lateral mobility of membrane proteins in GUVs

The distribution and mobility of membrane proteins in the plane of the membrane gives information on the proteins spatial organization and aggregation state. FCS provides such information by monitoring on a microscopic scale the temporal fluctuations in the concentration of a given molecule. The data presented clearly show that the proteins had not aggregated and were distributed homogeneously after sample preparation.

Analysis of our data shows that the diffusion coefficient of the lipid-anchored OppA ($7.5 \pm 0.9 \times 10^{-8}$cm^2/s) is similar to that of the fluorescent lipid analogue 3,3'-dioctadecyloxacarbocyanine perchlorate ($DiOC_{18}$, $7.7 \pm 0.8 \times 10^{-8}$cm^2/s), indicating that OppA does not interact with the membrane other than through its lipid anchor. The integral membrane proteins MscL and LacS diffused ~ 2-3 times slower compared to OppA. The difference in mobility of OppA and the integral membrane proteins is in accordance with the Saffman and Delbrück model for diffusion in biological membranes (37 and equation 1):

Equation 1.
$$D_T = \frac{kT}{4\pi\eta h}\left[\ln\frac{\eta h}{\eta_W A} - \gamma\right]$$

where k is the Boltzmann constant, η and η_W are the viscosity of the membrane and of the surrounding aqueous medium, respectively, h is the membrane thickness, A the cross sectional surface area (CSSA) of the particle and γ is Euler's constant. The mobility of LacS (dimer with a molecular mass of about 140kDa and CSSA of ~ 32nm^2; 38, 39) was ~ 1.3 times that of MscL (pentamer with a molecular mass of about 70kDa and CSSA of ~ 20nm^2 for the "closed" state; 40), which is in agreement with the Saffman and Delbrück model. Notice that due to the logarithmic dependence of the lateral mobility of membrane proteins on the cross-sectional area of the aggregate, diffusion measurements are not sensitive to small differences in molecular mass. (37, 41 and 42).

In conclusion, we developed a generic method to insert membrane proteins into GUVs without losing protein activity. The GUVs are suitable for single-molecule conductance recording as well as fluorescence correlation spectroscopy.

Acknowledgements

We thank L. Dijkink from the BioMaDe Technology Foundation for providing us with the plasmid encoding MscL K55C. This work was supported by funding from the Material Science Center (MSC^{plus}).

Reference List

1. Korlach, J., Schwille, P., Webb, W.W. and Feigenson, G.W. (1999) *Proc. Natl. Acad. Sci.* USA **96,** 8461-66
2. Bagatolli, L.A. and Gratton, E. (2000) *Biophys. J.* **78,** 290-305
3. Kahya, N., Scherfeld, D., Bacia, K., Poolman, B., and Schwille, P. (2003) *J. Biol. Chem.* **278,** 28109-15
4. Angelova, M.I., Soléau, S., Méléard, Ph., Faucon, J.F. and Bothorel, P. (1992) *Progr. Colloid Polym. Sci.* **89,** 127-31
5. Akashi, K., Miyata, H., Itoh, H., and Kinosita, K.Jr. (1996) *Biophys. J.* **71,** 3242-50
6. Angelova, M.I. and Tsoneva, I. (1999) *Chem. Phys. Lip.* **101,** 123-37
7. Kahya, N., Pécheur, E., de Boeij, W.P., Wiersma, D.A. and Hoekstra, D. (2001) *Biophys. J.* **81,** 1464-74
8. Sakmann, B. and Neher, E. (1995) Single-Channel Recording. New York: Plenum 2nd edition
9. Blount, P., Sukharev, S.I., Moe, P.C., Martinac, B. and Kung, C. (1999) *Methods Enzymol.* **294,** 458-82
10. Akashi, K., Miyata, H., Itoh, H. and Kinosita, K.Jr. (1998) *Biophys. J.* **74,** 2973-82
11. Dimitrov, D.S. and Angelova, M.I. (1986) *Stud. Biophys.* **113,** 15-20
12. Mueller P. and Chien, T.F. (1983) *Biophys. J.* **44,** 375-81
13. Akashi, K., Miyata, H., Itoh, H. and Kinosita, K.Jr. (1998) *Biophys. J.* **74,** 2973-82
14. Dimitrov, D.S. and Angelova, M.I. (1987) *Stud. Biophys.* **119,** 61-5
15. Folgering, J.H.A., Kuiper, J.M., de Vries, A.H., Engberts, J.B.F.N. and Poolman, B. (2004) *Langmuir* **20,** 6985-7
16. Doeven, M.K., Abele, R., Tampé, R. and Poolman, B. (2004) *J. Biol. Chem.* **279,** 32301-7
17. Picon, A., Kunji, E.R.S., Lanfermeijer, F.C., Konings, W.N. and Poolman, B. (2000) *J. Bacteriol.* **182,** 1600-8
18. Veenhoff, L.M., Geertsma, E.R., Knol, J. and B. Poolman, B. (2000) *J. Biol. Chem.* **275,** 23834-40
19. Kuipers, O.P., Beerthuyzen, M.M., Siezen, R.J. and de Vos, W.M. (1993) Eur. *J. Biochem.* **216,** 281-91
20. Kunji, E.R.S., Slotboom, D. and Poolman, B. (2003) *Biochim. Biophys. Acta* **1610,** 97-108
21. Blount, P., Sukharev, S.I., Schroeder, M.J., Nagle, S.K. and Kung, C. (1996) *Proc. Natl. Acad. Sci. USA* **93,** 11652-7
22. Sukharev, S.I., Blount, P., Martinac, B., Blattner, F.R. and Kung, C. (1994) *Nature* **368,** 265-8
23. Knol, J., Veenhoff, L., Liang, W.J., Henderson, P.J., Leblanc, G. and Poolman, B. (1996) *J. Biol. Chem.* **271,** 15358-66
24. Detmers, F.J.M., Lanfermeijer, F.C., Abele, R., Jack, R.W., Tampé, R., Konings, W.N. and Poolman, B. (2000) *Proc. Natl. Acad. Sci. USA* **97,** 12487-92

25. Doeven, M.K., Folgering, J.H., Krasnikov, V., Geertsma, E.R., van den Bogaart, G. and Poolman, B. (2005) *Biophys. J.* **88,** 1134-42
26. Schwille, P. (2001) *Cell Biochem. Biophys.* **34,** 383-408
27. Lowry, O.H., Rosebrough, N.J., Farr, A.L. and Randall, R.J. (1951) *J. Biol. Chem.* **165,** 265-75
28. Petrache, H.I., Dodd, S.W. and Brown, M.F. (2000) *Biophys. J.* **79,** 3172-92
29. Girard, P., Pécréaux, J., Lenoir, G., Falson, P., Rigaud, J. and Bassereau, P. (2004) *Biophys. J.* **87,** 419-29
30. Lee, J.C. and Timasheff, S.N. (1981) *J. Biol. Chem.* **256,** 7193-201
31. Arakawa, T. and Timasheff, S.N. (1985) *Biophys. J.* **47,** 411-4
32. Crowe, J., Crowe, L.M., Carpenter, J.F., Rudolph, A.S., Wistrom, C.A., Spargo, B.J. and Anchordoguy, T.J (1988) *Biochim. Biophys. Acta* **947,** 367-84
33. Crowe, L.M., Mouradian, R., Crowe, J., Jackson, S.A. and Womersley, C. (1984) *Biochim. Biophys. Acta* **769,** 141-50
34. Crowe, L.M., Reid, D.S. and Crowe, J.H. (1996) *Biophys. J.* **71,** 2087-93
35. Crowe, J., Hoekstra, F.A., Nguyen, K.H.N. and Crowe, L.M. (1996) *Biochim. Biophys. Acta* **1280,** 187-96
36. Ricker, J.V., Tsvetkova, N.M., Wolkers, W.F., Leidy, C., Tablin, F., Longo, M. and Crowe, J.H. (2003) *Biohys. J.* **84,** 3045-51 (JHC personal communication)
37. Saffman, P.G. and Delbrűck, M. (1975) *Proc. Natl. Acad. Sci. USA* **72,** 3111-13
38. Friesen, R.H.E., Knol, J. and Poolman, B. (2000) *J. Biol. Chem.* **275,** 33527-35
39. Veenhoff, L.M., Heuberger, E.H.M.L. and Poolman, B. (2001) *EMBO J.* **20,** 3056-62
40. Chang, G., Spencer, R.H., Lee, A.T., Barclay, M.T. and Rees, D.C. (1998) *Science* **282,** 2220-6
41. Kucik, D.F., Elson, E.L. and Sheetz, M. (1999) *Biophys. J.* **76,** 314-22
42. Lee, C.C. and Petersen, N.O. (2003) *Biophys. J.* **84,** 1756-64

Lipid-mediated light-activation of a mechanosensitive channel of large conductance

Joost H.A. Folgering, Johanna M. Kuiper, Alex H. de Vries, Jan B.F.N. Engberts and Bert Poolman

A modified version of this chapter was published: (2004) *Langmuir* **20,** 6985-7 and supplementary information (1)

Abstract

This paper describes the reversible activation of a mechanosensitive channel via a light-sensitive lipid mimic. For these experiments the, mechanosensitive channel protein MscL from *L.lactis* or *E.coli* was reconstituted in lipid bilayers composed of 80mol% 1,2-dioleoyl-*sn*-glycero-3-phosphocholine and 20mol% of di-(5-{[4-(4-butylphenyl)azo]-phenoxy}-pentyl)phosphate (4-Azo-5P). Light-induced isomerization of the azobenzene moiety of 4-Azo-5P from *trans* to *cis* was used to activate MscL. Through a second light-induced isomerization of the azobenzene moiety, back to the *trans* conformation, MscL activity was reduced to the initial level.

Introduction

The Mechanosensitive channel of Large conductance (MscL) serves as pressure relief valve that protects bacteria against severe osmotic downshifts. Equivalent systems for mechanosensation are also present in higher organisms. The determination of the crystal structure of MscL from *Mycobacterium tuberculosis* (2) and the large amount of biochemical data for the homologous protein from *Escherichia coli* (3) has made MscL the paradigm in the research on membrane-mediated mechanosensation. MscL opens at membrane tensions close to the lytic limit of the bilayer. Changes in the lateral tension in the membrane, asymmetric bending and membrane thinning are thought to be the main driving forces for channel opening (4-6). Although asymmetric bending can be elicited by applying a pressure across the membrane in patch clamp experiments, changing of the other membrane parameters requires other approaches of which reconstitution of MscL in different lipid mixtures and comparison of the channel properties in separate experiments is the easiest and most accurate. Here, we present the reconstitution of MscL in lipid bilayers with properties that can be altered via light-induced *trans*-*cis* isomerization of a lipid mimic (Fig. 1). The *trans*-to-*cis* and *cis*-to-*trans* isomerisations result in a reversible increase and decrease, respectively, of activity of the channel protein.

To obtain qualitative information on the conformations the 4-Azo-5P molecules adopt inside a bilayer in their *trans* and *cis* forms, and to get an idea of the consequences of *trans*-*cis* isomerisation for the gating threshold of MscL, molecular dynamics simulations were performed. We tested the hypothesis that 4-Azo-5P molecules are more elongated in the *trans* than in the *cis* form. More elongated molecules would presumably be more

compatible with the DOPC bilayer, and this would lead to a larger bilayer thickness and a smaller bilayer area. Because of the larger bilayer thickness, the open probability of MscL would be reduced.

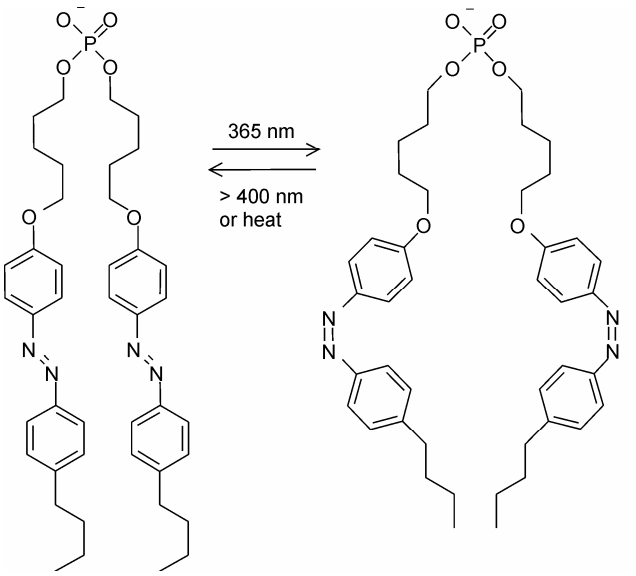

Figure 1: 4-Azo-5P structure in the *trans* (left) and *cis* (right) conformation. Switching between these conformations is elicited by illuminating at 365nm (from *trans* to *cis*) or at > 400nm (from *cis* to *trans*).

Materials and Methods

Formation of proteo-GUVs

The MscL proteins from *E. coli* and *Lactococcus lactis* were modified with a carboxyl-terminal 6-histidine tag and amplified in *E. coli* PB104, using the pB10b expression vector (7). Membranes isolated from the cells were solubilized with Triton X-100 and the proteins were purified by nickel affinity chromatography. Purified protein was reconstituted, at a 1:20,000 channel to lipid molar ratio, into lipid bilayers containing 80mol% of 1,2-dioleoyl-*sn*-glycero-3-phosphatidylcholine (DOPC) plus 20mol% of sodium di-(5-{[4-(4-butylphenyl)azo]-phenoxy}-pentyl)phosphate (4-Azo-5P) (Fig. 1) (8), or 80mol% of DOPC plus 20mol% 1,2-dioleoyl-*sn*-glycero-3-phosphatidylserine (DOPS). As a control liposomes without MscL were prepared. Subsequently, the (proteo)liposomes were dehydrated on glass cover slides coated with indium tin oxide (ITO) and then rehydrated in a flow chamber with 400µl of 0.25mM K-Hepes, pH 7.2, 10mM KCl, 2mM $MgCl_2$ plus 320mM sucrose; the sucrose was used to make the rehydration buffer equimosmolar to the buffer for patch-clamp analysis (5mM Hepes, pH 7.2, 200mM KCl, 40mM $MgCl_2$). The flow chamber was closed with two ITO-coated glass slides, one of which contained the dried proteoliposomes. A voltage of 1.2V at 10Hz was applied for at least 3h through electrodes sealed on the glass plates (For further details see chapter 3 and (9)). The resulting giant unilamellar vesicles (GUVs), 5-50µm in diameter, were used in patch clamp experiments.

Lipid switching in isolated membrane patches

After formation of a giga-ohm seal by suction through a patch clamp electrode, the membrane patch was excised from the respective GUV and analyzed for the presence of channel activity. If channels were observed, the patch was clamped at a negative pressure between –5mmHg and –15mmHg. At that point, the light was switched off except for a Hg lamp (Oriel 180W) to illuminate the sample using a 365nm mercury line filter with a bandwidth of 10nm. This resulted in switching of the azobenzene moiety of 4-Azo-5P from the *trans* to the *cis* conformation (8, 10). Subsequent illumination with the same light source, but using a mercury line filter at 436nm (bandwidth 10nm), shifted the 4-Azo-5P back to the *trans* conformation (10). The illumination and sampling protocols are schematically depicted in (Fig. 2).

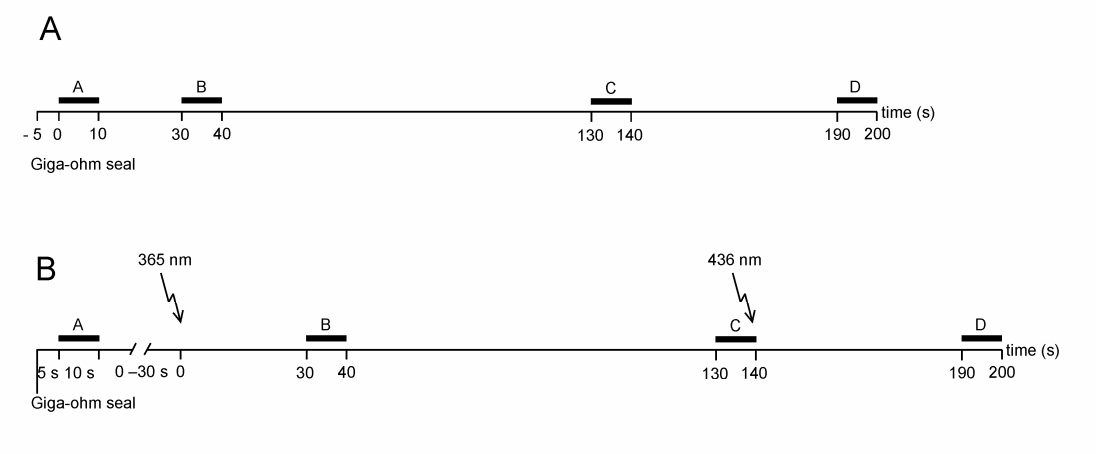

Figure 2: (A) Timeline for patch clamp analysis of a sample without lipid switching; the line represents the recording of channel activity. The bars A to D over the line indicate the time periods analyzed for open probability. (B) Timeline for patch clamp analysis of a sample with lipid switching; the line represents the recording of channel activity. The bars A to D over the line indicate the time periods analyzed for open probability.

Patch clamp recording and analysis

Channel activity was recorded using an Axopatch 200A amplifier together with a digital converter and Axoscope software (Axon Instruments, Foster City, USA). Data were acquired at a sampling rate of 33kHz and filtered at 10kHz. Offline analysis was performed using Pclamp 6.0 software (Axon Instruments). During the experiments the position of the patch in the pipette was followed with a Nikon DXM CCD camera. For each time period (A-D in Fig. 2A and B), 10s of recording was analyzed using Fetchan (Axon Instruments). Opening and closing events were evaluated by using half-maximal conductance ($G_{0.5}$) of a channel as a cut-off criterium (here, $G_{0.5}$ = 1.1nS for the *Lactococcus lactis* MscL and $G_{0.5}$ = 2.0nS for the *Escherichia coli* MscL). The resulting event lists were used to determine the mean open probabilities for each of the 10s time periods, using the Pstat program. Analysis was done on the first ten seconds of each patch (starting within 5s

after giga-ohm seal formation) and, for patches not subjected to 4-Azo-5P switching, the 30-40s, 130-140s and 190-200s were analyzed (A-D in Fig. 2A). For patches subjected to light-induced switching, the periods 30-40s and 130-140s after the start of illumination at 365nm were used; after 140s the patch was illuminated at 436nm for at least 50s before another 10s period of the recording was used for analysis (A-D in Fig. 2B).

The open probabilities in each time period from one patch were compared to the open probability of the first ten seconds of the same patch. The relative values, obtained from separate patches, were then averaged and the standard deviation was calculated. If the relative open probability of a given time period differed more than 4 standard deviations from the mean of the remaining data, the trace was evaluated more extensively. Some time-periods were eliminated from the analysis because of suspect disturbances in the seal (indicated by a baseline shift), which might have resulted in a change in membrane tension. In other cases, a new 10s period of recording around the same time point was analyzed for open probability. In all reevaluated cases, this resulted in an open probability that was within 2 times the standard deviation, indicating that the initially selected dataset was not typical for the patch of interest.

Molecular dynamics simulations

Molecular dynamics simulations were performed on a small patch of a membrane, containing sixteen DOPC and three 4-Azo-5P molecules (16% 4-Azo-5P) in each monolayer of the bilayer (full details of the simulations are given below). Furthermore, 6 Na^+ ions were added to neutralize the charges of the phosphate groups of 4-Azo-5P, and the system also contained 39 water molecules per lipid. The shape of the 4-Azo-5P molecules was quantified by the difference between the largest and the smallest eigenvalues of the tensor of inertia. The tensor of inertia of a molecule is defined as: $I_{\alpha\beta} = \Sigma\, m_i\, (r_{i\alpha} - r_{0\alpha})\, (r_{i\beta} - r_{0\beta})$ in which m_i is the mass of atom i, $r_{i\alpha}$ is a Cartesian coordinate (α, β = {x, y, z}) of atom i, $r_{0\alpha}$ is a Cartesian coordinate of the center of mass of the molecule, and the sum runs over all atoms of the molecule. For a spherical molecule, the eigenvalues of the tensor of inertia are equal, and the difference between the largest and smallest eigenvalue is zero. For non-spherical molecules the difference between the largest and smallest eigenvalues increases with increasing anisotropy (in this case, elongation). The difference between the largest and smallest eigenvalues of the tensor of inertia will be refered to as the anisotropy of the molecule. The values of the anisotropy from simulations of 4-Azo-5P molecules in a DOPC bilayer are given in Table 1, second row.

Simulation details

Simulations were performed using semi-isotropic pressure (P = 1bar) conditions. A twin-range cut-off was used. Interactions between particles within the short-range cut-off of 1.0nm were updated every step. Interactions between particles within the long-range cut-off of 1.4nm were updated every 10 steps. A time-step of 2.5fs was employed. The cut-off for the Lennard-Jones interactions was 1.0nm. The cut-off for the electrostatic interactions,

evaluated using a reaction-field correction (with ε = 54), was 1.4nm. Periodic boundary conditions were employed. For pressure and temperature coupling the Berendsen barostat and thermostat were used, respectively. All simulations were performed with the GROMACS code (11) version 3.0.5.

Table 1: Properties of 4-Azo-5P molecules in their *trans* and *cis* forms while in a bilayer of DOPC, and of the bilayer containing 4-Azo-5P molecules

Property	*trans*	*cis*	difference	t	p
Anisotropy	0.41 (0.02)	0.29 (0.05)	0.12	3.2	0.004
Area of patch (nm^2)	10.9 (0.10)	11.1 (0.10)	-0.2	2.0	0.025
System repeat distance (nm)	8.58 (0.05)	8.44 (0.06)	0.16	2.5	0.007
Compressibility of the area (Nm^{-1})	1.4	1.1			

The average properties for the *trans* and *cis* forms are given, together with their standard deviations (in brackets). Student's t-test, t- and p-values (one-sided), for testing the hypothesis that the anisotropy is larger for the *trans* conformation than for the *cis* conformation, are also given. The averages are calculated for 6 molecules of 4-Azo-5P in each simulation. Similarly, student's t-tests were performed for the differences in the area of the bilayer and the repeat distance. Averages are obtained over 10ns of simulation.

The force fields used for DOPC and water are as described in (12). The sodium ions were modeled using the GROMACS force field. Force field parameters for 4-Azo-5P, entirely compatible with the DOPC force field used, were not available in the literature. Standard parameters from the GROMACS force field were used for the alkyl, phenyl, and phosphate groups. The azo-link was modeled by taking bond lengths, bond angles and Lennard-Jones parameters from aromatic five- and six-ring N-atoms in GROMACS. Charge distributions were chosen to resemble those in similar aromatic systems. All these force-field values are tentative but reasonable. The conformation of the azo-link was ensured by specifying a torsional potential around the N=N bond that strongly favored either the *trans* or *cis* form. Spontaneous switches between these two forms were not observed for any 4-Azo-5P molecule during the simulations. All relevant non-standard force field parameters are given in Table 2.

The systems simulated contained 16 DOPC lipids in each monolayer of the bilayer. The number of 4-Azo-5P molecules in each monolayer was 3 (16%). Six Na^+ ions were added to neutralize the negative charge on the phosphate group of 4-Azo-5P. The number of water molecules was 1482 (corresponding to full hydration, 39 waters per lipid) in all simulations. An initial conformation was prepared by taking a snapshot from a pure DOPC bilayer simulation. From this, all water molecules, and 20% of DOPC molecules were removed. 4-Azo-5P molecules in the *cis* form were inserted by attempting to place conformations from a 4-Azo-5P molecule *in vacuo* in the box. Eight 4-Azo-5P molecules were placed in the box. The system was hydrated and 8 Na^+ ions were added by replacing 8 water molecules after energy minimization and a short equilibration run. During the subsequent MD run, 7 of the 8 4-Azo-5P molecules inserted spontaneously into the DOPC

bilayer in the first 15ns. Two 4-Azo-5P molecules were removed to obtain a bilayer in which the number of DOPC and 4-Azo-5P molecules was the same in each monolayer. After a further 10ns of equilibration, a production run of 10ns was performed. Starting configurations, containing the *trans* form of 4-Azo-5P, were prepared from a configuration of the *cis* form by changing the appropriate torsional potential around the N=N bond. A short (10ps) MD run with a small time-step (0.5fs) sufficed to switch all *cis* molecules to the *trans* form. Subsequent production runs with *trans* 4-Azo-5P molecules were then performed.

Table 2: Non-standard force field parameters for the Azo-link region in 4-Azo-5P

Bonds			
CBN-NAZ	b_0 = 0.133nm	k = $4.184e^{+05}$kJmol^{-1}nm^2	
NAZ-NAZ	b_0 = 0.120nm	k = $4.184e^{+05}$kJmol^{-1}nm^2	
Angles:			
CR6-CBN-NAZ	θ_0 = 120degrees	k = 418.4kJmol^{-1}rad^{-2}	
CBN-NAZ-NAZ	θ_0 = 120degrees	k = 418.4kJmol^{-1}rad^{-2}	
Torsions:			
CBN-NAZ-NAZ-CBN	*cis*: θ max = 180 degrees	k = 50kJmol^{-1}	multiplicity: 1
CBN-NAZ-NAZ-CBN	*trans*: θ max = 0degrees	k = 50kJmol^{-1}	multiplicity: 1
Charges:			
CBN	+0.20	NAZ: -0.20	

CBN: aromatic carbon bound to Azo N; NAZ: Azo nitrogen; CR6: aromatic carbon in 6-ring

Results

Fig. 3 shows a continuous trace of *L. lactis* MscL in DOPC:4-Azo-5P (4:1 mol/mol) before and after *trans* to *cis* and subsequent *cis* to *trans* switching of 4-Azo-5P. A large increase in channel activity was observed when 4-Azo-5P was switched from *trans* to *cis* (light of 365nm); the channel activity decreased when the patch was subsequently illuminated at 436nm. It is also clear from this figure that the response to illumination at 365nm is slower than the response to illumination at 436nm. Upon illumination at 436nm the channel activity did not fully return to the initial value. Details of switch-induced changes in channel activity are shown in Fig. 4. At constant pipette pressure, illumination at 365nm resulted in 4-Azo-5P lipid switching from the *trans* to the *cis* conformation and, when channels were present in the patch, also an increase in channel openings upon switching was observed (Fig. 4A, B). Subsequent illumination with the same light source, but using a mercury line filter at 436nm shifting the 4-Azo-5P back to the *trans*

conformation, resulted in a decrease in channel activity as shown in Fig. 4C. The channel activities shown in Fig. 4 correspond to several substates (ca. 0.8nS and 1.5nS) and full openings at ca. 2.2nS, which are typical for MscL from *L.* lactis (13).

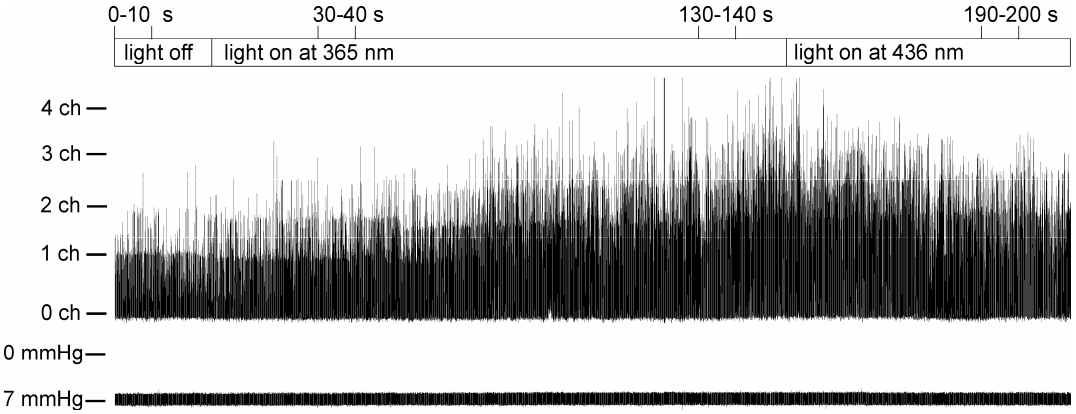

Figure 3: A continuous trace of MscL activity in a patch composed of DOPC:4Azo5P (4:1 mol%) with the light off and light on at 365 and 436nm. The patch contains MscL from *L. lactis*. Top bar indicates time scale; the marked periods were used for analysis. No illumination and illumination at 365nm and 436nm are indicated inside the timebar. The number of channels and pressures are marked on the left of the figure.

After 90s of illumination at 365nm, 73% of the 4-Azo-5P lipid is in the *cis* conformation (10) and the channel activity was increased about 4 times (n=13), (Fig. 5). At the applied pressures (generally around –10mmHg), it was not possible to activate all channels in the patch with the light-dependent switch of the lipids. The whole cycle of lipid switching and channel activation relaxation in a single patch could be repeated at least five times. After 50s of illumination at 436nm, when 89% of the *cis*-4-Azo-5P lipid is back in the *trans* position (10), the channel activity (after one cycle of switching) was about 1.3 times higher than at the start of the experiment (Fig. 3, Fig. 4A and C; Fig. 5). This increase may (partly) be due to the small fraction (11%) of 4-Azo-5P still in the *cis* conformation, but more probably, it is caused by migration of the lipid patch inside the pipette (Fig. 6). The observed patch movement was at a rate of about 1µm/min away from the tip of the pipette. Because the pipette is tapered, the movement towards a larger pipette diameter will stretch the membrane. Assuming lipids are not added to the patch, the increase in area per lipid will increase the tension in the membrane and shift the open probability of the channel, and this would explain why channel activity did not return to its initial value upon switching of *cis* 4-Azo-5P back to the *trans* conformation. Alternatively, one could argue that lipids are added from the tip of the pipette to the patch while it is moving. At a given pressure gradient a migrating will become less curved and this will also increase the open probability of the channel. Although movement of the patch inside the pipette has been observed by others (14), in our hands, movement of the patch was

not observed for 80 mol% of DOPC in combination with other lipids (20 mol% DOPE or DOPS) and it was more characteristic of the presence of 4-Azo-5P.

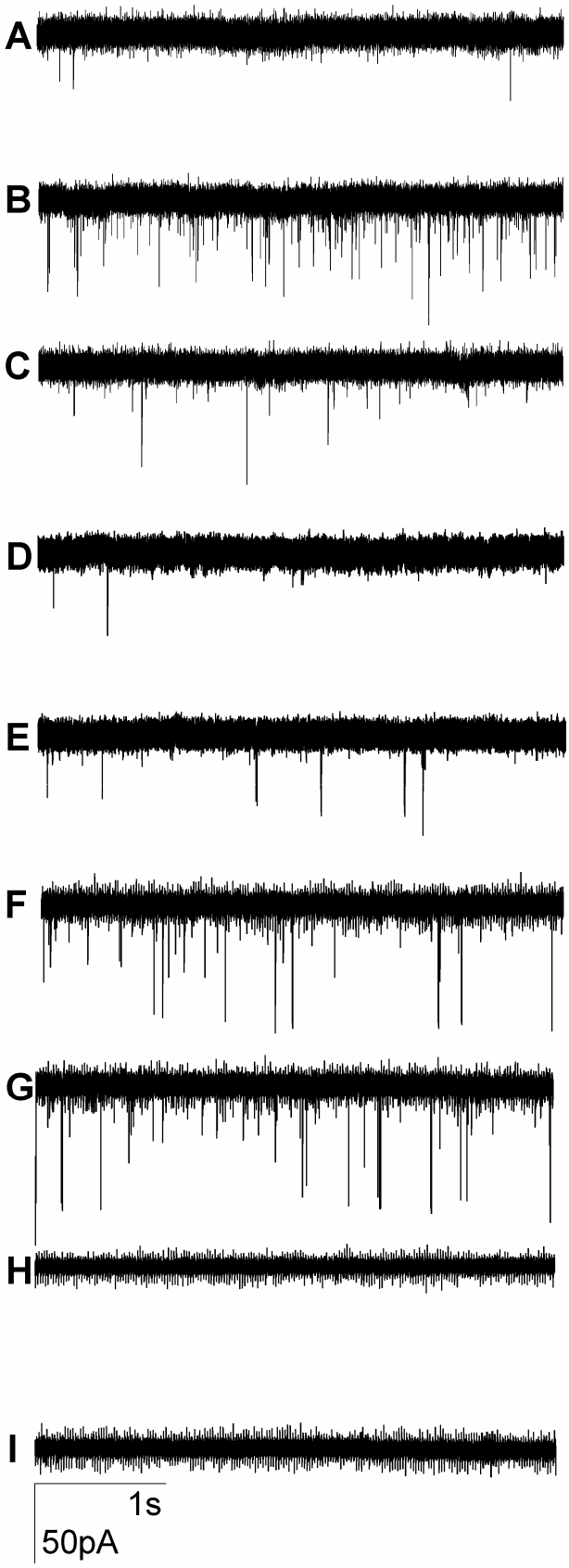

Figure 4: Channel activity of a single patch composed of DOPC: 4-Azo-5P (4:1 mol/mol), containing the *L. lactis* MscL channel. (A) before illumination of the sample (4-Azo-5P in *trans* conformation); (B) after 30s min of illumination at 365nm (4-Azo-5P in *cis* conformation); (C) after subsequent 60s of illumination at 436nm (4-Azo-5P back in *trans* conformation). (D) and (E), channel activity of a patch of DOPC:4-Azo-5P (4:1 mol/mol), containing the *L. lactis* MscL without illumination (D was recorded shortly after seal formation, E after 60s) . (F) and (G), channel activity of a patch of DOPC:DOPS (4:1 mol/mol), containing the *L. lactis* MscL before illumination (as soon as the seal had formed; F) and after 30s of illumination at 365nm (G). (H) and (I), activity of a patch of DOPC:4-Azo-5P (4:1 mol/mol) without channels (H was recorded shortly after seal formation, I after 30s illumination at 365nm). All patches were clamped at –20mV and a pipette pressure of around –10mmHg.

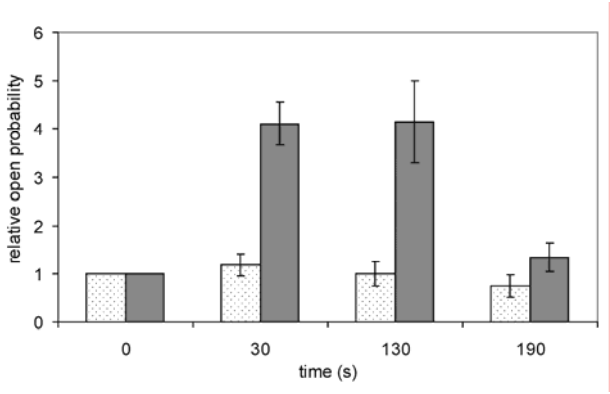

Figure 5: Quantification of the increase in open probability of MscL upon *trans* to *cis* isomerization of 4-Azo-5P. The open probability from 0 - 10s was indexed at 1. The bars indicate the mean relative open probability in patches without switching (dotted bars) and with switching (gray bars); 30 - 40s and 130 - 140s of illumination at 365nm and subsequent 50s illumination at 436nm (190 - 200s). Error bars indicate standard error of the mean.

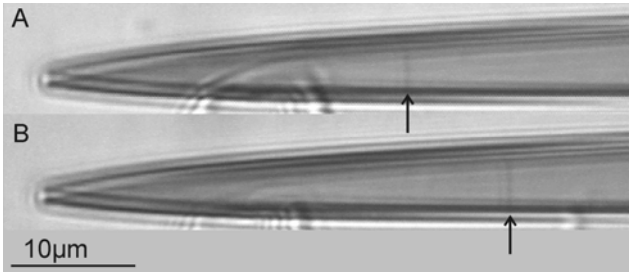

Figure 6: Movement of the lipid patch inside the pipette. (A) the patch immediately after formation of a giga-ohm seal; (B) the same patch 10 minutes later (and after one cycle of switching from *trans* to *cis* and back to *trans*). The arrows indicate the position of the patch inside the pipette.

A control experiment, in which the channel activity was monitored in the dark, with 4-Azo-5P lipids kept in the *trans* conformation for the duration of the experiment (3min), is shown in Fig. 4D, E. In 21 independent experiments without lipid switching, a small increase in channel activity was observed during the first two minutes (Table 3). In a second control experiment, the 4-Azo-5P lipid was replaced by DOPS (Fig. 4F, G). In four independent patches with DOPC and DOPS as membrane lipids, the channel activity did not significantly increase (Table 3). Finally, empty liposomes containing 20mol% of 4-Azo-5P showed no change in electrical signal upon illumination at 365nm (Fig. 4H, I).

Molecular dynamics simulations

Table 1 shows that the shape of the 4-Azo-5P molecules in a DOPC bilayer, as measured by the anisotropy of the tensor of inertia, is significantly different in the *trans* and *cis* forms. In the *trans* form, the 4-Azo-5P molecules are more elongated than in the *cis* form. This should lead to a smaller area of the bilayer and a larger bilayer thickness. The area of the patch and the

bilayer repeat distance were observed to differ significantly for the bilayers containing the *trans* and *cis* forms. It should be noted, however, that the confidence from the student's t-test may be too high, because it is known that the area of bilayers may relax very slowly to their equilibrium values (15). The 10ns of equilibration and 10ns of data collection used here may not have been enough. The shortness of the simulation is the reason for not performing the student's t-test for the compressibility of the area (defined as $K_A = k_B T A_0 / \sigma_A^2$; A_0 is the average area and σ_A is the fluctuation in the area). The error in the compressibility of the area can only be estimated roughly as ~0.5Nm^{-1}, but should improve when performing longer simulations. The compressibility of the area is given in Table 1. It is seen to be smaller for the bilayer with cis 4-Azo-5P than for the bilayer with trans 4-Azo-5P, but the difference may not be significant.

Table 3: Open probabilities of switched and unswitched membrane patches

Time period (s)		Patches with lipid switching		
		Open probability	s.e.m.	n
0-10	(A)	1.00	n.a.	n.a.
30-40	(B)	4.11	0.45	13
130-140	(C)	4.15	0.85	5
190-200	(D)	1.34	0.30	6
		Patches without lipid switching		
		Open probability	s.e.m.	n
0-10	(A)	1.00	n.a.	n.a.
30-40	(B)	1.18	0.23	21
130-140	(C)	1.00	0.25	7
190-200	(D)	0.75	0.23	7
		Patches without switchable lipid		
		Open probability	s.e.m.	n
0-10	(A)	1.00	n.a.	n.a.
30-40	(B)	1.34	0.12	4
130-140	(C)	4.15	0.85	5
190-200	(D)	1.34	0.30	6

Open probabilities of switched (illuminated at 365nm) and unswitched membrane patches (DOPC:4-Azo-5P at 4:1 mol/mol) and of membrane patches without switchable lipid (DOPC:DOPS at 4:1 mol/mol) are presented together with the standard error of the mean (s.e.m.) and the number of time-periods (n) on which the values are based. All open probabilities were indexed to the open probability of the first time-period (A, see also Fig. 2), which was set at 1. All patches had 4-Azo-5P for 100% in the *trans* configuration at t = 0; at 190s and after subsequent illumination at 365 (*trans* to *cis*) and 436 nm (*cis* to *trans*), D in Fig. 2B, a fraction (about 10%) of 4-Azo-5P is still in the *cis* form (8). At t = 30-40 (B) and 130-140s (C), the switched patches had 4-Azo-5P (> 70%) in the *cis* configuration and the unswitched patches had 4-Azo-5P only in the *trans* configuration.

An impression of the consequences of the different shapes of the 4-Azo-5P molecules in their *trans* and *cis* forms for the electron distribution

across the bilayer is given in Fig. 7. The total electron distribution across the system is given (top lines), as well as the contribution from the 4-Azo-5P molecules (bottom lines). The total electron distribution across the system is similar for the systems containing the *trans* (dashed lines) or the *cis* (drawn lines) form of 4-Azo-5P. Thus, it appears that the thickness of the bilayer is not affected significantly by switching between the two forms of 4-Azo-5P. Focusing on the contribution of 4-Azo-5P, however, it can be seen that the electron density distribution of the two forms is different, in accordance with the difference in their shapes. The distribution is wider and more homogeneous for the molecules in the *trans* than for the molecules in the *cis* form. It is likely that this difference influences the lateral pressure profile, but the exact nature of the changes can only be speculated about.

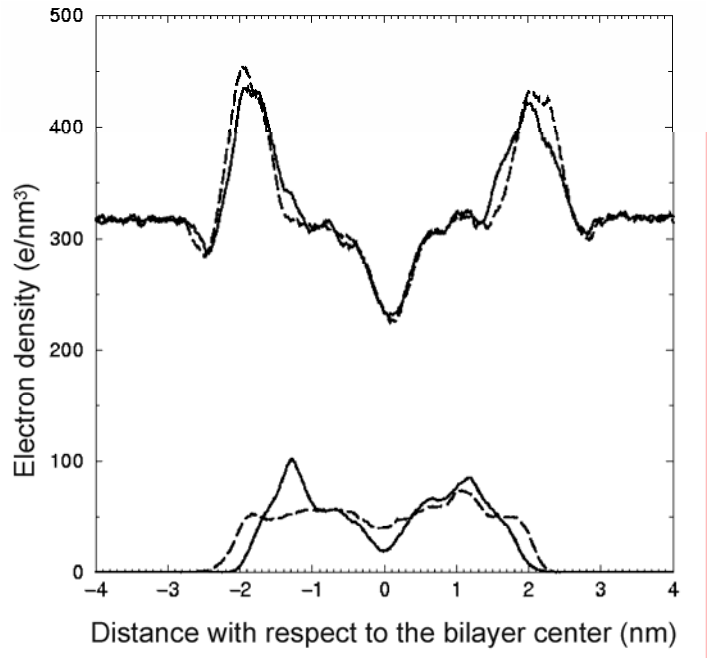

Figure 7: Electron density profiles, obtained from molecular dynamics simulations, across the simulation box for bilayers containing 32 DOPC, 6 Na^+ ions, 1482 water molecules, and 6 4-Azo-5P molecules. The solid lines represent the system with 4-Azo-5P in the *cis* form; the dashed lines represent the system with 4-Azo-5P in the *trans* form. The top two curves represent the total electron density; the bottom two lines the contribution of the 4-Azo-5P molecules only. The profile is not symmetric around the center of the bilayer because of limited statistics.

Discussion

We have shown that we can reversibly activate MscL by switching the 4-Azo-5P fraction (20mol%) of the membrane from the *trans* to the *cis* conformation. During the experiments, the position of the patch in the pipette was followed with a Nikon DXM CCD camera (Fig. 6). With the current camera set-up it was not possible to take pictures of the patch in the *cis* conformation, as this required light of longer wavelengths which caused switching back to the *trans* conformation. The increase in channel activity shown in Figure 4B must be the result from the light-dependent switching of 4-

Azo-5P from the *trans* to the *cis* conformation. Since 4-Azo-5P is present in both leaflets of the patch membrane, it is not likely that activation is caused by a change in curvature strain (or elastic stress) of one leaflet relative to the other as is the case when amphipaths such as 1-Acyl-2-hydroxy-*sn*-glycero-3-phosphocholine (LysoPC) or 4-[butylamino]benzoicacid-2-[dimethylamino]-ethyl-ester (tetracain) are used (4). This means that the channel is activated by a more subtle change in the overall lateral pressure profile or by membrane thinning.

The molecular dynamics simulation showed that the shape of 4-Azo-5P molecules in a DOPC bilayer adopt is different for the *trans* and the *cis* conformations. The mass distribution across the bilayer due to the 4-Azo-5P molecules is wider and more homogeneous for the *trans* conformation than for the *cis* conformation. Such changes probably affect the lateral pressure profile, but are difficult to quantify. More elongated molecules such as *trans* 4-Azo-5P are presumably more compatible with the chain packing in the DOPC bilayer, leading to a larger bilayer thickness and a smaller bilayer area. This could lead to a larger compressibility of the bilayer, that is, it would require more energy to stretch the bilayer to the same extent in the presence of *trans* 4-Azo-5P than in the presence of *cis* 4-Azo-5P. Although the differences in gating threshold of MscL when switching between *trans* and *cis* forms of 4-Azo-5P correlate with the properties calculated from the simulations, the mechanism for MscL opening cannot be elucidated on the basis of these simulations.

Additional DSC studies on vesicles formed from 75mol% 4-(dihexadecylmethyl)-1-methylpyridinium chloride and 25mol% 4-Azo-5P showed that the main phase transition temperature decreased from 28°C to 17°C upon *trans*-*cis* isomerisation (16). Similarly, deuterium NMR experiments on POPC-d_2 bilayers upon incorporation of 20 mol% of 4-Azo-5P indicated that the acyl chain order decreased when the molecule was switched from the *trans* to *cis* form (16), these changes correlate with the molecular dynamics simulation data.

In summary, we have shown that we can reversibly activate MscL from both *L. lactis* and *E. coli* (not shown) by switching the 4-Azo-5P fraction (20mol%) of the membrane from the *trans* to the *cis* conformation. Switching from *trans* to *cis* probably causes a change in the lateral pressure profile, resulting from a change in collisional pressure along the acyl chains of the lipid, and some thinning of the membrane, but elucidation of the mechanism leading to MscL opening requires more extensive molecular dynamics simulations. Importantly, the rapid and reversible alteration of the lipid bilayer via *trans*-*cis* isomerization of lipids allows monitoring of the effect of membrane perturbation on the conformational states of membrane proteins.

Acknowledgements

This work was financially supported by the Material Science Center (MSC^{plus}).

Reference List

1. Http://pubs.acs.org/subscribe/journals/langd5/suppinfo/la048942v/la048942vsi20040623_055807.pdf
2. Chang, G., Spencer, R.H., Lee, A.T., Barclay, M.T. and Rees, D.C. (1998) *Science* **282,** 2220-6
3. Perozo, E. and Rees, D.C. (2003) *Curr. Opin. Struct. Biol.* **13,** 432-42
4. Perozo, E., Kloda, A., Cortes, D.M. and Martinac, B. (2002) *Nat. Struct. Biol.* **9,** 696-703
5. Elmore, D.E. and Dougherty, D.A. (2003) *Biophys. J.* **85,** 1512-24
6. Martinac, B., Adler, J. and Kung, C. (1990) *Nature* **348,** 261-3
7. Sukharev, S.I., Blount, P, Martinac, B., Blattner, F.R. and Kung, C. (1994) *Nature* **368,** 265-8
8. Kuiper, J.M., Hulst, R. and Engberts, J.B.F.N. (2003) *Synthesis* 695-8
9. Doeven, M.K., Folgering, J.H., Krasnikov, V., Geertsma, E.R., van den Bogaart, G. and Poolman, B. (2005) *Biophys. J.* **88,** 1134-42
10. Kuiper, J.M. and Engberts, J.B.F.N. (2004) *Langmuir* **20,** 1152-60
11. Lindahl, E., Hess, B., van der Spoel, D. (2001) *J. Mol. Mod.* **7**, 306-17
12. de Vries, A.H., Mark, A.E. and Marrink, S.J., (2004) *J. Phys. Chem. B* **108**, 2454-63
13. Folgering, J.H.A., Moe, P.C., Schuurman-Wolters, G.K., Blount, P. and Poolman, B. (2005) *J. Biol. Chem.* **280,** 8784-92
14. Sukharev, S.I., Sigurdson, W.J., Kung, C. and Sachs F. (1999) *J. Gen. Physiol.* **113,** 525-40
15. Anézo, C., de Vries, A.H., Holtje, H.-D., Tieleman, D.P. and Marrink, S.J. (2003) *J. Phys. Chem. B* **107**, 9424
16. Kuiper, J.M.; Chupin, V.; Engberts, J.B.F.N. to be published **2005**

The oligomeric state of the mechanosensitive channel of large conductance from *Escherichia coli*

Joost H.A. Folgering, Justina C. Wolters and Bert Poolman

Part of this chapter has been submitted for publication in *Protein Science*

Abbreviations: GUV: Giant Unilamellar Vesicle; ITO: Indium-Tin-Oxide; NTA: Nitrilo-Triacetic Acid; DOPS: 1,2-dioleoyl-*sn*-glycero-3-phosphatidylserine; DOPC: 1,2-dioleoyl-*sn*-glycero-3-phosphatidylcholine; SEC: Size Exclusion Chromatography

Abstract

To determine the quaternary structure of the mechanosensitive channel MscL from *E. coli* and to obtain a gene construct for making single substitutions per channel, covalent oligomers (monomer to hexamer) were constructed by gene fusion; up to six copies of the *mscL* gene were fused in tandem. All the multimeric tandem constructs yielded functional channels with wild-type conductance and dwell times. Importantly, only the covalent pentamer opened at the same relative pressure (compared to the pressure required to open MscS) as the wild-type MscL channel. After membrane solubilization, the wildtype channels and the covalent pentameric channel migrated similarly in a size exclusion chromatography (SEC) experiment. This indicates that the solubilized wild-type MscL-detergent-lipid complex is of the same size as the pentameric tandem-detergent-lipid complex. Overall, the data strongly suggest that the pentameric MscL represents the functional state of the channel.

Introduction

Mechanosensitive (MS) channels play a critical role in the survival of microorganisms upon a decrease of the external osmolarity. The biochemically and biophysically best characterized MS channel is the Mechanosensitive Channel of Large conductance (MscL) from *Escherichia coli*. MscL gates in response to tension in the cell membrane, which is caused by the influx of water into the cell upon osmotic downshift. After opening of MscL, osmolytes and excess water leave the cell, which prevents cell lysis.

When MscL activity was first described and the corresponding gene identified in *Escherichia coli* (1), it was clear that the channel, with a conductance of 2.5-4nS, had to be an oligomer of the relatively small (136 α-amino acid) polypeptide. Moreover, octyl-β-glucopyranoside-solubilized MscL migrated through a gel filtration column as a complex of 60-80kDa rather than the expected 17kDa predicted for a monomeric species (and ignoring the contributions from bound detergent). On the basis of these experiments a tetrameric channel was proposed (2). However, the exact number of subunits per functional channel has been a matter of discussion ever since.

Purified MscL, which had been reconstituted into liposomes in the presence of antibodies, was not able to form functional channels, this was taken as evidence that the subunits of MscL exist in the membrane as monomers (2). However, the mere presence of antibodies could also affect channel activity by blocking the pore, or inhibiting the mechanosensing parts of the protein. It has also been shown that the response to sustained membrane tension is different when a small number of channels (an activity burst is followed by inactivation) instead of a large number of channels (sustained or increasing channel activity) is present in a patch. From these observations it has been suggested that the channels assemble in the membrane upon application of mechanical force (2), but conclusive experiments have never been presented. Studies in which wild-type MscL and a dimeric version of the polypeptide were subjected to cross-linking resulted in the proposition that the functional unit consisted of six subunits (3, 4). This hexameric conformation was also supported by a two-dimensional crystallization / electron microscopy study (5).

A major breakthrough came when the structure of MscL from *Mycobacterium tuberculosis* was determined by X-ray crystallography (6). This not only gave insight into the pore structure and potential gating mechanism but also showed that the *M. tuberculosis* channel consists of five subunits. Subsequently, the quaternary structure of MscL from *E. coli* was examined by cross-linking, size exclusion chromatography (SEC) and analytical ultracentrifugation, using the wild-type, dimeric and trimeric tandem constructs. Although the reported analytical ultracentrifugation, crosslinking and SEC data are not unambiguous, this work is most consistent with the proposal that also MscL from *E. coli* forms a channel of five subunits (7). More recently, an electron microscopic study on a homogeneous population of MscL particles confirmed a pentameric structure (8).

Although there is no evidence that the oligomeric structure of MscL differs from species to species, such information does exist for other membrane-bound protein complexes, e.g., the F_IF_O-ATP synthase (in yeast it contains 10 *c* subunits, in chloroplasts 14 and in *Ilyobacter tartaricus* 11 (9)). Recently, pore-forming toxins were identified in *Staphylococcus aureus* that vary in their subunit composition. These pores consist of subunits of LukF and Hlg2 in either a 3:4 or a 4:3 ratio and are thought to play a role in hemolysis of human erythrocytes (10). Both these examples demonstrate that oligomeric structures of proteins (or protein complexes) may differ between species and even within a single species.

Here, we present in *vivo* evidence for the pentameric structure of MscL from *E. coli*, based on expression and characterization of covalently linked subunits. We also present SEC data showing that the pentameric tandem construct migrates similar to wildtype MscL. The covalent pentameric channel offers unique possibilities to further study the gating of the channel by making single or multiple specific α-amino acid substitutions or introducing pairs of fluorophores at specific positions in the channel.

Materials and Methods

Strains and growth conditions

All experiments were carried out with *E. coli* PB104 (*recA*$^-$ and *ΔmscL::Cm*^{res}) as a host for the recombinant plasmids (11). Cells were grown under aerating conditions at 37°C in Luria broth, supplemented with 100µg/mL ampicillin and 30µg/mL chloramphenicol. To search for optimal expression conditions of *mscL*, temperatures of 25°C and 30°C and different L-arabinose concentrations were tested. For growth on solid medium, 1.5% (w/v) agar was added to the broth.

Table 1: List of plasmids used in this study and their characteristics

Plasmid	Relevant characteristics	Reference
pB10b	pBR322 *ori*; *lacUV5* promoter; *Xba*I, *Xho*I in multiple cloning site, *Amp*^{res}	(11)
pB10bmscL	pB10b with *mscL*, with a C-terminal 6 histidine tag inserted in *Xba*I, *Xho*I	(11)
pBAD	pBR322 *ori*; P_{BAD} promoter; *Nco*I, *Hind*III in multiple cloning site, *Amp*^{res}	(12)
pGFPCR	pUC *ori*; *GFPuv*, *Nco*I, *Xho*I and *Sac*I in multiple cloning site, *Amp*^{res}	(24)
pBADMscL5	pBAD with subunit MscL1-10H inserted in *Eco*RI, *Hind*III	This work
pBADMscL45	pBADMscL1 with subunit MscL2 inserted in *Kpn*I, *Eco*RI	This work
pBADMscL345	pBADMscL1,2 with subunit MscL3 inserted in *Bgl*II, *Kpn*I	This work
pBADMscL2345	pBADMscL1,2,3 with subunit MscL4 inserted in *Bgl*II, *Sac*I	This work
pBADMscL12345	pBADMscL1,2,3,4 with subunit MscL5 inserted in *Sac*I, *Nco*I	This work
pBADMscL1AB2345	pBADMscL1,2,3,4,5 with subunit MscL5 replaced by subunit MscL5AB from pGFPCRMscL5AB using *Sac*I, *Nco*I	This work
pGFPCRMscL1A	pGFPCR with subunit MscL5A inserted in *Xho*I, *Sac*I	This work
pGFPCRMscL1AB	pGFPCRMscL5A with subunit MscL5B inserted in *Nco*I, *Xho*I	This work

Construction of plasmids

The plasmids used in this study are listed in Table 1. The tandem constructs were made by ligating *mscL* genes one by one into the pBADmyc-HisB vector as shown in Fig. 1A. The individual genes were amplified by PCR, using the primers listed in Table 2. During PCR amplification, restriction sites were created upstream and downstream of the *mscL* gene for directional insertion and positioning of the DNA into the vector. PCR amplifications, using Expand High-Fidelity DNA polymerase (Roche Applied Science, Indianapolis)

were performed according to the manufacturer's instructions. The DNA was amplified by PCR using pB10bMscL as template, an annealing temperature of 53°C, and an elongation time of 60sec.

Table 2: Primers and plasmids and their relevant characteristics

Subunit	Primers	Sequence	Site
MscL5	Fw	5'-ATATAT*GAATTC*ATGAGCATTATTAAAGAATTTCGCG	*Eco*RI
MscL5-7H	Rev	5'-GTGGTGATGGTGATGGTGATGAGAGCGGTTATTCT GCTCTTTCAGC	
MscL5	Fw	5'-ATATAT*GAATTC*ATGAGCATTATTAAAGAATTTCGCG	*Hind*III
MscL5-10H	Rev	5'-ATATAT*AAGCTT*TTAATGGTGATGGTGGTGATGGTG ATGGTGATGAGAGC	
MscL4	Fw	5'-ATATAT*GGTACC*ATGAGCATTATTAAAGAATTTCGCG	*Kpn*I
MscL4	Rev	5'-ATATAT*GAATTC*AGAGCGGTTATTCTGCTCTTTCAGC	*Eco*RI
MscL3	Fw	5'-ATATAT*AGATCT*ATGAGCATTATTAAAGAATTTCGCG	*Bgl*II
MscL3	Rev	5'-ATATAT*GGTACC*AGAGCGGTTATTCTGCTCTTTCAGC	*Kpn*I
MscL2	Fw	5'-ATATATGAGCTCATGAGCATTATTAAAGAATTTCGCG	*Sac*I
MscL2	Rev	5'-ATATAT*AGATCT*AGAGCGGTTATTCTGCTCTTTCAGC	*Bgl*II
MscL1	Fw	5'-ATATAT*CCATGG*GCATTATTAAAGAATTTCGCG	*Nco*I
MscL1	Rev	5'-ATATAT*GAGCTC*AGAGCGGTTATTCTGCTCTTTCAGC	*Sac*I
MscL1A	Fw	5'-ATATAT*CTCGAG*ATGAGCATTATTAAAGAATTTCGCG	*Xho*I
MscL1	Rev	5'-ATATAT*GAGCTC*AGAGCGGTTATTCTGCTCTTTCAGC	*Sac*I
MscL1	Fw	5'-ATATAT*CCATGG*GCATTATTAAAGAATTTCGCG	*Nco*I
MscL1B	Rev	5'-ATATAT*CTCGAG*AGAGCGGTTATTCTGCTCTTTCAGC	*Xho*I

To the first inserted gene (*mscL5*), a sequence coding for a C-terminal 10-histidine tag was added in a two step PCR. Primers MscL1 Fw and MscL1-7H Rev were used to introduce a 7-histidine tag. In a second step, using the product of the first amplification as template and primers MscL1 Fw and MscL1-10H Rev, another three histidines, a stop codon and a restriction site for further cloning were introduced. The gene was then inserted into the pBAD plasmid, using *Eco*RI and *Hind*III restriction enzymes and T4 ligase (Roche Applied Science, Indianapolis) according to the manufacturer's instructions, forming pBADMscL5. *mscL4* was inserted into pBADMscL5 using the *Kpn*I and *Eco*RI restriction sites, resulting in pBADMscL45. Next *mscL3*, *mscL2* and *mscL1* were inserted sequentially using the restriction sites shown in Fig. 1A and Table 2, resulting in pBADMscL345; pBADMscL2345 and pBADMscL12345, respectively. To introduce the sixth *mscL* gene into pBADMscL12345, the fifth gene (*mscL1*) was replaced by a two gene fusion (*mscL1AB*) constructed in pGFPCR. First, *mscL1B* was inserted into pGFPCR, using *Xho*I and *Sac*I restriction sites, and then *mscL1A* was inserted, using *Nco*I and *Xho*I restriction sites, resulting in pGFPCRMscL1AB.

The oligomeric tandem constructs were used to transform *E. coli* PB104, and after isolation and purification of the plasmids (Qiagen, Chatsworth, CA), the DNA sequence was analyzed to confirm fidelity. Sequencing showed that *mscL5* contained a silent mutation. In addition,

mscL4 contained a methionine to leucine substitution at position 1 of the MscL coding region.

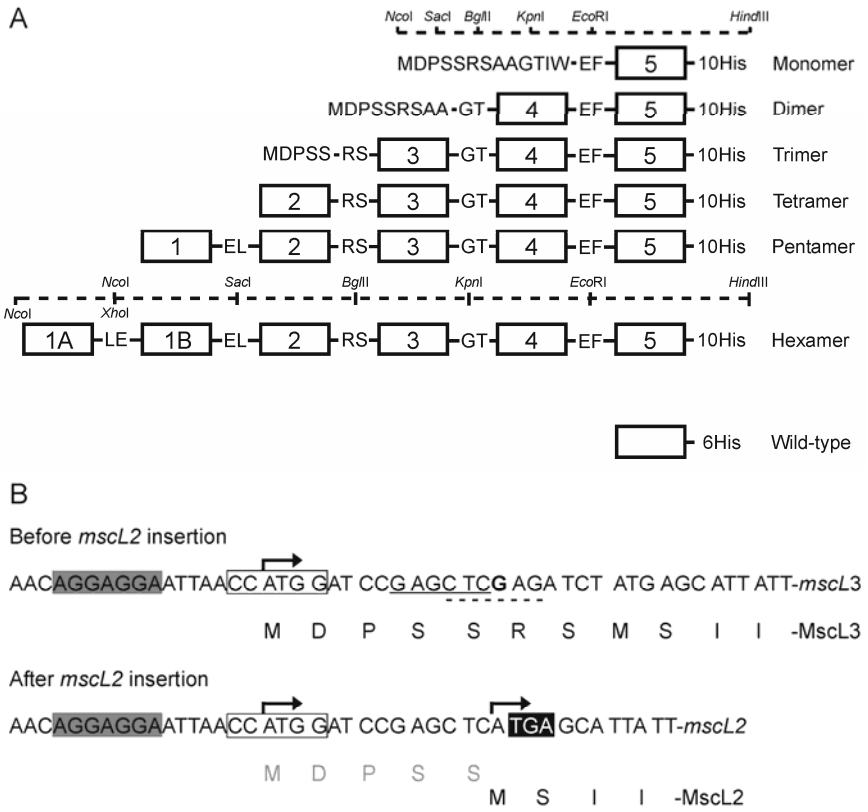

Figure 1: (A) Schematic representation of the multimeric MscL constructs. Top dashed line indicates relevant restriction sites in the multiple cloning site of the pBAD plasmid before cloning. The α-amino acid sequences of the linkers of the multimeric tandem constructs are indicated. The monomeric, dimeric and trimeric tandem constructs each start at the ATG of the *Nco*I restriction site in the plasmid and therefore contain N-terminal extensions as indicated. Each box represents the full sequence of one wild-type MscL from *E. coli*, the numbers inside the boxes indicate the number of the MscL units (Table 1 and 2). The 10 his-tag at the C-terminus of the proteins is also shown. The second dashed line indicates the position of the relevant restriction sites in the multiple cloning site of the pBAD plasmid after cloning of the DNA fragments. Positions of the relevant restriction sites in the pentameric tandem construct are shown above the second dashed line; additional changes in restriction sites for the hexameric tandem construct are indicated below the second dashed line. For comparison, wild-type MscL is also shown. (B) Ribosome-binding site (indicated in grey box) and translation initiation sites (indicated with arrows) before and after insertion of *mscL2*, using the *Sac*I restriction site, (underlined, solid). The insertion of *mscL2*, using the *Sac*I restriction site removes the guanine (bold) from the *Xho*I restriction site (underlined, dashed), resulting in a frameshift relative to the ATG of the *Nco*I restriction site (boxed). Translation from that ATG would result in a 5 α-amino acid peptide (indicated in grey) as the sixth triplet corresponds to a stop-codon (indicated as black box). Most likely, the tetrameric MscL fusion is expressed from the second ATG, which represents the start of the wild-type *mscL* gene. The sequences of the peptides resulting from translation at the indicated translation initiation sequences are shown below the DNA sequence.

Expression

E. coli PB104 containing the plasmids with the *mscL* tandem constructs were grown in LB medium to an OD_{600} of 0.8, after which expression was triggered by addition of L-arabinose (0.0025% - 0.25% w/v) and induction for different time periods as suggested in (12). Inside-out membrane vesicles were prepared by lysing the bacteria (20mg/mL protein) by a two-fold passage through a French pressure cell at 10,000psi and removal of unlysed cells and cell wall debris by centrifugation at 30,000xg. The membrane vesicles were washed once by centrifugation at 150,000xg and then resuspended in 50mM KPi, pH 6.5. Aliquots of 0.5mL were frozen in liquid nitrogen and stored at -80°C until use.

Purification

Membrane vesicles, containing overexpressed oligomeric tandem protein, were solubilized in 50mM KPi, 10mM imidazole, 300mM NaCl, pH 7.0, plus 0.5% Triton X-100 [or 0.5% *n*-dodecyl-β-D-maltoside (DDM) or 3% octyl-β-D-glucoside (octyl-glucoside)] at 4°C for 20min, under continuous mixing of the suspension. The solubilized proteins and remaining membrane material were separated by ultracentrifugation at 270,000xg for 20min at 4°C. The supernatant was then loaded onto Ni-NTA affinity resin (20mg total membrane protein per ml of resin) pre-equilibrated with solubilization buffer, or applied to the SEC column as described below. The Ni-NTA column was washed with 40 column volumes of solubilization buffer, containing 0.1% Triton X-100 (or 0.1% DDM, or 1% octyl-glucoside). In some experiments, 0.5mg/mL of purified *E. coli* lipids and/or 20% glycerol (v/v) were present during the membrane solubilization and protein purification. Next, the column was washed with the same buffer containing 50mM imidazole (instead of 10mM), after which the proteins were eluted in the same buffer containing 500mM imidazole.

Reconstitution

Membrane reconstitution was performed essentially as described (13). The purified protein was mixed with Triton X-100-destabilized preformed liposomes (10mg/mL of lipid); the lipid mixtures were composed of dioleoyl 18:1 (Δ9 cis) phospholipids DOPC and DOPS in a 3 to 1 ratio. Typically, reconstitutions were performed at protein-to-lipid ratios of 1 to 200 w/w. The resulting proteoliposomes were converted to proteo-GUVs for patch-clamp analysis by dehydration and rehydration in the presence of an AC electrical field as described (14;15).

Spheroplast preparation

Giant spheroplasts were prepared from *E. coli* PB104, carrying the plasmids with the *mscL* oligomeric tandem constructs, essentially as described (16), except that protein synthesis was triggered using 0.25% L-arabinose for 30min.

Electrophysiology

Experiments were performed as described previously (14-16). Samples of 1-5μL of spheroplast (0.2 - 0.8mg/mL of total protein) or proteo-GUVs (0.1mg/mL of protein) suspensions were transferred to a sample chamber

containing a ground electrode and 300µL of patch clamp buffer: 5mM HEPES, pH 7.2, 200mM KCl, 90mM $MgCl_2$, plus 10mM $CaCl_2$ for spheroplasts; 5mM HEPES, pH 7.2, 200mM KCl plus 40mM $MgCl_2$ for proteo-GUVs. Channel activity was recorded using an Axopatch 200A amplifier together with a digital converter and Axoscope software (Axon Instruments, Foster City, USA). Data was acquired at a sampling rate of 33kHz and filtered at 10kHz. Offline analysis was performed using PClamp 6.0 software (Axon Instruments).

Size exclusion chromatography

Samples were prepared as described above under "*purification*". Detergent-solubilized samples (0.5-1mg of total protein, from 2.5mg wet weight of membranes) were applied to the column immediately after solubilization and ultracentrifugation. Alternatively, purified protein samples were applied after a 10min centrifugation step at 13,000×g. The protein was analyzed on an ÄKTA™ chromatography system (Amersham, Uppsala Sweden) equipped with a Superdex 200 10/300 GL column. The column was pre-equilibrated with the wash buffer indicated below and subsequentially calibrated using HMW and LMW gel-filtration standards (Pharmacia). After sample injection, the column was eluted with 50mM KPi, pH 7.0, 300mM NaCl plus the detergent, lipid and glycerol concentration, used during solubilization or purification, at a flow-rate of 0.5mL/min and 0.5mL fractions were collected. The collected fractions were analyzed on SDS-PAGE and by immuno-detection.

Miscellaneous

Purified proteins were analyzed on 5-20% polyacrylamide gradient SDS-PAGE (17). Protein expression levels in membrane vesicles were analysed by immuno-detection, using antibodies raised against the his-tag (Amersham) and the Western-light chemoluminescence detection kit (Tropix Inc., Bedford, MA).

Results

Expression of the tandem constructs

On the basis of expression screening (comparing different L-arabinose concentrations, induction times and growth temperatures) with the covalent pentameric *mscL* gene (data not shown), L-arabinose at 0.0025% (w/v) and two hours of induction at 30°C were used for further studies with all the tandem constructs. An immuno-blot was used to visualize the protein levels as shown in Fig. 2. Except for the tetrameric fusion, translation of the constructs started from the ATG codon at the beginning of the multiple cloning site in pBAD, resulting in different N-terminal extensions relative to wild-type MscL for the mono- di- and trimeric constructs (Fig. 1A). As shown in Fig. 1B the insertion of the *mscL2* gene into the *Sac*I site resulted in a single base pair frame shift, 11 nucleotides downstream of the ATG translation initiation codon at the beginning of the multiple cloning site in pBAD. Most likely, the tetrameric construct is translated from the second ATG and starts like the wild-type, pentameric and hexameric constructs of MscL with the sequence MSII (Fig. 1B). The final level of expression of the tetrameric construct was

lower than that of the other constructs (Fig. 2), probably because the distance between the Shine-Delgarno sequence and translation initiation of *mscL2* is too long. It is also possible that an alternative weaker Shine-Delgarno sequence closer to the *mscL2* ATG is used (Fig. 1B).

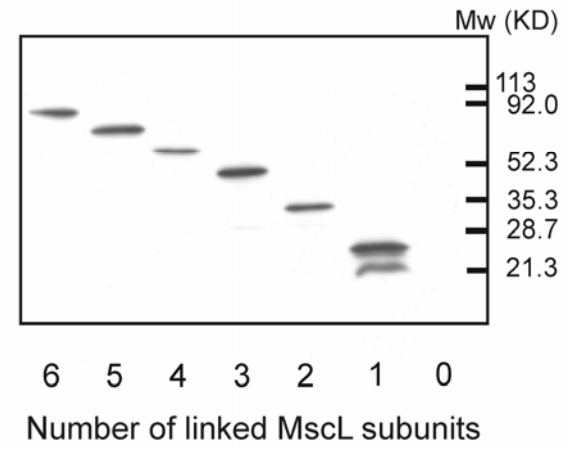

Figure 2: Immuno-blot of *E. coli* PB104 membranes expressing the different MscL tandem constructs. The double band observed in the lane marked "1" is typical for monomeric (wild-type) MscL (1, 4). All lanes are marked according to the number of MscL units in the construct.

Longer exposures of the immunoblots showed that the anti-his antibody had also reacted with some smaller sized proteins or protein fragments (data not shown). Most of these bands were also present in the empty plasmid control and are therefore aspecific. However, some of the smaller bands were related to the expression of a particular tandem construct, indicating that some degradation had taken place, possibly during the preparation of the membrane vesicles.

All tandem constructs encode functional channels

Patch clamp experiments with spheroplasts expressing the different MscL tandem constructs revealed that all covalent oligomers formed active mechanosensitive channels with a unitary conductance of around 3.0nS (Fig. 3). In the empty plasmid control, indicated by 0 in Fig. 3, only MscS activity was observed. The number of channels observed per patch was generally between one and five for all the multimeric constructs except for the tetrameric fusion, where in a number of patches no channel activity was observed, which is in accordance with the lower expression level (Fig. 2). Dwell times and substate preference of the oligomeric tandem channels were found not to differ significantly from those of the WT channel (data not shown). This is in contrast to previous findings (7), where it was reported that the dimeric and trimeric tandem showed a slower open-to-closed transition.

Next, giant spheroplasts of *E. coli* PB104 were used to examine the pressure at which the oligomeric tandem channels first opened fully relative to the pressure at which MscS opened. The pressure ratio of the monomeric construct was 1.69 ± 0.10, which is comparable to the ratio found for wild-type MscL (1.64 ± 0.08) (18). The pressure ratios for the di-, tri-, tetra- and

hexameric tandem constructs were significantly higher and tended to increase with the number of linked subunits (Fig. 4). Importantly, the pressure ratio of the pentameric tandem construct was similar to that of the wild-type MscL, strongly suggesting that it represents the native oligomeric state.

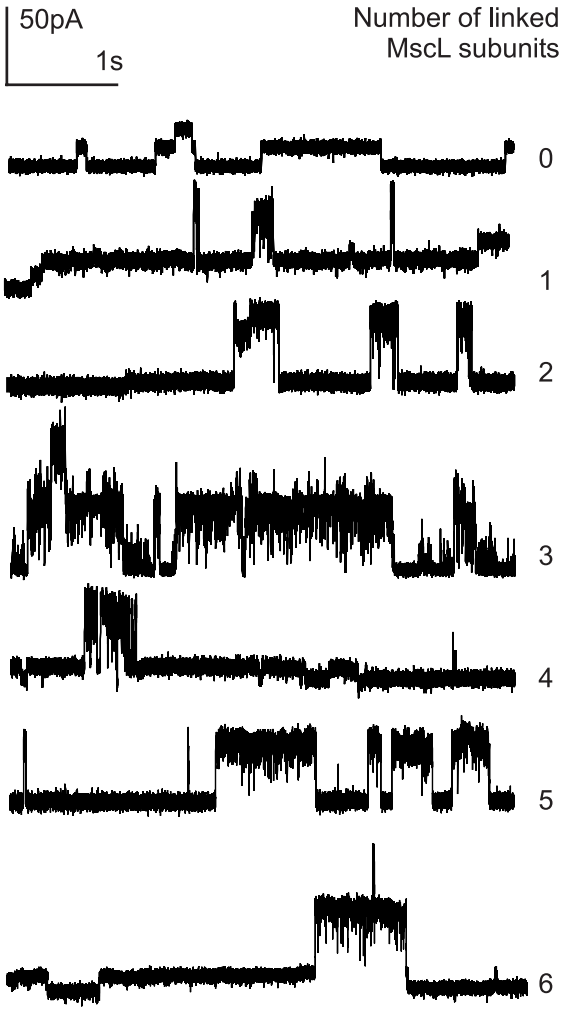

Figure 3: Traces of electrophysiological recordings of spheroplasts from *E. coli* PB104 expressing the different multimeric constructs. Patches were not saturated, but tension was set to a level where only one or two channels were activated. Time and current scale bars for all traces are indicated at the top of the figure. All traces are marked according to the number of MscL units in the construct. The trace marked "0" corresponds to *E. coli* PB104 (containing the empty pBAD control plasmid), that is, the MscL null mutant in which MscS activity can still be observed.

Wild-type, monomeric and pentameric tandem constructs form complexes of equal size

After Ni-NTA purification, wild-type MscL and the oligomeric tandem channel constructs were loaded onto a SEC column. Each sample had a tendency to form aggregates that eluted in or around the void volume of the column. Even wild-type MscL aggregated to some extent, but most of the protein formed a protein-detergent complex of around 300kDa in the presence of Triton X-100 (data not shown). A number of conditions were explored to diminish the aggregation of the tandem constructs. Three different detergents, *i.e.* Triton X-100, DDM and octyl-glucoside, the absence or presence of 20% glycerol, and the absence and presence of 0.5mg/mL of purified *E. coli* lipids were tested. In each case, the medium composition during Ni-NTA purification and gel filtration was the same. The only medium, yielding a somewhat reduced aggregation of the pentameric tandem construct, was composed of

50mM KPi, pH 7.0, 300mM NaCl, plus 0.1% Triton X-100, 0.5mg/mL of purified *E. coli* lipids and 20% glycerol (v/v) as additions. Under these conditions, a small fraction (~ 10% of the total amount of MscL protein) formed a detergent protein complex with an apparent molecular mass of 220 to 300kDa. Changing expression conditions (shorter induction / induction with a lower concentration of L-arabinose / induction at 35°C, 30°C or 25°C) or even changing the expression vector (from the arabinose to the IsoPropyl-β-D-ThioGalactopyranoside inducible *trc* promoter) did not improve the ratio between aggregated and non-aggregated protein.

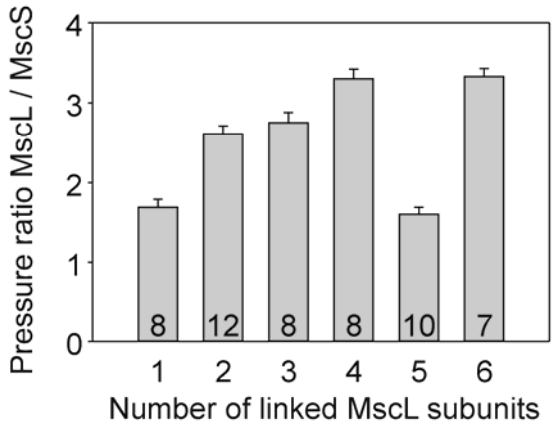

Figure 4: Pressure ratios of MscL / MscS. For each of the tandem constructs, the pressure required to fully open the first MscL channel was determined relative to the pressure required to open MscS in the same patch. The number of patches analyzed is indicated inside the bars. Error bars indicate s.e.m.

Previously, it was shown that the MscL-detergent complex in octyl-glucoside (3% w/v) solubilized membranes formed a discrete molecular species with a mass around 80kDa, as assessed by SEC (7). This experiment was repeated for the monomeric and pentameric tandem constructs, but most of the MscL protein was found to be aggregated. Next, the experiment was repeated using the conditions found to be optimal for the purified protein (Fig. 5). Again, all samples (including the wild-type) showed a tendency to aggregate as most clearly observed for the pentamer, where around 70% of the total protein migrated at an apparent molecular mass of 500-1000kDa. However, the fraction with a retention time of 23min showed an increase in pentameric tandem construct. The increase was at least 3-fold based on quantification of the bands by immuno-detection (Fig. 5). This indicates that with 0.1% Triton X-100 as detergent the wild-type, monomeric and pentameric tandem constructs form complexes with an apparent mass between of 220-300kDa (discrete fractions of 0.5mL were analyzed therefore, the mass could not be determined more accurately). It also means that wild-type and monomeric MscL form protein-lipid-detergent complexes of similar size as the pentameric tandem, confirming that the pentamer is the native oligomeric state of the channel.

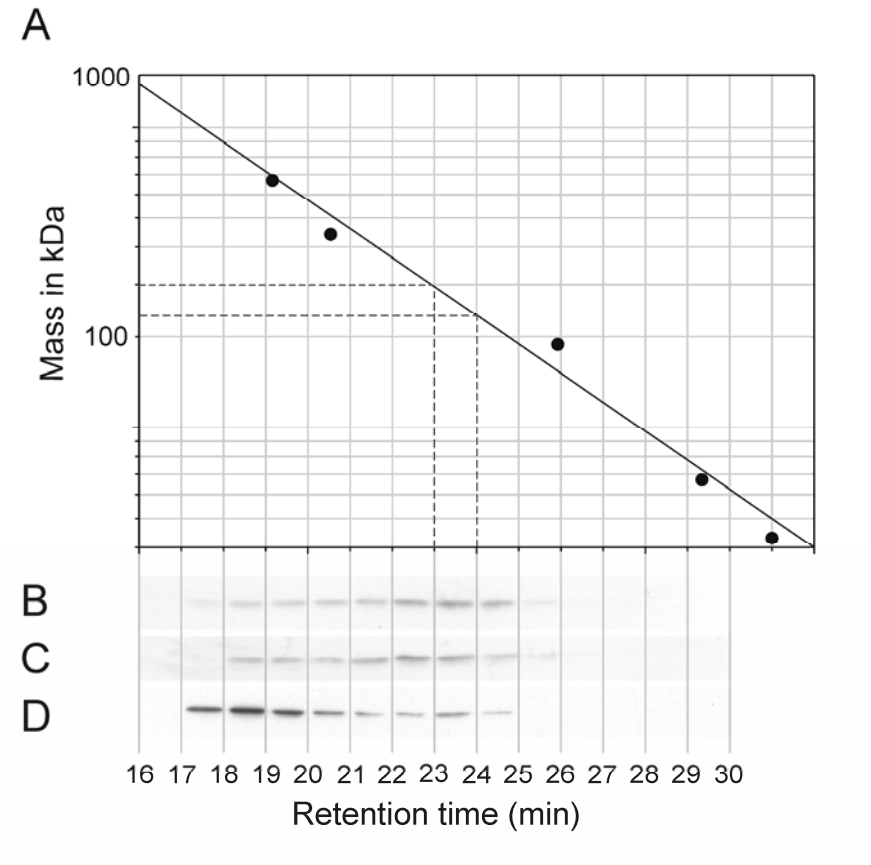

Figure 5: (A) SEC calibration curve obtained with thyroglobulin (669kDa), ferritin (440kDa), catalase (232kDa), aldolase (158kDa), albumin (67kDa), ovalbumin (43kDa), chymotrypsin (25kDa) and ribonuclease (13.7kDa) as markers. The chromatography medium is described in the text. (B) 20µL of 0.5mL fractions, collected from SEC of solubilized membranes containing wild-type MscL, were used for SDS-PAGE analysis. MscL was identified by immuno-detection. (C) As (B) for the monomeric MscL construct. (D) As (B) for the pentameric MscL construct. Values below the immuno-blots indicate retention time on the Superdex 200 10/300 GL column.

Patch-clamp analysis of Ni-NTA purified pentameric tandem MscL in proteoliposomes

From Ni-NTA purification, > 90% pure (based on SDS-PAGE analysis) pentameric tandem protein could be obtained at reasonable concentrations (0.1mg/mL). After reconstitution into detergent-destabilized liposomes, channel activity could be detected using patch clamp. However, most of the observed activity did not resemble wild-type MscL activity. High conductance openings, and a large number of dwell levels were observed. The activity also seemed to be tension independent (Fig. 6). This indicates that the pentameric tandem protein was not inserted into the membrane in a native conformation, probably because it had already aggregated during the isolation.

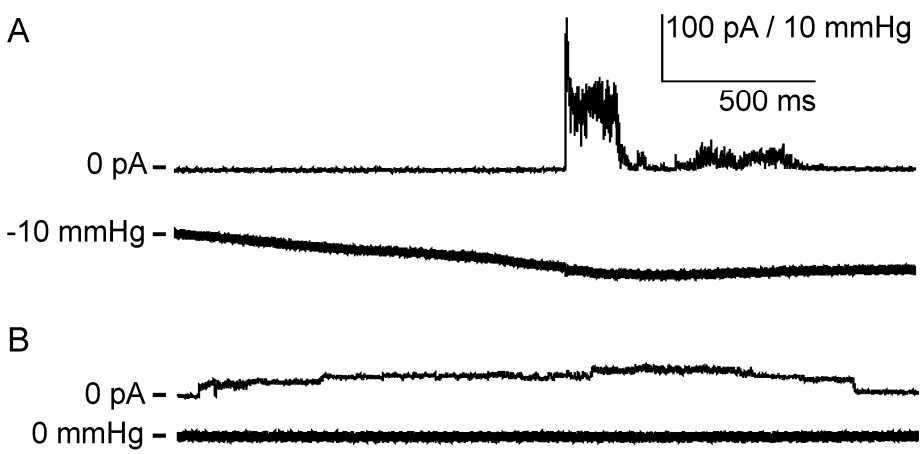

Figuge 6: Typical traces of aberrant channel activity in proteo-GUV patches containing reconstituted pentameric MscL. (A) Short high conductance openings, followed by a number of lower conductance bursts were observed. After further increase of the pressure, channel activity was no longer observed. (B) Longer openings were also observed, but a unitary conductance level could not be determined. Often channel activity was tension independent.

Discussion

MscL from *E. coli* forms a pentameric structure

Based on the relative pressure ratios for full channel opening (Fig. 4), it can be concluded that the covalently-linked pentameric construct behaves similar to the wild-type MscL channel. The higher pressure ratio required for the opening of the covalent dimeric, trimeric, tetrameric and hexameric constructs may be explained from the way these polypeptides form functional channels (Fig. 7). If it is assumed that one functional channel comprises of five subunits, one or more non-participating subunits must lie at the periphery of the channel in the case of the covalent dimeric, trimeric, tetrameric and hexameric constructs, as originally suggested by Sukharev and colleagues (7). We propose that in the dimeric, trimeric and hexameric constructs, one of the linked subunits is not participating in channel formation and is located at the periphery of the channel (Fig. 7B, C and F). For the tetrameric construct, it would imply that three subunits are not participating in channel formation (Fig. 7D). It is actually surprising that these constructs form functional channels, with relatively little detrimental effects of the non-participating subunits. The peripherally-located subunits, however, do hinder the opening of the channel, as can be inferred from the increased pressures needed for initial MscL gating (Fig. 4). This implies that the presence of subunits, which do not participate in the formation of the pore, requires additional energy for the cooperative opening of the channel. The linkers between the subunits may also influence the pressure ratios by restricting the channel flexibility. However, we feel that this is not likely as the pentameric tandem behaves like wild-type MscL.

It could be argued that the covalent hexameric tandem construct is not in the conformation proposed in Fig. 7F, but in a conformation in which all six subunits participate in channel formation. In that case, the 6th subunit would

lead to a 1.2 fold increase of the circumference of the channel and possibly a 1.2 fold increase in the pore diameter as compared to the suggested pentameric structure. The conductivity of such a channel could be calculated from the following equation (19):

$$R_c = \left(l + \frac{\pi r}{2} \right) \frac{\rho}{\pi r^2}$$

This equation relates the channel resistance (R_c, which is the reciprocal of the conductance) to the pore radius (r), the pore length (l) and the conductivity of the solution inside the channel (ρ). Using previously proposed values (19) for channel length (l = 42Å) and recording solution conductivity (ρ = 0.5Ωm), the pore radius of a pentameric channel of 3.0nS conductance would be 18.2Å. If we increase this radius by a factor 1.2, the conductance of the hexameric channel would be around 4.0nS. Such an increase in conductance would have been noticed with our experimental set-up but was not observed. We therefore propose that the hexameric construct also forms a channel with a pentameric structure, that is, with one subunit not participating in the channel. Along the same line of reasoning, it can be concluded that the dimeric, trimeric and tetrameric constructs must be composed of the number of polypeptide chains indicated in Fig. 7B and C.

The SEC experiments showed that the wild-type protein and pentameric construct form complexes with similar mass, suggesting that subunits in the wild-type form strongly interacting pentameric channels. Again, this indicates that the in *vivo* oligomeric state of the wild-type MscL channel from *E. coli* is pentameric. The solubilised wild-type MscL, the monomeric construct and the covalent pentameric tandem construct migrated on the SEC column with an apperent molecular mass of 220 - 300kDa. The protein mass of the pentameric tandem construct (as shown in Fig. 1A) corresponds to only 76.9kDa and the difference between the apparent and calculated mass must be due to detergent and lipid binding, if one ignores possible differences in the molecular shape of MscL and the proteins in the calibration set. This difference amounts to 200-300 detergent and/or lipid molecules, which is in the same range as the binding of detergent to other types of integral membrane proteins with a comparable membrane-embedded domain (20).

The SEC experiments were also performed to rule out the possibility that the channel formed by the pentameric construct is composed of multiple pentameric units (e.g., as shown in Fig. 7G). Because of the strong tendency of the pentamer to aggregate, this possibility cannot be ruled out completely. On the other hand, a channel structure as depicted in Fig. 7G would not very likely result in channel activity resembling that of wild-type MscL. As the pentameric construct was found to be active in the spheroplasts, but appeared to be aggregated after solubilization, it seems that this pentameric construct starts aggregating once it is outside the native membrane.

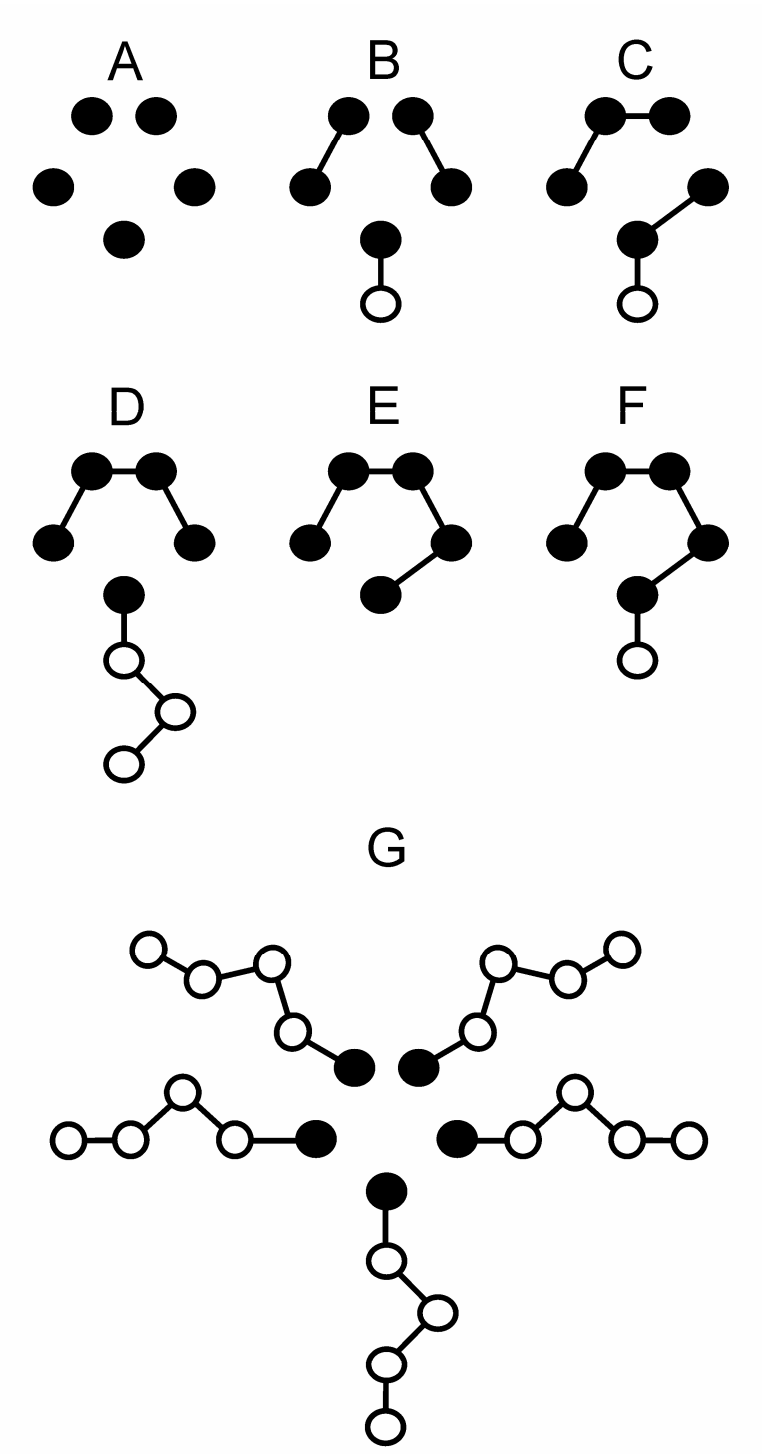

Figure 7: Schematic depiction of the possible ways the covalently linked multimeric MscL constructs might form functional channels with a "pentameric" structure. Each filled circle indicates a subunit participating in the formation of an active channel. The open circles indicate non-participating subunits. Dimer and trimer schemes are as suggested previously (7). (A) monomeric construct, (B) dimeric tandem construct, (C) trimeric tandem construct, (D) tetrameric tandem construct, (E) pentameric tandem construct, (F) hexameric tandem construct, and (G) alternative structure formed from pentameric tandem constructs.

Implications of linker length for the structure of the pentameric construct

In the covalently-linked MscL constructs, the C-terminus of MscL 1 to 4 is conjugated to the N-terminus of the next MscL by a linker of only two α-amino acids. As all constructs were able to form functional channels, this implies that in the open and closed conformations the N- and C-terminus of the protein can be close together. This is in contrast to the situation in the 3-dimensional structure of MscL from *M. tuberculosis*, where the N- and C-terminus are about 35Å apart (6). In *E. coli* this distance may be different, as MscL from *E. coli* is 15 α-amino acids shorter than MscL from *M. tuberculosis*. Studies, in which the C-terminal helices of MscL from *E. coli* were subjected to cysteine cross-linking with the channel in the open or closed state (21), showed that these helices form a rigid helix bundle that is probably directed towards the cytoplasm. It is also known that MscL tolerates relatively large truncations of up to 27 residues from the C-terminus (22), and separately expressed N- and C-terminal halves of the protein still form functional channels (23). This, together with our results, suggests that the position and structure of the C-terminus is not very critical for the formation of functional channels.

In summary: we have shown that covalently-linked multimeric constructs of up to six MscL proteins are capable of forming functional pores and that the pentameric construct resembles wild-type MscL in its channel properties. SEC experiments showed that the wild-type MscL and the pentameric construct form molecular species with similar mass. From this, we conclude that the oligomeric state of MscL from *E. coli* is pentameric. The pentameric gene cassette with unique restriction sites between the individual genes allows easy exchange of wild type for mutant alleles. This means that the covalent pentameric construct represents an important tool for analyzing the effect of single and multiple α-amino acid substitutions per pore unit, rather than per subunit, on channel function.

Acknowledgements

We would like to thank W.H.C. Huibers and D.J. Slotboom for assistance in the SEC experiments, E.R. Geertsma and the channel protein group at the BioMaDe Technology Foundation for helpful discussions, and MSC^{plus} for financial support.

Reference List

1. Sukharev, S.I., Blount, P., Martinac, B., Blattner, F. R. and Kung, C. (1994) *Nature* **368,** 265-8
2. Hase, C.C., Le Dain, A.C. and Martinac, B. (1995) *J. Biol. Chem.* **270,** 18329-34
3. Blount, P., Sukharev, S.I., Moe, P.C., Schroeder, M.J., Guy, H.R. and Kung, C. (1996) *EMBO J.* **15,** 4798-805
4. Hase, C.C., Le Dain, A.C. and Martinac, B. (1997) *J. Membr. Biol.* **157,** 17-25
5. Saint, N., Lacapere, J.J., Gu, L.Q., Ghazi, A., Martinac, B. and Rigaud, J.L. (1998) *J. Biol. Chem.* **273,** 14667-670
6. Chang, G., Spencer, R.H., Lee, A.T., Barclay, M.T. and Rees, D.C. (1998) *Science* **282,** 2220-6
7. Sukharev, S.I., Schroeder, M.J. and McCaslin, D.R. (1999) *J. Membr. Biol.* **171,** 183-93
8. Becker, C.F., Strop, P., Bass, R.B., Hansen, K.C., Locher, K.P., Ren, G., Yeager, M., Rees, D.C. and Kochendoerfer, G.G. (2004) *J. Mol. Biol.* **343,** 747-58
9. Stahlberg, H., Muller, D.J., Suda, K., Fotiadis, D., Engel, A., Meier, T., Matthey, U. and Dimroth, P. (2001) *EMBO Rep.* **2,** 229-33
10. Sugawara-Tomita, N., Tomita, T. and Kamio, Y. (2002) *J. Bacteriol.* **184,** 4747-56
11. Ou, X., Blount, P., Hoffman, R.J. and Kung, C. (1998) *Proc. Natl. Acad. Sci. USA* **95,** 11471-5
12. Guzman, L.M., Belin, D., Carson, M.J. and Beckwith, J. (1995) *J. Bacteriol.* **177,** 4121-30
13. Knol, J., Sjollema, K. and Poolman, B. (1998) *Biochemistry* **37,** 16410-5
14. Folgering, J.H., Kuiper, J.M., de Vries, A.H., Engberts, J.B. and Poolman, B. (2004) *Langmuir* **20,** 6985-7
15. Doeven, M.K., Folgering, J.H., Krasnikov, V., Geertsma, E.R., van den, Bogaart. G. and Poolman, B. (2004) *Biophys. J.* **88,** 1134-42
16. Blount, P., Sukharev, S.I., Moe, P.C., Martinac, B. and Kung, C. (1999) *Methods Enzymol.* **294,** 458-82
17. Laemmli, U.K., Beguin, F. and Gujer-Kellenberger, G. (1970) *J. Mol. Biol.* **47,** 69-85
18. Yoshimura, K., Batiza, A., Schroeder, M., Blount, P. and Kung, C. (1999) *Biophys. J.* **77,** 1960-72
19. Cruickshank, C.C., Minchin, R.F., Le Dain, A.C. and Martinac, B. (1997) *Biophys. J.* **73,** 1925-31
20. Poolman, B., Doeven, M.K., Geertsma, E.R., Biemans-Oldehinkel, E., Konings, W.N. and Rees, D.C. (2005) *Meth. Enzymol.,* in press
21. Anishkin, A., Gendel, V., Sharifi, N.A., Chiang, C.S., Shirinian, L., Guy, H.R. and Sukharev, S. (2003) *J. Gen. Physiol* **121,** 227-44
22. Blount, P., Sukharev, S.I., Schroeder, M.J., Nagle, S.K. and Kung, C. (1996) *Proc. Natl. Acad. Sci. USA* **93,** 11652-7

23. Park, K.H., Berrier, C., Martinac, B. and Ghazi, A. (2004) *Biophys. J.* **86,** 2129-36
24. Cormack, R.S., Hahlbrock, K. and Somssich, I.E. (1998) *Plant J.* **14,** 685-92

Bacterial mechanosensation: lessons and challenges

Joost H.A. Folgering, Ana A. Arteni, Johanna M. Kuiper, Jan B.F.N. Engberts and Bert Poolman

Abbreviations: ABC, ATP-binding cassette; GUV, Giant Unilamellar Vesicle; FCS, Fluorescence Correlation Spectroscopy; LUV, Large Unilamellar Vesicle; AC, alternating current; AFM, Atomic Force Microsopy; DOPE, L-α-dioleoyl phosphatidylethanolamine; DOPC, 1,2-dioleoyl-*sn*-glycero-3-phosphatidylcholine; CCD, charge-coupled device; DIC, differential interference contrast; MTSET, [2-(trimethylammonium)ethyl] methanethiosulfonate; FRET, fluorescence resonance energy transfer

Introduction

All cells in nature are surrounded by a lipid membrane that is semi-permeable. This means they allow passage of water and small hydrophobic molecules into and out of the cell, but block diffusion of large and hydrophilic molecules like ions and sugars (Fig 1A). The cell volume is determined by the mechanic and elastic properties of the cell envelope, that is, the membrane in combination with an internal and/or external skeleton and by the water activities inside and outside the cell. The turgor pressure is the hydrostatic pressure difference that balances the internal and external osmolyte concentrations. The relation can be summarized as follows:

$$\Delta\pi = \pi_i - \pi_o = (RT / \overline{V}) \ln (a_o / a_i) \approx RT (c_i - c_o)$$

The equation relates turgor pressure ($\Delta\pi$) of the cell with the water activity outside and inside the cell (a_o and a_i, respectively); the partial molal volume of the solvent ($\overline{V}$); R is the gas-constant and T is the absolute temperature; π ($= (RT / \overline{V}) \ln a$) is the osmotic pressure. Water activity of the internal and external environment of the cell is inversely related to the osmolyte concentrations (c_i and c_o; 1). If the solute concentration outside the cell increases (hyperosmotic stress), the external water activity will decrease, and there will be a net efflux of water from the cell. Also, the turgor pressure will decrease and ultimately the cell will plasmolyse (when $\Delta\pi = 0$; Fig. 1B; 2). A decrease in cell volume will increase the crowding of the cytoplasm, which in turn may cause aggregation of the proteins and so affect essential processes in the cell. Bacteria will generally respond to this type of stress by importing and/or synthesizing compatible solutes (1, 3 and 4), and thereby counteract the loss of water and the accompanying decrease in volume and turgor pressure. The most important transporter for the uptake of compatible solutes in *Lactococcus lactis* is the ATP binding cassette (ABC) transporter OpuA, which transports glycine betaine at the expense of ATP. OpuA is activated when the ionic strength of the cytoplasm increases as a result of volume decrease, the ion-sensing activity of OpuA is dependent on the presence of charged lipids (5-7). The actual osmosensing domain of the protein has recently been identified and corresponds to a specific, so-called CBS-domain

(this domain was first identified in the cystathionine-β-synthase protein, hence it is called CBS) that interacts with the cell membrane (8).

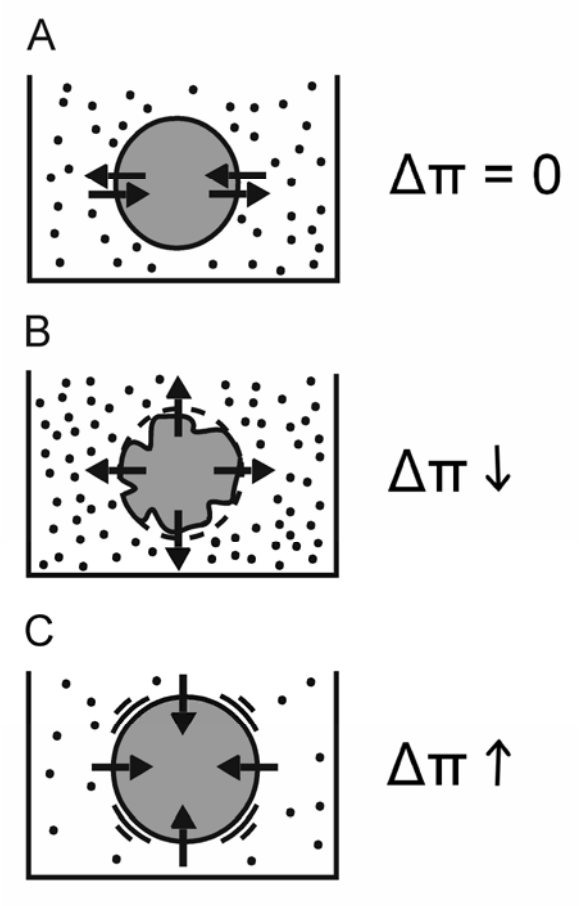

Figure 1: In their natural environments bacteria are often challenged by osmotic stress. (A) Osmostatic conditions correspond to osmolarities of the medium optimal for growth when exogenous osmoprotectants are absent. When the concentration of osmolytes in the environment increases, the bacteria become (B) hyper-osmotically stressed and lose water. If, on the other hand, the external medium is diluted the cell becomes (C) hypo-osmotically stressed and water will flow into the cell. The adaptation mechanisms of the cell to counteract the negative effects of these stresses are discussed in the text. Arrows indicate the (net) flow of water immediately after the stress is imposed.

Rapidly increasing external osmolarities are often encountered by bacteria in nature, for instance during droughts. High medium osmolarities are exploited in biotechnological applications, for instance, the growth of microorganisms in food products to inhibit spoilage. The reverse process, i.e., the rapid decrease of the external osmolarity is also common in natural environments (e.g., dilution of the external osmolyte concentrations by rainfall). In those situations, water will diffuse into the cell, increasing the cell volume. However, the cell membrane and surrounding cell-wall cannot be stretched without limit, neither can it be synthesized at a rate fast enough to keep up with the volume increase. Initially this would mean that the turgor pressure will increase but, eventually, if the cell is not protected, it will lyse (Fig. 1C). The Mechanosensitive channel of Large (MscL) conductance is one of the proteins that actually protect the bacterial cell against lysis. The channel works like a pressure relief valve; it opens near the lytic tension of the membrane and allows osmolytes and water to flow out of the cell, thereby decreasing the cell volume and relieving the membrane tension.

Even though OpuA and MscL both have functions in the process of cell volume regulation, their mode of regulation is very different. Whereas OpuA is

activated by an electrostatic switching mechanism involving protein-lipid headgroup interactions, MscL is activated by a change in the lateral pressure (profile) of the membrane. The lateral pressure is composed of the components of the interactions between the various membrane constituents, specifically the derivative of their Gibbs free energy with respect to area. The lateral pressure profile is the depth-dependent distribution of lateral stresses within the membrane (9). Here, we have used the lateral pressure profile as a description of the lateral stresses in lipid membranes. The lateral pressure can be influenced by the asymmetric bending or thinning of the membrane. When activated the turnover of transporters like OpuA is around 1-10 glycine betaine molecules translocated per second, whereas MscL in the open state allows the flow of 10^8-10^9 ions per second. The ion-flux through MscL results in a current that is measurable at the level of individual channel molecules. The MscL channel is the main research topic of this thesis. The set-up used to study the channel is described in detail in Text-box 1.

Historical perspective

As described in chapter 1, the road to finding the conditions under which single channel activities could be studied started over 250 years ago with Galvani and Volta trying to elucidate why frog leg muscles would contract in reaction to a physical stimulus. Only after the realization that biological cells are surrounded by a membrane, the knowledge of Galvani and Volta could be applied and explained. It became possible to measure potentials across and later even currents through membranes, both in rest and during muscle contraction. It even became possible to measure the current through the muscle cell membrane. However, the current measurements always represented the activity of an ensemble of channels. It was not until the 1970s, that the patch clamp technique and the black lipid membrane system allowed the study of individual ion channel activities (10).

Text-box 1:

Preparing patch pipettes

Before patching of a sample one needs to prepare the glass microelectrodes. The micropipettes were pulled from 100µL borosilicate glass capillaries (2-000-200; Drummond Scientific Company, Broomall PA, USA) using the P-97 Micropipette puller (Fig. A1 and details shown in A2; Sutter Instruments Company, Novato CA, USA). The capillaries were positioned using slidebars (d) and heated with a heating filament (c). When the glass is warm enough, the sliding bars pull on the capillary, thereby elongating and thinning it. When the movement of the sliding bars exceeds a preprogrammed value, the heating is stopped and the glass and heating filament are air cooled, using compressed (a) and dried air (b). The heating cycle can now be restarted. The temperature of the filament, the maximal speed of the sliding bar, the cooling time and the number of heating cycles can all be programmed (f). The display (e) shows the pulling program that is

activated, and, after pulling, it shows the number of heating cycles and the total time the filament was heated. A pulled pipette is shown in Fig. A3 (divisions on scale bar are 1mm); the diameter of the pipette tip is approximately 1µm.

When the radius of curvature of a patch is determined by differential interference contrast (DIC), the tip of the pipette used must be at an angle so that it can be placed in the focal plane of the microscope. To bend the pipette to the correct angle a microforge is used (Fig. A4; MF-830 Narishige International USA, Inc., East Meadow NY, USA). The pulled pipette is placed in micromanipulator (h) and placed close to heating filament (g). Using foot-switch (j) the filament is heated; the heat is transferred by convection and the pipette is heated on one side, causing it to bend towards the filament. The heat of the filament can be adjusted using knob k. One of the eyepieces (i) of the microforge contains a graded scale that can be used to exactly determine the angle of the pipette tip.

The patch clamp set-up

The patch-clamp set-up used for the experiments described in this thesis is shown in Fig. B. After pulling the pipettes, a sample is loaded into the patch clamp chamber (j). The bath is placed on the inverted microscope (c; Nikon, Tokyo, Japan) inside the Faraday cage (a), which decreases electrical noise around the set-up. The sample can be viewed using visible light (f). After connecting the glass micropipette to the electrode on the headstage (k), it can be brought into proximity of the sample using the coarse (d) and fine (e) tuning knobs of the micromanipulator. Using a manometer (h; World Precision Instruments Ltd., Stevenage, United Kingdom), a small positive pressure is applied inside the pipette to prevent sealing of unwanted particles in the sample. When the tip of the pipette is close to the desired spheroplast or membrane blister, the pressure is released (or even a negative pressure is applied), resulting in a giga-ohm seal.

The patch inside the pipette can be visualized with the charge-coupled device camera (b; Nikon, Tokyo, Japan). If the patch is visualized by a difference in calcein concentration across the patch membrane, the fluorescent light (g) from the back of the microscope is used in combination with the correct dichroic mirror settings inside the microscope. For illumination of the patch to effect the switching of azobenzene substituted amphiphiles, an external Hg-lamp (i; 180W, Newport Oriel Instruments, Irvine CA, USA) is added to the set-up. The light from the lamp has to be directed towards the bath using a fiber-optic cable as shown in Fig. B3 (m).

The channel currents measured by the electrode are transferred to the amplifier (n; Axopatch 200B, Axon instruments, Union city CA, USA) through an electrically isolated wire, the digidata® 1322A box (o; Axon instruments, Union city CA, USA), which converts the amplified current to a 0 – 1V signal that can be read by the computer (q). The computer records

the signal from the patch using Clampex software (Axon instruments, Union city CA, USA), which can also be used for the signal analysis. The final piece of peripheral equipment (Fig. B4) is the computer (p), which is used for recording images from the charge-coupled device camera (b).

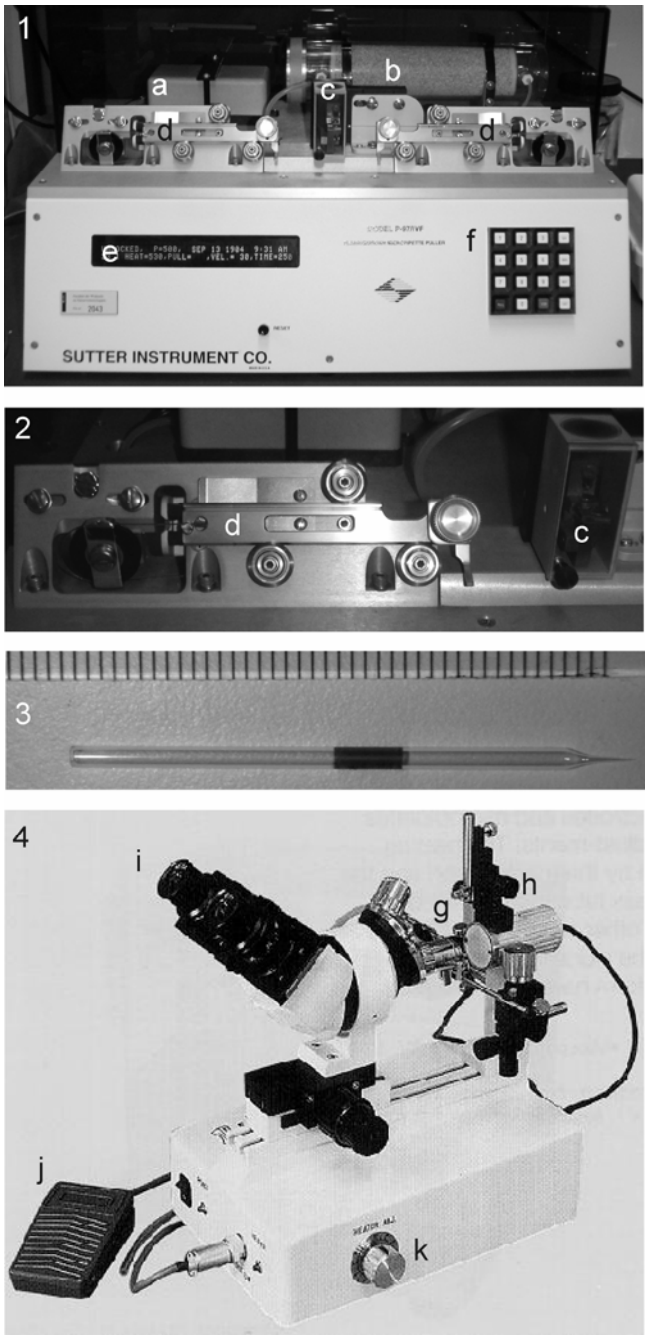

Figure A: Pulling micropipettes. (1) puller, (a) air compressor, (b) air drying compartment, (c) heating filament, (d) sliding bars (2x), (e) display and (f) keyboard; (2) detail of pipette puller; (3) pipette after pulling; (4) microforge, (g) heating filament, (h) pipette micromanipulator, (i) eyepiece, (j) foot-switch and (k) knob to set filament heat. For practical details see text.

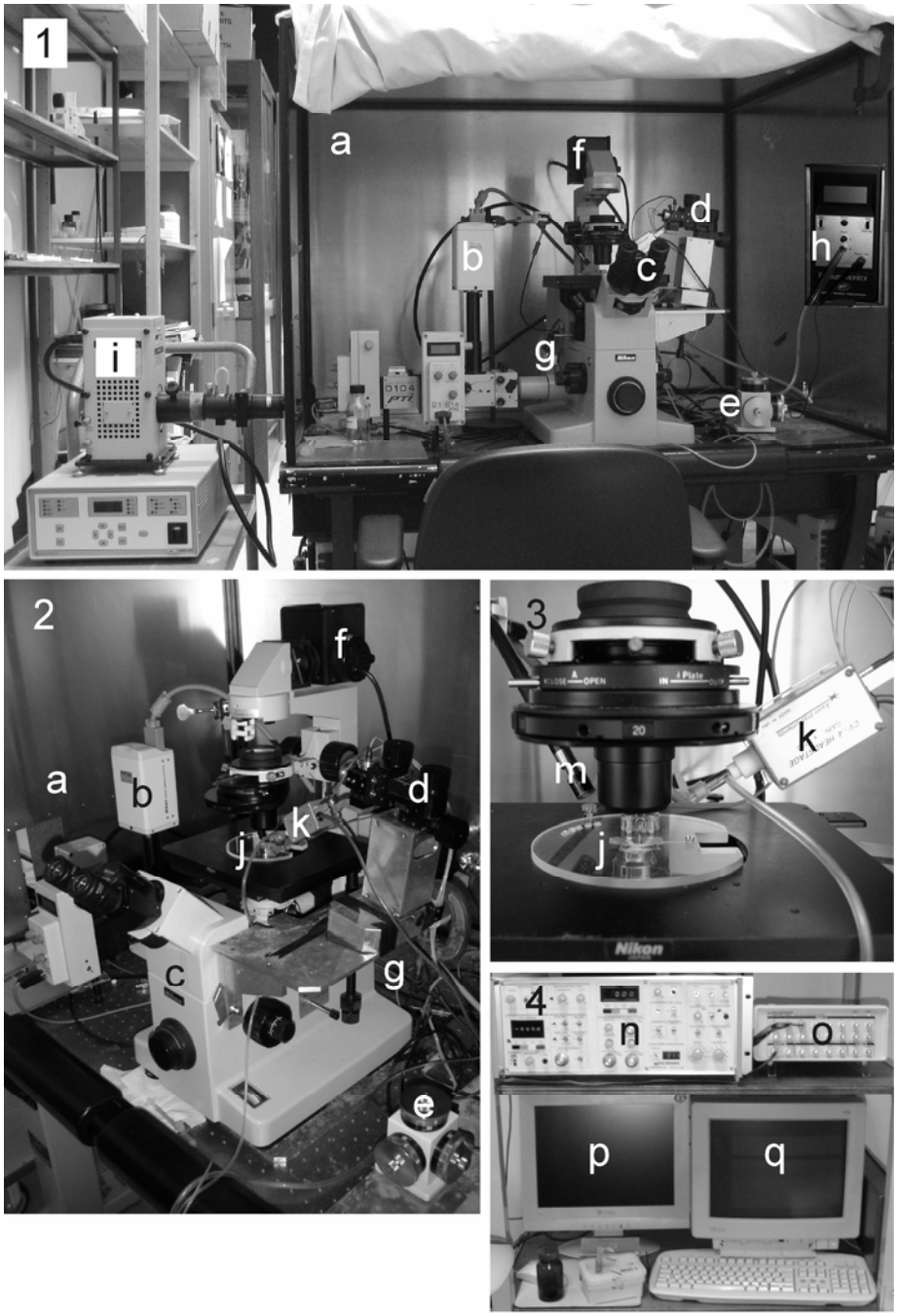

Figure B: The patch clamp set-up. (1) general overview of set-up, (a) Faraday cage, (b) charge-coupled device camera, (c) inverted microscope, (d) coarse tuning micromanipulator, (e) fine tuning micromanipulator, (f) visible light source for microscope, (g) light for fluorescence microscopy, (h) manometer and (i) Hg-light; (2) detail of inverted microscope showing (j) patch clamp chamber (or bath) and (k) headstage; (3) detail showing (j) chamber, (m) fiber-optic cable and (k) headstage; (4) peripheral equipment, (n) the signal amplifier, (o) the digi-data box, (p) computer for imaging and (q) Computer for electrical recordings. For practical details see text.

In developing single channel recordings relatively few modifications have been made to the basic techniques introduced by Müller and Rudin (who

introduced black lipid membrane technique) and Neher and Sackmann (who introduced the patch clamp technique). The improvements were mainly directed towards a higher signal to noise ratio, which was accomplished by the use of better amplifiers and improvements in the membrane seal. The membrane seal was improved by using micropipettes made from borosilicate glass, but also by decreasing the size of the pipette opening. Smaller pipette openings, and the resulting smaller patches led to a lower influence of membrane capacitive currents (in the order of ~ 1pA) on the channel current recording (11). Recently, developments have been directed towards high-throughput systems, which allow fast screening of channel activity in multiple patches in parallel and their in response to ligands or other stimuli. The first systems to be used as on-site user-friendly bio-sensors (12) and high-throughput drug-screening facilities (13) are now available. One area that seems to be underexposed is the use of the patch clamp technique in combination with other biophysical or biochemical methods. In chapter 3, we explore the possibilities of using proteo-GUVs for fluorescence correlation spectroscopy and patch clamp analysis, but other combinations of techniques seem possible and will be discussed further under ”Giant Unilamellar Vesicles”.

Using a modification of the patch clamp technique developed by Naher and Sackmann (14), the mechanosensitive channels of large and small conductance have been identified and characterized. The proteins responsible for these activities have also been crystallized to obtain structural insights into the functioning of the channel. However, the structure of only one conformation is available for each channel: for MscL (15), the (partially) closed conformation; for MscS (16), the (largely) open conformation. Ever since the structure of MscL has been available, researchers have attempted to link function to specific α-amino acid residues in the protein (17-20). An important recent result involves the assembly of the channel from split polypeptides. Oligomers of the N-terminal half, containing transmembrane helix 1 (TM 1), were able to form tension-insensitive channels. Oligomers assembled from the C-terminal part, containing transmembrane helix 2 (TM 2), were not able to form functional channels. However, if the two channel halves were expressed together, a fully functional channel was formed. The only difference with wild-type MscL was a higher gating tension for the channel made of the two split polypeptides. This work nicely showed that TM 1 is involved in channel formation, whereas TM 2 seems to play a major role in sensing the tension in the membrane (21).

Two applications of the MscL channel were discussed in chapter 1. The first application concerns the development of liposomal drug delivery systems, where the channel facilitates diffusion of hydrophilic compounds (e.g. anti-tumor drugs) across the membrane (22). A similar (channel-independent) application, based on polymer chemistry has recently been described (23). The polymers composed of poly(sodium 4-styrenesulfonate) and poly(allylamine hydrochloride) were mixed with the drug of interest, a stabilizer (4-(dimethylamino)pyridine) and gold particles of around 6nm in

diameter. The particle was subsequently coated with a single lipid bilayer, and the resulting capsules could be activated by 10ns light pulses from a near-infrared laser, which melted the gold-polymer particles and released the encapsulated drug. The second application involved the engineering of MscL to a pore with a metal-binding site, which essentially converted MscL to a ligand gated channel. This result shows that it is possible to add functionality to MscL, which may aid the further development of biosensors based on this channel (24).

A major challenge for the future is the elucidation at high resolution of the open conformation of MscL. Currently, several models for channel gating based on the closed structure and molecular modeling are available. Even though it is a powerful technique, modeling of molecular dynamics is always dependent on the parameters that are entered into the model by the experimenter. The open conformation would provide an end-point for the modeling of the gating mechanism. A mutant that can be locked in the open state is available, but so far, no crystals have been obtained using this mutant (25).

Characterisation of the mechanosenstive channels from Lactococcus lactis

Chapter 2 describes the identification and characterization of MscL and MscS from *Lactococcus lactis*. Both channels have properties similar to those previously reported for the corresponding *E. coli* proteins. MscS from *L. lactis* is the third characterized MscS-like channel and the second from a Gram-positive bacterium. An unexpected finding was that even though both *mscL* and *mscS* are expressed (at least at the level of mRNA), efflux of glycine betaine from *L. lactis* seems to be mediated mainly by MscL. This was confirmed by patch clamp measurements on membranes from an MscL disruption strain, in which mechanosensitive channel activity was no longer observed. However, when the MscS channel was produced in *Escherichia coli*, it did form functional mechanosensitive channels. As the mRNA for the MscS protein was normally produced, one would expect the protein to be synthesized by the cell, which leaves the question of how and why MscS activity in *L. lactis* is down-regulated. In a recent paper by Akitake *et al*. (26), it has been described that the activity of MscS from *E. coli* is influenced by the membrane potential. It is however unlikely that this parameter is the cause for the failure to detect any MscS activity in *L. lactis*, because, when the protein was heterologously produced in *E. coli*, channel activity was readily observed. Obviously, more research on the regulation of MscS synthesis and activity is required.

Giant Unilamellar Vesicles

Membrane protein studies are often carried out in so-called proteoliposomes. Frequently the formation of proteoliposomes involves the use of purified detergent-solubilized protein and detergent-destabilized liposomes, followed by removal of the detergent molecules (by dilution, dialysis or adsorption to polystyrene beads). Proteoliposomes have a

diameter of ~ 200nm and are called Large Unilamellar Vesicles (or LUVs). Although these LUVs are very useful for the analysis of transport across liposomal membranes, they are too small for techniques such as patch clamp or single molecule spectroscopy. In chapter 3, a method is presented for the preparation of Giant Unilamellar Vesicles (or GUVs), ranging in diameter from 5 to 50µm, into which a number of membrane proteins (MscL, OppA and LacS) have been successfully incorporated. Formation of GUVs is not a new in the sense of forming pure lipid vesicles (27-30). However, functional incorporation of membrane proteins in these GUVs is a challenge, as it requires the conservation of functional integrity of the membrane proteins, that is, during the de- and rehydration steps of the GUV formation process. This problem was overcome by the addition of low amounts of sucrose (or trehalose). These co-solvents are thought to stabilize proteins through hydrogen bonding with the polar groups of proteins during dehydration (31).

When (proteo)liposomes prepared from unsaturated lipids are dried the transition temperature (T_M) increases by 70-80°C (32). This means that the lipids go from a liquid crystalline to a gel phase, which causes lateral phase separation and may cause protein aggregation. Thus, sucrose most likely also plays a role by preventing this lateral phase separation (and presumably protein aggregation) by maintaining the membrane in the liquid crystalline phase; the sugars lower the T_M during drying with about 70°C (32). The sugar molecules exert this effect (replacing the evaporating water) by hydrogen-bonding to the lipid headgroups, thereby maintaining the spacing between the headgroups and preventing the membrane from going from the liquid-crystalline to the gel phase. The interactions of sucrose with the proteins and the maintenance of the liquid-crystalline phase of the membrane are most probably the determining factors for the stabilization of the studied proteins. However, while these co-solvents stabilized the proteins during dehydration, they inhibited fusion of the lipid membranes and thereby the formation of GUVs, when using conventional rehydration procedures (both in the presence and absence of divalent cations). This problem was largely overcome by the application of an AC electrical field (~ 6V/cm, 10Hz) during the rehydration process. The formed GUVs have been successfully used in FCS, patch clamp and biochemical assays (Chapter 3).

It has also been possible to prepare proteo-GUVs at low co-solvent concentrations in the absence of an AC electrical field, provided anionic lipids were present in the proteoliposomes (33). Still, if one would like to use GUVs in a high osmolarity medium, it is advisable to rehydrate proteo-GUVs in the presence of a high-concentration of co-solvents to prevent the liposomes from collapsing upon transfer to a high osmolarity medium. In these cases, the AC electrical field is required for proteo-GUV formation.

A potentially important development would be the combination of fluorescence microscopy and electrophysiology. For supported lipid bilayers, in which the support was sealed to the bottom of a chamber containing a buffer, such a set-up has already been realized. After placing the chamber inside a larger buffer-filled chamber, electrodes were placed in the inner

smaller chamber and outer larger chamber, and single channel currents could be measured. For FCS measurements, the lens of the confocal scanning microscope was submerged in the inner chamber (34). A similar set-up could be envisioned with GUVs. The added value would be that by using a fluorescent dye, different lipid domains (rafts), and possibly the partitioning of fluorescently-labeled proteins in these domains, can be observed by confocal scanning. By patching specific membrane domains, the channel functioning in the different lipid environments could be determined. If one of the electrodes would be inserted into the proteo-GUV (using a micropipette), the set-up would no longer require the use of the support and matching chamber combination.

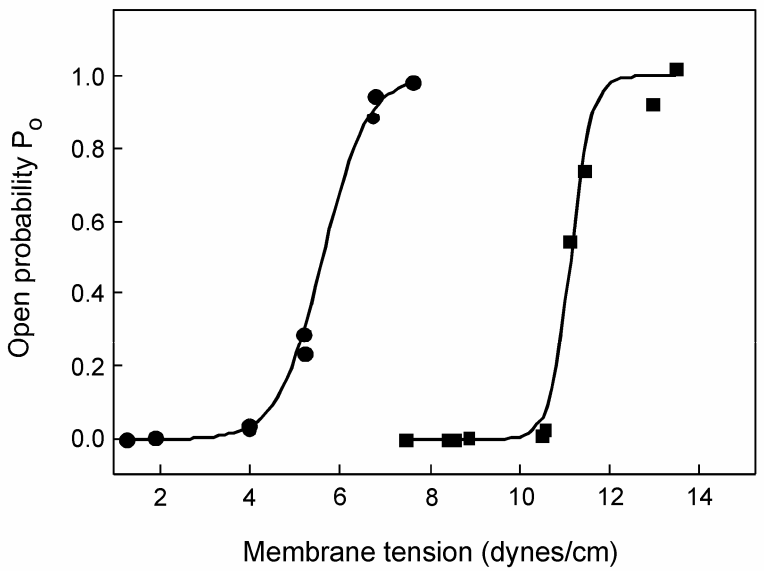

Figure 2: Dependence of MscL open probability on membrane tension for two lipid compositions. MscL from *E. coli* was reconstituted in liposomes with DOPC:DOPE at a ratio of 3:1 (●) or 1:3 (■). The shift in tension dependence shows that more energy is required to open MscL when the fraction of the non-bilayer forming lipid DOPE is increased. Graph after (35).

GUVs have also contributed to the analysis of the effect of lipid head-group composition on the MscL open probability. Previously, this was done by de- and rehydration of MscL proteoliposomes prepared from the desired lipid composition. However, the yield of membrane blisters suitable for forming giga-ohm seals is low and highly dependent on lipid composition of the membrane. Although the effect of variations in the DOPE:DOPC lipid ratio on the MscL open probability has been reported (Fig. 2 and 35), it is experimentally demanding to obtain these results. With a success rate of GUV formation of nearly 100%, it is now possible to prepare and study proteo-GUVs with a range of lipid compositions. Unfortunately, the next step in the process of patch clamp analysis is not straightforward and makes it laborious to obtain complete data-sets. The remaining problem relates to the stability of the membranes inside the pipette. To obtain open probability curves, it is

required that a patch can be loaded with tension until channel activity is saturated. Often the membrane seal ruptures before this point is reached. Many experiments, using proteo-GUVs, composed of different lipids, thus resulted in incomplete data sets.

To determine the tension dependence of channel opening, one does not only need to measure the channel activity, but also the membrane tension. According to Laplace, tension in the membrane can be calculated from T = ½ (p × r), in which p represents the applied pressure and r the radius of curvature of the patch (measured in the direction of the applied pressure, Fig. 3A). Therefore, to determine the tension, the applied pressure and the radius of the patch need to be known. The radius can be estimated from images obtained with a charge-coupled device (CCD) camera in combination with differential interference contrast (DIC) optics, as shown in Fig. 3B (35). However, DIC is not always suitable to accurately determine patch curvature, as the images often lack clear contrast between the patch and the surrounding medium. An alternative method was developed, in which 0.25mM calcein was added to the medium inside the patch-pipette. After seal formation, the patch would form a barrier between the bath solution, containing a low concentration of calcein (leaked from the pipette through diffusion before seal formation), and the buffer inside the pipette. Images obtained after illumination of the sample in the fluorescence mode of the microscope (Text-box 1) reflect the concentration of the probe on either side of the membrane, which simplifies accurate determination of the curvature of the membrane (barrier) inside the pipette (Fig. 3C).

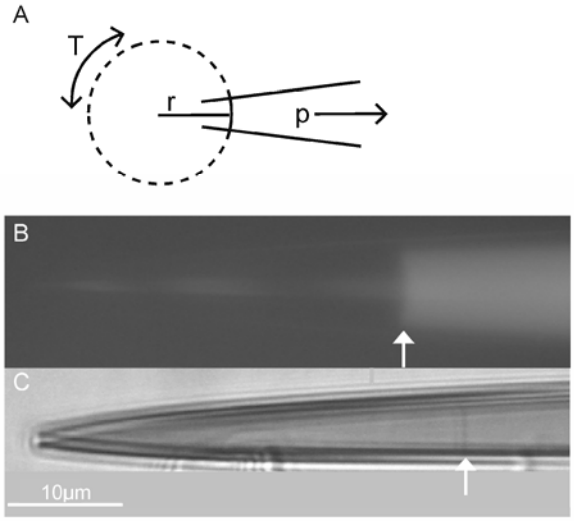

Figure 3: Using CCD images of a membrane inside a patch clamp pipette to determine radius of curvature of a patch. (A) Laplace's law defines the tension (T) developed within a bilayer as a function of the radius of curvature (r), and pressure (p) across the membrane. (B) Image taken in fluorescence mode. The patch separates a high (inside pipette) from a low concentration (bath solution) of calcein. (C) Image taken in differential interference contrast mode. The patch is visible as a dark line inside the pipette. Because of lower contrast, it is harder to determine curvature from this type of image than when a fluorophore is used. Size bar is 10µm; arrow indicates the position of the patch.

After full data-sets have been obtained, the tension dependence of the channel, in combination with pressure profile data (obtained from molecular modeling) for the MscL-containing membranes composed of different lipids, may help elucidate the osmosensing mechanism of MscL. In this respect, the mutants in the outward facing rim of MscL, seemingly involved in tension sensing (36), may be useful for such an analysis.

Switchable lipid mimic

Not only the lipid head-group properties determine the membrane lateral pressure profile and thereby the open probability of the MscL channel. Also, the packing of the lipid tails influence the profile in the membrane. Combining the heretofore described method of GUV formation with a lipid mimic with a switchable tail provided a method to modulate the lateral pressure profile within a single patch. Chapter 4 shows that 4-Azo-5P in a matrix of DOPC, switches from a *trans* to a *cis* conformation upon illumination with light at 365nm. With 20mol% of 4-Azo-5P in the membrane, the alteration of the membrane properties were large enough to increase the open probability of the MscL channel 4-fold. Not only could the channel be activated in this way, but when light with a wavelength > 400nm was used, the process was reversed and the open probability decreased.

The azobenzene-substituted amphiphiles might be used in future studies to further analyze the sensing moiety of MscL. Chapter 4 deals with a switch in the centre of the lipid tail. However, one could consider using similar mimics with the switchable azo-moiety closer to the lipid headgroup or closer to the center of the membrane bilayer (37). This could provide information on the depth in the membrane where MscL senses membrane tension. However, using the currently available azobenzene-substituted amphiphiles may not be optimal for this type of experiment as the *trans* conformation has a tendency to form H-aggregates during bilayer formation (37). One solution to this problem may be the synthesis of genuine phospholipids with the azobenzene moieties at different positions in the lipid tail.

Unfortunately, it was not possible to open MscL by switching the azobenzene-substituted amphiphiles from *trans* to *cis* alone. This problem was overcome by applying a small additional negative pressure in the patch pipette. A number of alternative approaches to make the light-dependent switching more effective were considered. One was increasing the mol% of azobenzene-substituted amphiphiles in the membrane, but previous studies had shown that this would result in leaky membranes upon switching (37). Alternatively, a lipid mimic with a single tail was considered as this would introduce asymmetric membrane bending in the membrane (38-40), that is, when it is added to one side of the membrane (and assuming slow transmembrane flip-flop). This bending together with the switch might result in a strong enough perturbation of the membrane tension to result in MscL activity without additional negative pressure. Although the amphipath has been synthesized (41), the patch clamp experiments still have to be carried out. Not only asymmetric bending, but also thinning of the membrane is

known to increase the open probability of MscL, so a 4-Azo-5P in combination with lipids of shorter tail lengths is another possibility to consider. Finally, one could mix 4-Azo-5P, 4-Azo-6P and 4-Azo-9P, with their switching moieties at different positions in the lipid tail, to elicit MscL activity without additional negative pressure. A combination of these azobenzene-substituted amphipaths may also minimize the tendency of the molecules to form H-aggregates.

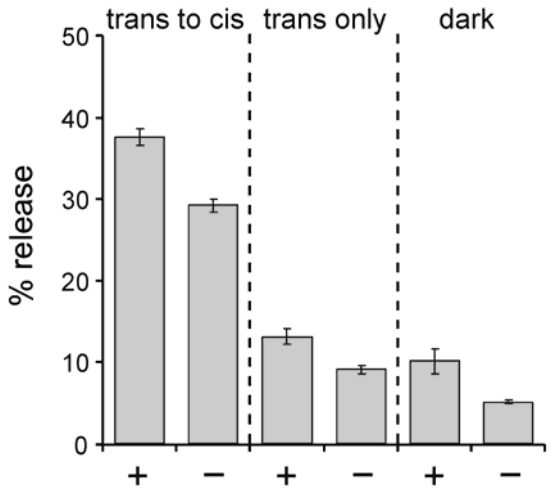

Figure 4: Calcein efflux from liposomes with (+) and without (–) MscL from *E. coli*. The lipid composition was DOPC:DOPE:4-Azo-5P in a 3:5:2 ratio. The first two bars indicate release from samples illuminated at 365nm (for 7min), left in the dark (for 5min) and then switched back by illumination at 436nm (for 1min). The second two bars indicate release from samples that were left in the dark (for 5min) and then illuminated at 436nm (for 1min). The last two bars indicate release from control samples which had been left in the dark for 6 min. The samples that had not been illuminated at 365nm, all released between 5 and 10% of the internal calcein. The samples that were switched released 28% (without MscL) and 37% (with MscL) of calcein, indicating that part of the release is MscL mediated. The 0% release (background) corresponds to the fluorescence intensity of the sample measured at t = 0; 100% release corresponds to the fluorophorescence intensity after the addition of 0.5% Triton X-100. The presented values correspond to the fluorescence intensity measured after treatment (illumination/dark) minus the background, relative to the fluorescence intensity after the addition of 0.5% Triton X-100 minus the background. Error bars indicate standard deviations; n = 3 for each bar.

An alternative method to monitor MscL channel activity in proteoliposomes is to determine the release of a fluorophore (Text-box 2). Using MTSET-mediated release of calcein (623Da) from G22C-MscL containing proteoliposomes, up to 60% of the calcein could be released via MscL. For the wild-type channel in combination with the 4-Azo-5P the release was 37% (± 1%), whereas the switching in liposomes without MscL resulted in a release of around 28% (Fig. 4). The possibilities to increase the efficacy of the lipid switch on MscL activity as described for the patch clamp experiments

could also be applied here. This was already done for the single tail 4-Azo-5P substituted amphipath, but the release of calcein was not improved (41).

Size exclusion limits of MscL in the open state

There has been a discussion in the literature about the release of small proteins like Thioredoxin (15kDa) and DnaK (21kDa) by MscL (46). To demonstrate that MscL could indeed facilitate the release of relatively large solutes, which does not necessarily imply that it actually happens *in vivo*, a modified efflux assay was used to follow the release of fluorescently-labeled macromolecules (Text-box 3).

It was observed that dextran (~ 2kDa) and Insulin (~ 6kDa) could be released via MscL G22C from *E. coli* upon MTSET treatment of the proteoliposomes (Fig. 5). It is evident that insulin release from proteoliposomes is slower than release of calcein or dextran, and that the larger molecule seems to be hindered in its passage through the MscL pore. In future experiments, Thioredoxin and DnaK should be considered, to resolve the issue, whether these even larger molecules can also pass through the MscL channel. Importantly, before other proteins are tested, one needs to be aware that the molecules may stick to the membrane surface of the proteoliposome or even to the filter itself, and proper controls need to be preformed.

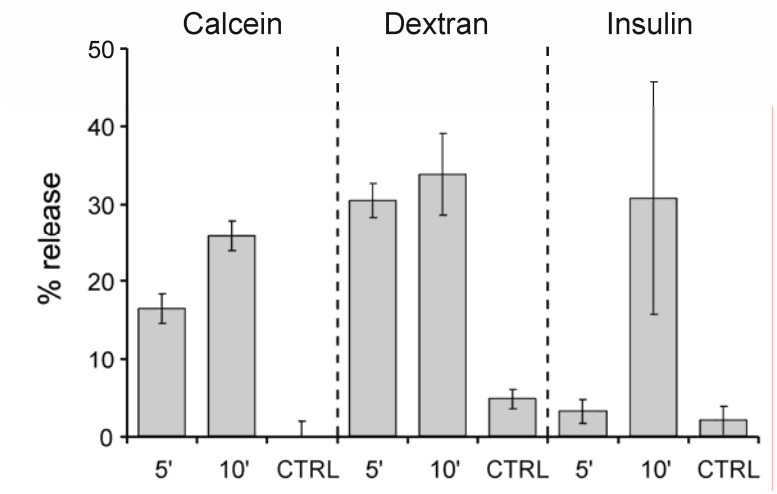

Figure 5: Macromolecule efflux from proteoliposomes containing MscL (G22C) from *E. coli*. The liposome composition was DOPC:Cholesterol in a 9:1 ratio. Samples were taken at 5 or 10min after addition of MTSET, or after 10min without any addition (CTRL). The first three bars indicate release of calcein, the middle three bars release of dextran (2 kDa), and the last three bars release of insulin (6kDa). The 0% release (background) corresponds to the fluorescence intensity of the sample measured at t = 0; 100% release corresponds to the fluorophorescence intensity after the addition of 0.5% Triton X-100. The presented values correspond to the fluorescence intensity measured after treatment (illumination/dark) minus the background, relative to the fluorescence intensity after the addition of 0.5% Triton X-100 minus the background. Error bars indicate standard deviations; n = 3 for each bar.

Text-box 2:

Release of calcein from MscL proteoliposomes (calcein efflux assay)

This method was developed in close collaboration with Robert Friesen from BioMaDe Technology Foundation. For experimental details see (42). In brief: proteoliposomes containing MscL were prepared as described (43). Calcein (final concentration of 25mM) was included by rapid-freezing (liquid nitrogen) and slow-thawing of the proteoliposomes. The external free calcein was removed by size exclusion column chromatography, using Sephadex G75 resin and isoosmotic wash buffer (10mM potasium phosphate, pH 8, 150mM NaCl, 1mM EDTA). For detection of fluorophore release, a 10-15µl proteoliposome fraction was placed in 2-4ml of wash buffer. Activity was measured as the increase in fluorescence upon calcein dequenching after release through the channel. Fluorescence was monitored at 520nm (slit-width 5nm; excitation at 490nm slit-width 2nm) using a SLM 500 spectrofluorometer. Release was expressed as percentage of the value obtained after lysing the proteoliposomes by the addition of 0.5% Triton X-100 (final concentration) and background subtraction.

Triggering release of calcein through MscL activation was performed in two ways:

1) It has been demonstrated that MscL can be activated by introduction of a charge at the pore constriction site. This has been achieved through modification by MTSET of a cysteine introduced at position 22 (44, 45). Using the G22C mutant of MscL from *E. coli*, the release of calcein from an MTSET-modified sample was up to 60% higher than the release from a non-treated sample.
2) Alternatively, MscL in proteoliposomes containing 20mol% of 4-Azo-5P can be activated by light (chapter 4). In this case activation occurs through illumination at 365nm for 7 min in the presence of 1mM tetracaine. Tetracaine was added to overcome the problem that 20mol% of 4-Azo-5P alone was not sufficient to activate MscL. Tetracaine causes asymmetric bending of the membrane which decreases the energy barrier required for MscL opening (39). The concentration of tetracaine was chosen such that opening of MscL in the dark was minimal. After illumination, the samples were left in the dark for 5min to allow maximal release of calcein through the channel. To create an end-point to the release, the activation was reversed by illumination for 60s using light at 436nm. To compensate for the effect of the second illumination, control samples were left in the dark for 6min before measuring; to compensate for the effect of the 60s illumination at 436nm, samples were left in the dark for 5min and then illuminated at 436nm for 1min. An additional control involved the use of liposomes, not containing MscL, prepared via the same reconstitution procedure as the proteoliposomes. These liposomes were subjected to the same illumination schemes.

Text-box 3:

Release of macromolecules

Release of macromolecules from MscL containing proteoliposomes was monitored with carboxy-fluorescein-labeled proteins or dextrans that were included in the proteoliposome lumen. As the concentration of these probes was not high enough for self quenching, the liberated probes had to be separated from the proteoliposomes. This was done by filtration of the proteoliposomes over 200nm nitrocellulose filters. The release was determined as a percentage of the total amount of fluorophore labeled macromolecule inside the proteoliposomes; the 100% value was obtained by lysing the proteoliposomes with 0.5% Triton X-100 (final concentration) and background subtraction.

Pentamer

The final chapter of this thesis deals with a structural aspect of MscL. It has been shown that MscL from *Mycobacterium tuberculosis* has a pentameric arrangement of its subunits (16). In this thesis, we show that *in vivo* MscL from *E. coli* also assumes a pentameric quaternary structure. For future studies, it is important to purify and functionally reconstitute the pentameric tandem construct. Two relatively simple adaptations to the purification method described in chapter 5 should be considered to prevent protein aggregation and/or degradation. Firstly, the fused gene construct could be transferred to *L. lactis*, where the machinery for protein synthesis might be better capable of coping with the stress associated with membrane protein amplification. Secondly, one could consider preparing longer linkers between the sub-units, thereby diminishing potential folding problems that may arise from the two-amino acid linkers that were used (also see discussion of chapter 5). Introduction of a protein cleavage site in these linkers would enable cleavage of the subunits after reconstitution, which might release potential strain in the subunit interactions as a result of the short linkers. The channel would still be formed from the same originally linked subunits, assuming that subunits are not exchanged between channels once they are assembled in the membrane.

Using the covalently linked pentameric construct (or the complex after specific proteolytic cleavage), mutations could be introduced into individual subunits so that only one (rather than five) substitution is present per channel. This could, for instance, be used to determine the number of charges (MTSET molecules) required to open the MscL (G22C) from *E. coli*, which would provide an estimate of the strength of electronic repulsion needed for channel gating. Alternatively, a donor-acceptor pair (e.g., a single Trp combined with single Cys labeled with a coumarin-derived fluorophore (e.g. Alexa 350) as a fluorescence acceptor (47)) could be used to obtain distance information of the channel in the open and closed conformations by using fluorescence resonance energy transfer (FRET). Also, fluorophores could be linked to the

constriction site of the channel and passage of acceptor / quencher molecules could be monitored.

Conclusions

In the past decade a lot of information has been gathered on the structure, function and mechanism of MscL. Even so many questions remain about the actual gating mechanism of the channel. Application of MscL in drug delivery systems also requires further insight into the channel functioning. Other challenges can be found in the functioning of MscS and MscK, the regulation of channel expression, and the importance of protein lipid interactions. Ultimately, many of these questions rely on the availability of high-resolution structures of the channels in the closed, partially open, and fully open conformation.

Reference List

1. Poolman, B., Blount, P., Folgering, J.H.A., Friesen, R.H., Moe, P.C. and van der Heide,T.H. (2002) *Mol. Microbiol.* **44,** 889-902
2. Csonka, L.N. and Hanson, A.D. (1991) *Annu. Rev. Microbiol.* **45,** 569-606
3. Morbach, S. and Kramer, R. (2002) *Chembiochem.* **3,** 384-97
4. Wood, J.M., Bremer, E., Csonka, L.N., Kraemer, R., Poolman, B., van der, H.T. and Smith, L.T. (2001) *Comp. Biochem. Physiol. A Mol. Integr. Physiol.* **130,** 437-60.
5. van der Heide,T. and Poolman,B. (2000) *J. Bacteriol.* **182,** 203-6
6. van der Heide,T., Stuart,M.C., and Poolman,B. (2001) *EMBO J.* **20,** 7022-32
7. Poolman, B., Spitzer, J.J. and Wood, J. (2004) *Biochim. Biophys. Acta* **1666,** 88-104
8. Biemans-Oldehinkel, E. and Poolman, B (2005) to be published
9. Cantor, R.S. (1999) *Biophys. J.* **76,** 2625-39
10. Picolini, M. (1998) *Brain Res. Bull.* **46,** 381-407
11. Auerbach, A. and Sachs, F. (1984) *Ann. Rev. Biophys. Bioeng.* **13,** 269-302
12. www.nanion.de
13. www.axon.com
14. Neher, E. and Sakmann, B. (1976) *Nature* **260,** 799-802
15. Chang, G., Spencer, R.H., Lee, A.T., Barclay, M.T. and Rees, D.C. (1998) *Science* **282,** 2220-6
16. Bass, R.B., Strop, P., Barclay, M. and Rees, D.C. (2002) *Science* **298,** 1582-7
17. Blount, P., Schroeder, M.J. and Kung, C. (1997) *J. Biol. Chem.* 1997 **272,** 32150-7
18. Blount, P., Sukharev, S.I., Schroeder, M.J., Nagle, S.K. and Kung, C. (1996) *Proc. Natl. Acad. Sci. USA* **93,** 11652-7
19. Maurer, J.A. and Dougherty, D.A. (2003) *J. Biol. Chem.* **278,** 21076-82
20. Yoshimura, K., Batiza, A., Schroeder, M., Blount, P. and Kung, C. (1999) *Biophys. J.* **77,** 1960-72
21. Park, K.H., Berrier, C., Martinac, B. and Ghazi, A. (2004) *Biophys. J.* **86,** 2129-36
22. www.biomade.nl/channel.htm
23. Radt, B., Smith, T.A. and Caruso, F. (2004) *Adv. Mater.* **16,** 2184-9
24. Iscla, I., Levin, G., Wray, R., Reynolds, R. and Blount, P. (2004) *Biophys. J.* **87,** 3172-80
25. Shapovalov, G., Bass, R., Rees, D.C. and Lester, H.A. (2003) *Biophys. J.* **84,** 2357-65
26. Akitake, B., Anishkin, A. and Sukharev, S. (2005) *J. Gen. Physiol.* **125,** 143-54
27. Angelova, M.I., Soléau, S., Méléard, Ph., Faucon, J.F. and Bothorel, P. (1992) *Progr. Colloid Polym. Sci.* **89,** 127-31

28. Akashi, K., Miyata, H., Itoh, H., and Kinosita, K.Jr. (1996) *Biophys. J.* **71,** 3242-50
29. Akashi, K., Miyata, H., Itoh, H. and Kinosita, K.Jr. (1998) *Biophys. J.* **74,** 2973-82
30. Korlach, J., Schwille, P., Webb, W.W. and Feigenson, G.W. (1999) *Proc. Natl. Acad. Sci.* USA **96,** 8461-6
31. Crowe, J., Crowe, L.M., Carpenter, J.F., Rudolph, A.S., Wistrom, C.A., Spargo, B.J. and Anchordoguy, T.J (1988) *Biochim. Biophys. Acta* **947,** 367-84
32. Ricker, J.V., Tsvetkova, N.M., Wolkers, W.F., Leidy, C., Tablin, F., Longo, M. and Crowe, J.H. (2003) *Biohys. J.* **84,** 3045-51 (JHC personal communication)
33. Doeven, M.K., Folgering, J.H., Krasnikov, V., Geertsma, E.R., van den Bogaart, G. and Poolman, B. (2005) *Biophys. J.* **88,** 1134-42
34. Hemmler, R., Böse, G.,Wagner, R. and Peters, R. (2005) *Biophys. J.* **88,** 4000-7
35. Moe, P.C. and Blount, P. (2002) *Biophysical Chemistry: Membranes and Proteins (Ed: Templer, R.H. and Leatherbarrow, R.)* 199-207
36. Yoshimura K, Nomura T, Sokabe M. (2004) *Biophys. J.* **86,** 2113-20
37. Kuiper, J.M. and Engberts, J.B.F.N. (2004) *Langmuir* **20,** 1152-60
38. Perozo, E., Kloda, A., Cortes, D.M. and Martinac, B. (2002) *Nat. Struct. Biol.* **9,** 696-703
39. Elmore, D.E. and Dougherty, D.A. (2003) *Biophys. J.* **85,** 1512-24
40. Martinac, B., Adler, J. and Kung, C. (1990) *Nature* **348,** 261-3
41. Kuiper, J.M. and Engberts, J.B.F.N. (2005) Chapter 5: Single tailed azobenzene-substituted phosphates Ph.D. *Thesis* 107-126
42. Koçer, A., Walko, M., Meijberg, W. and Feringa, B.L. (2005) *Science* in press
43. Folgering, J.H.A., Moe, P.C., Schuurman-Wolters, G.K., Blount, P. and Poolman, B. (2005) *J. Biol. Chem.* **280,** 8784-92
44. Batiza,A.F., Kuo,M.M., Yoshimura,K., and Kung,C. (2002) *Proc. Natl. Acad. Sci. USA* **99,** 5643-8
45. Yoshimura,K., Batiza,A., and Kung,C. (2001) *Biophys. J.* **80,** 2198-206
46. Vazquez-Laslop, N., Lee, H., Hu, R. and Neyfakh, A.A. (2001) *J.Bacteriol.* **183,** 2399-404
47. probes.invitrogen.com/handbook/sections/0203.html

Nederlandse samenvatting voor niet vakgenoten

Inleiding

De cellen van levende organismen zijn omgeven door een celmembraan. De celmembraan scheidt het interne van de cel van het externe milieu. De membraan is semi-permeabel, wat betekent dat het wel water doorlatend is, maar dat grotere en geladen deeltjes de membraan niet kunnen passeren. Om in leven te blijven moeten de cellen ervoor zorgen dat er een balans is tussen stoffen die de cel in komen en verlaten. We noemen die balans "homeostase".

Door een proces dat osmose (Figuur 1) wordt genoemd, stroomt het water door een semi-permeabel membraan van de kant waar de concentratie van opgeloste stoffen laag is naar de kant waar deze hoger is, totdat een evenwicht is bereikt. Wanneer de stroming wordt beperkt door een barrière (bij de bacterie is dat de celwand, die nog om de membraan heen zit en zorgt voor de versteviging van de cel), kan er een druk worden opgebouwd. Deze zogenaamde osmotische druk is gerelateerd aan het aantal opgeloste deeltjes. Voor het beschrijven van deze osmotische druk heeft de Nederlander Johannes van 't Hoff in 1901 de Nobelprijs ontvangen. Doordat de oplossingen in de cel sterk geconcentreerd zijn, kan de osmotische druk oplopen tot enkele honderden malen de atmosferische druk. Deze hoge druk wordt door bijvoorbeeld plantencellen gebruikt voor de stevigheid van de plant. Als de druk in de plantencellen wegvalt, zal de plant verwelken. Om dit onder normale omstandigheden te voorkomen, zijn er in de cel eiwitsystemen aanwezig, die erop gericht zijn om een bepaalde druk aan te leggen en/of in stand te houden.

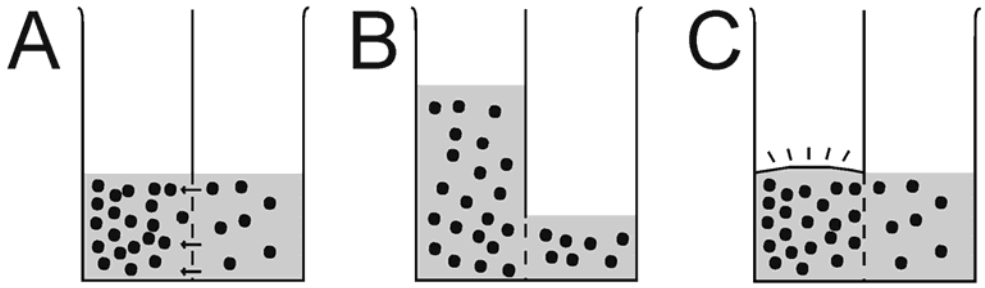

Figuur 1: Osmose. In afbeelding A wil het water van het rechter compartiment naar het linker, om zo ervoor te zorgen dat de verdeling van deeltjes links en rechts gelijk is. Afbeelding B laat het eindresultaat van de herverdeling van het water zien. In afbeelding C is het volume in het linker compartiment vastgezet. Hierdoor kan het water niet meer verder het compartiment instromen, en ontstaat er een osmotische druk in dat compartiment.

Bacteriën zijn eencellige organismen die op de meest uiteenlopende plaatsen kunnen worden gevonden. Zo zijn er bacteriën die leven in het poolijs, maar ook die leven op een vulkaan. Ook wat osmotische condities betreft zijn bacteriën te vinden in uiteenlopende milieus. Zo komen ze voor in een plas regenwater, maar er zijn ook soorten die leven in de zoutpannen waar zout uit zeewater wordt gewonnen. Deze omgevingen hebben echter geen constante osmotische waarde. Als het bijvoorbeeld regent wordt het

zout in de zoutpan verdund (dit noemen we een neerwaartse osmotische verschuiving), of als de zon schijnt verdampt het water uit een plas regenwater, waardoor de daarin opgeloste deeltjes worden geconcentreerd (dit noemen we een opwaartse osmotische verschuiving). De bacteriële cel heeft verschillende mechanismen om de gevolgen van beide typen osmotische verschuivingen op te kunnen vangen. Het gevolg van een opwaartse osmotische verschuiving is dat water de cel zal verlaten waardoor deze ineen krimpt. Hierdoor zullen processen in de cel worden verstoord. Om het verschrompelen te voorkomen kan een bacteriecel osmotisch actieve deeltjes aanmaken of uit het milieu opnemen.

Het gevolg van een neerwaartse osmotische verschuiving voor een bacterie is dat water van buiten de cel naar binnen zal stromen. Hierdoor zal het volume van de cel toenemen. De membraan en celwand, die de cel aan de buitenkant verstevigen, kunnen niet onbeperkt worden uitgerekt, en zullen uiteindelijk knappen net als een ballon waar teveel lucht in wordt geblazen. Om dit te voorkomen, beschikken bacteriën over eiwitten die als veiligheidsventielen werken en in reactie op de rek (tensie) in de membraan openen. Als de ventielen open zijn, kunnen water en opgeloste deeltjes de cel verlaten en het osmotische evenwicht tussen de cel en zijn omgeving kan worden hersteld. Als dat is gebeurd, sluiten de ventielen zich weer. De ventielen worden mechanogevoelige (of ook wel mechanosensitieve) kanalen genoemd, en zij zijn het onderwerp van studie geweest voor dit proefschrift.

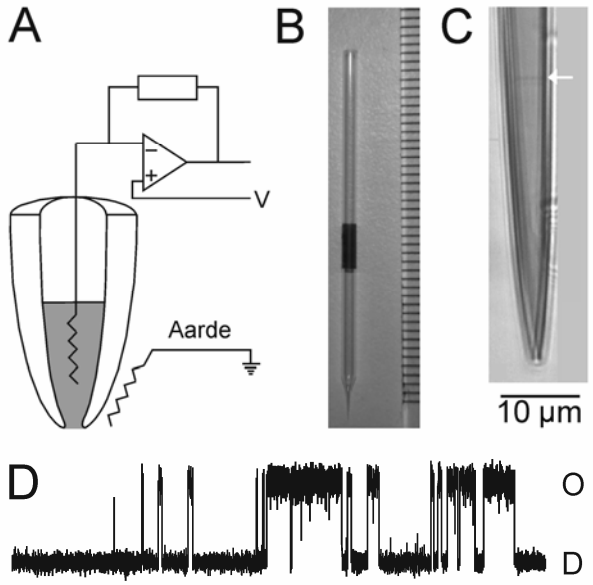

Figuur 2: Patch-clamp. Afbeelding A geeft een schematische weergave van een patch pipet aangesloten op een versterker weer. Het drijvende voltage (dat uiteindelijk de ionen-stroom drijft) wordt gezet over de electrode in de pipet en de geaarde electrode buiten de pipet (zig-zag lijnen geven de electrodes weer). Afbeelding B laat een volledige glazen pipet zien, de schaal ernaast is in milimeters. Afbeelding C laat een microscopische uitvergroting van de punt van de pipet zien, bij het pijltje zit een patch (stukje van een celmembraan). De schaal onder de afbeelding is 10 micrometer. Afbeelding C laat een typerend gemeten elektrisch signaal in de loop van de tijd zien. Helemaal links op tijdstip 0 is de stroom 0 pico-ampère, verder naar rechts zien we dan dat in de loop van de tijd het electrisch signaal omhoog gaat, en later weer omlaag. Het hoge signaal weerspiegelt de open toestand van het kanaal (rechts aangegeven met een O), het lage signaal de dichte toestand (rechts aangegeven met een D).

Het bestuderen van mechanosensitieve en andere eiwitkanalen

Een van de manieren waarop kanaaleiwitten kunnen worden bestudeerd is door middel van patch-clamp. Hierbij wordt een klein stukje van de celmembraan (een "patch") vastgepakt (ge-"clamped") met een glazen buisje (pipet) met een tipdiameter van slechts 1 micrometer (µm). Zowel in de pipet als rond de cellen zijn veel opgeloste ionen (zouten) aanwezig (Figuur 2A-C). Door een voltage over de membraan aan te leggen zou een stroom gemeten kunnen worden als de membraan niet impermeabel was voor ionen. Als door een onderdruk in de pipet de membraan onder tensie komt te staan zullen de mechanosensitieve kanalen openen. Door een open kanaal kunnen per seconde 100 miljoen ionen stromen. Het aangelegde voltage zorgt ervoor dat dit ook gebeurt, en er kan een stroom (van enkele pico-Ampères) gemeten worden. Om deze stroom te kunnen meten moet hij eerst worden versterkt. Hiervoor is in de opstelling een versterker aanwezig. De versterker geeft het signaal door aan een computer die de grootte van de gemeten stroom opslaat. Met de door de computer opgeslagen gegevens is het mogelijk om te zien wanneer het kanaal open staat (Figuur 2D). Een meer gedetailleerde beschrijving van de opstelling is te vinden in hoofdstuk 6 (text-box 1). Met behulp van het aangelegde voltage en de gemeten stroom kan de zogenaamde geleiding (doorlaatbaarheid van het kanaal voor ionen) van een kanaal worden bepaald. Geleiding is het omgekeerde van elektrische weerstand; met behulp van de wet van Ohm kan de geleiding als volgt worden uitgedrukt: G = I / V (geleiding = stroom / voltage).

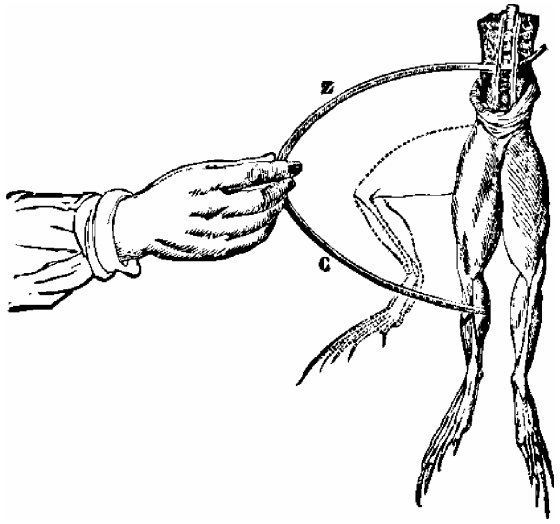

Figuur 3: De experimenten van Volta en Galvani. Een vrij geprepareerde kikkerpoot wordt met een passer op 2 plaatsen gelijktijdig aangeraakt. Door deze prikkeling trekt de pootspier samen en buigt. Ditzelfde gebeurt als de pootspier met behulp elektrische prikkels wordt gestimuleerd.

Hoewel het meten van kanaalactiviteit tegenwoordig een relatief eenvoudige bezigheid is, is dat niet altijd zo geweest. Tot het einde van de 18^{e} eeuw was het onbekend dat bepaalde biologische processen (zoals het samentrekken van een spier) geregeld werden door elektrische signalen van cellen. In die tijd onderzochten Luigi Galvani en Allesandro Volta spiersamentrekkingen van kikkerpoten door deze met fysieke of elektrische prikkels te stimuleren (Figuur 3). Halverwege de 19^{e} eeuw werden ook de eerste succesvolle pogingen ondernomen om de elektrische signalen van

spiercellen te meten. Pas in 1976 werd het ook mogelijk om de activiteit van individuele kanalen te meten, met behulp van speciale signaalversterkers en kleine glazen pipetten (Figuur 2A-C). Erwin Neher en Bert Sakmann die het systeem hebben ontwikkeld kregen in 1991 hiervoor de Nobelprijs voor de geneeskunde. De eerste bacteriële mechanosensitieve kanalen werden ontdekt in de bacterie *Escherichia coli* en beschreven in 1994 door Sergei Sukharev, Paul Blount, Boris Martinac, Frederic Blattner en Ching Kung. De kanalen werden geïdentificeerd op basis van de grootte van de geleiding en kregen de namen mechanosensitief kanaal van grote geleiding (in het Engels: Mechanosensitive channel of Large conductance of kortweg MscL) en mechanosensitief kanaal van kleine geleiding (in het Engels: Mechanosensitive channel of Small conductance of kortweg MscS).

Functie en vorm van mechanosensitieve kanalen

Het tweede hoofdstuk van dit proefschrift beschrijft de identificatie van deze twee typen kanalen uit de melkzuurbacterie *Lactococcus lactis*. Tevens worden eigenschappen als geleiding, gevoeligheid voor membraanspanning en de overgangen en tijdsduur van het open en dichtgaan van het kanaal beschreven. *Lactococcus lactis* wordt gebruikt in de bereiding van bijvoorbeeld kaas en yoghurt. De osmotische druk van de omgeving van de bacteriën wordt tijdens de bereidingsprocessen steeds hoger. Om te kunnen overleven als de osmotische druk van de omgeving plotseling zou dalen, hebben de bacteriën een eigen veiligheidsventiel. Wat betreft geleiding en gevoeligheid voor membraanspanning lijken de kanalen van *Lactococcus lactis* erg op die van *Escherichia coli*. Een duidelijk verschil is dat MscL van *Lactococcus lactis* veel korter open blijft staan dan MscL van *Escherichia coli*. Daarnaast blijkt dat het MscL kanaal voor deze bacterie het belangrijkste veiligheidsventiel is, en dat het MscS kanaal onder de geteste omstandigheden niet gebruikt wordt. Dit is bijzonder, aangezien tot nu toe werd aangenomen dat beide kanalen in alle bacteriën een vergelijkbare bijdrage leverden aan de vermindering van spanning in de cel membraan.

Figuur 4 laat een sterke uitvergroting zien van het MscL kanaal uit de bacterie *Mycobacterium tuberculosis*. Het is te zien dat het eiwit is opgebouwd uit vijf identieke eenheden. Voor het maken van de uitvergroting is een groot aantal kanalen uit hun natuurlijke omgeving (de celmembraan) gehaald en bekeken met behulp van Röntgenstraling. De zo verkregen informatie over hoe het kanaal eruit ziet, geldt dus niet noodzakelijk voor hoe het kanaal eruit ziet in de membraan. Ook wil het niet zeggen dat in alle andere bacteriën het kanaal er zo uit ziet. Zo zijn er in het verleden aanwijzingen gevonden dat het MscL kanaal in *Escherichia coli* opgebouwd zou kunnen zijn uit zes dezelfde eenheden. In hoofdstuk 5 van het proefschrift wordt een methode gepresenteerd om te bepalen wat het aantal eenheden is dat nodig is om een normaal functionerend MscL kanaal te maken.

De methode hield in dat de bacteriën genetisch werden gemodificeerd, zodat de eenheden niet los van elkaar konden worden geproduceerd. Eerst werden twee eenheden aan elkaar vastgezet, daarna ook drie, vier, vijf en zelfs zes. De aan elkaar gezette eenheden worden ook wel multimeren genoemd. Het blijkt dat bij vijf eenheden aan elkaar de tensiegevoeligheid van de kanalen die gevormd werden door deze multimeren gelijk was aan die van kanalen die opgebouwd waren uit de oorspronkelijke, losse eenheden. Voor

alle andere multimeren gold dat de kanalen meer tensie nodig hadden voordat ze open gingen. Daarnaast zijn er aanwijzingen gevonden dat kanalen opgebouwd uit losse eenheden net zo groot zijn als kanalen die zijn gevormd met de vijf aan elkaar vastzittende eenheden. Beide waarnemingen wijzen er op dat ook in de membraan van *Escherichia coli* het MscL kanaal is opgebouwd uit vijf dezelfde eenheden.

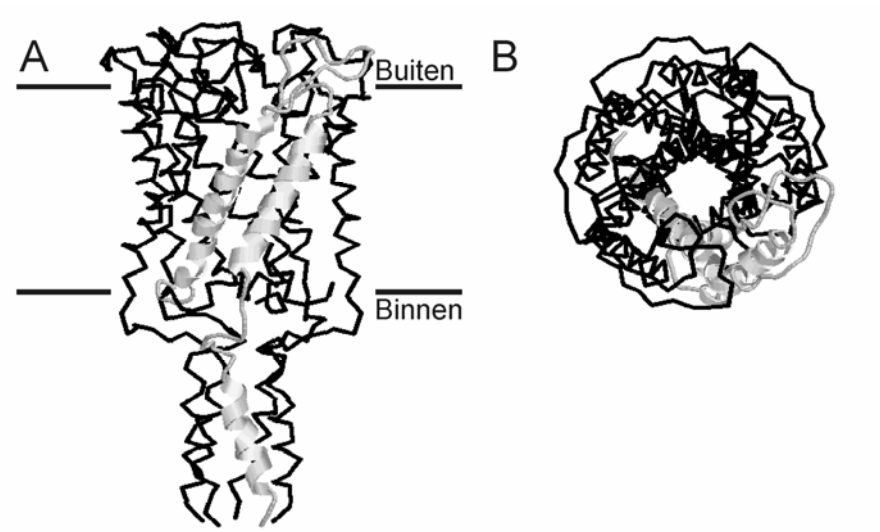

Figuur 4: Uitvergroting van het MscL kanaal van *Mycobacterium tuberculoses*. Afbeelding A laat het kanaal van de zijkant zien, afbeelding B laat een bovenaanzicht zien. In afbeelding A is met strepen ook weergegeven waar men verwacht dat de membraan zich bevindt ten opzichte van het kanaal. Bij de membraan staan aangegeven wat de binnen- en buitenkant van de bacteriecel zou zijn. Vooral in het bovenaanzicht is de vijfvoudige symmetrie van het kanaal goed te zien. Een van de vijf eenheden waaruit het kanaal is opgebouwd is in grijs weergegeven.

Het meten van kanaalactiviteit in kunstmatige systemen

In veel situaties is het handig om eiwitten te bestuderen buiten hun natuurlijke omgeving, zodat er geen invloeden zijn van processen in de cel. Om dit te doen is het mogelijk de eiwitten uit de bacteriecellen te halen waarin ze zijn geproduceerd. Voor membraaneiwitten is het echter lastig om de functie te bestuderen in de afwezigheid van de membraan. Om die reden worden membraaneiwitten regelmatig in kunstmatige cellen teruggeplaatst. Deze kunstmatige cellen, die alleen bestaan uit een membraan en het te bestuderen eiwit, worden proteo-liposomen genoemd. De membraan van de proteo-liposoom is opgebouwd uit dezelfde stoffen als de membraan van een bacterie, namelijk uit lipiden.

De meeste proteoliposomen zijn na preparatie tussen de 0.1 en 0.5µm in doorsnede en worden ook wel Large Unilamellar Vesicles of kortweg LUVs genoemd. Het bekijken van de kanaalactiviteit in deze LUVs levert gezien hun geringe grootte een probleem op: immers, de doorsnede van de pipetten die bij patch-clamp worden gebruikt is 1µm. Het is dus niet mogelijk om een stukje uit de membraan vast te pakken met de pipet. In plaats daarvan zouden de LUVs in hun geheel verdwijnen in de pipet. In hoofdstuk 4 van dit proefschrift wordt een methode beschreven voor het prepareren van extra grote proteoliposomen.

De LUVs worden volgens een standaardmethode geprepareerd en vervolgens gedroogd op een glazen plaatje. Dit plaatje is voorzien van een

dunne laag van elektrisch geleidend materiaal. Het plaatje met de gedroogde proteoliposomen wordt vervolgens op een afstand van ongeveer één millimeter geplaatst tegenover een zelfde plaatje zonder proteoliposomen (Figuur 5A). De ruimte tussen de plaatjes wordt gevuld met een oplossing met heel weinig zout. Het drogen en rehydrateren van de proteoliposomen zorgt ervoor dat deze samensmelten. Hierdoor ontstaan grote proteoliposomen met een diameter van 5 tot 50µm. Deze proteoliposomen zijn dus tot 100 keer groter dan de LUVs, en worden daarom ook wel Giant Unilamellar Vesicles (kortweg GUVs) genoemd.

Om te voorkomen dat de eiwitten tijdens het drogen op het glasplaatje kapot gaan moet in sommige gevallen een stabiliserende stof worden toegevoegd. Echter hoe meer van de stabiliserende stof wordt toegevoegd, hoe moeilijker de proteoliposomen samensmelten om GUVs vormen. Om toch GUVs te krijgen, kunnen de plaatjes worden aangesloten op een wisselspanningsbron, die met een frequentie van 10Hz (10 keer per seconde) de spanning wisselt van + naar – 1.2 Volt (Figuur 5B). Het elektrische veld dat zo ontstaat tussen de twee plaatjes versterkt het versmeltingproces zodat toch GUVs gevormd kunnen worden. Voor de formatie van GUVs met MscL kanalen is zelfs een extra hoge concentratie van de stabiliserende stof, en daarom ook het elektrische veld nodig. Zou deze hoge concentratie niet aanwezig zijn, dan zouden de GUVs ineen schrompelen, omdat ze vanuit een omgeving met weinig zout (tijdens de rehydratatie) worden overgebracht naar een omgeving met hoog zout (nodig om de stroom te kunnen meten) in de patch-clamp opstelling. Dit is vergelijkbaar met een bacterie- of plantencel in een situatie met een opwaartse osmotische verschuiving (de plant gaat slap hangen).

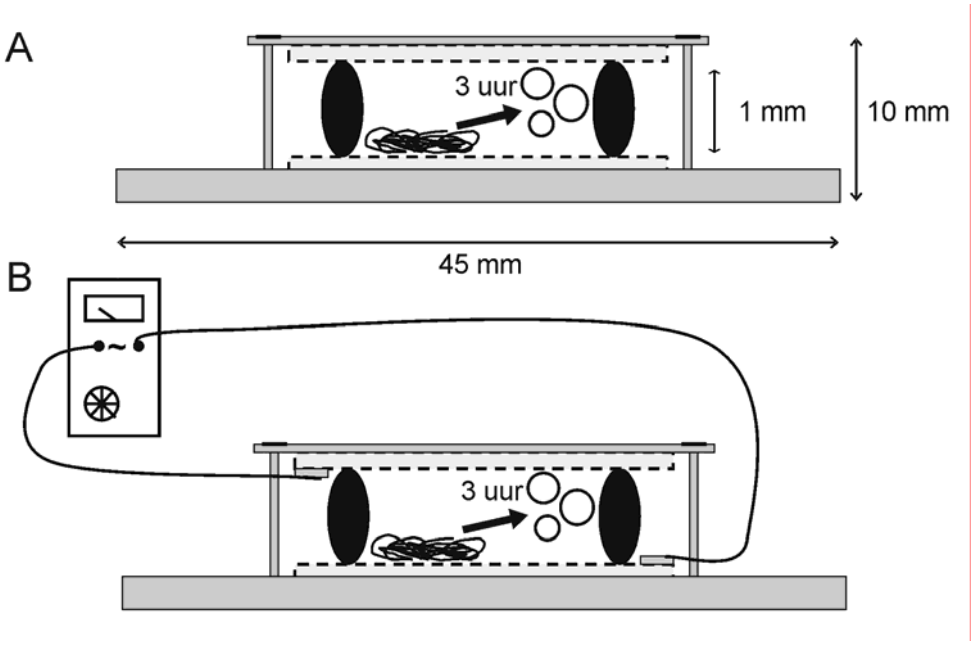

Figuur 5: Formatie van GUVs. Afbeelding A laat een dwarsdoorsnede zien van de rehydratatie kamer voor de formatie van GUVs zonder stabiliserende stoffen. Afbeelding B laat een zelfde dwarsdoorsnede zien, maar nu zijn de glazen plaatjes met het laagje geleidend materiaal (omgeven door een stippellijn) aangesloten op een wisselspanningsbron (1.2 Volt, 10Hz). In beide gevallen ontstaan de GUVs na 3 uur rehydrateren.

De gevormde GUVs kunnen niet alleen worden gebruikt voor patch-clamp, maar ook om de mobiliteit en verdeling van eiwitten in een kunstmatig membraan te bepalen. Dit is ook gedaan voor een het MscL kanaal. Uit deze experimenten blijkt dat het MscL kanaal homogeen is verdeeld over de proteo-liposomen na herplaatsing in een kunstmatig membraan. Daarnaast blijkt ook dat het MscL kanaal zich in de membraan beweegt met snelheden die vergelijkbaar zijn met andere membraaneiwitten van dezelfde grootte.

Gecontroleerde afgifte van geneesmiddelen

Op dit moment worden de meeste geneesmiddelen zo toegediend dat de werkzame stof over het hele lichaam wordt verspreid. De concentratie van de werkzame stof wordt meestal precies zo afgestemd dat de stof geen schadelijke gevolgen (bijwerkingen) heeft voor het lichaam als geheel, maar wel effectief is tegen de ziekte van de patiënt. Voor een maximaal effect van het geneesmiddel zou echter beter zijn om de concentratie op de plek van bestemming (bijvoorbeeld een tumor) heel hoog te kunnen maken, maar in de rest van het lichaam minimaal. Om het geneesmiddel op de plek van bestemming te brengen en daar af te leveren is de stichting BioMaDe bezig met het ontwerpen van een afleversysteem voor geneesmiddelen. Dit systeem (Figuur 6A en B) maakt voor de aflevering van het geneesmiddel gebruik van mechanosensitieve kanalen.

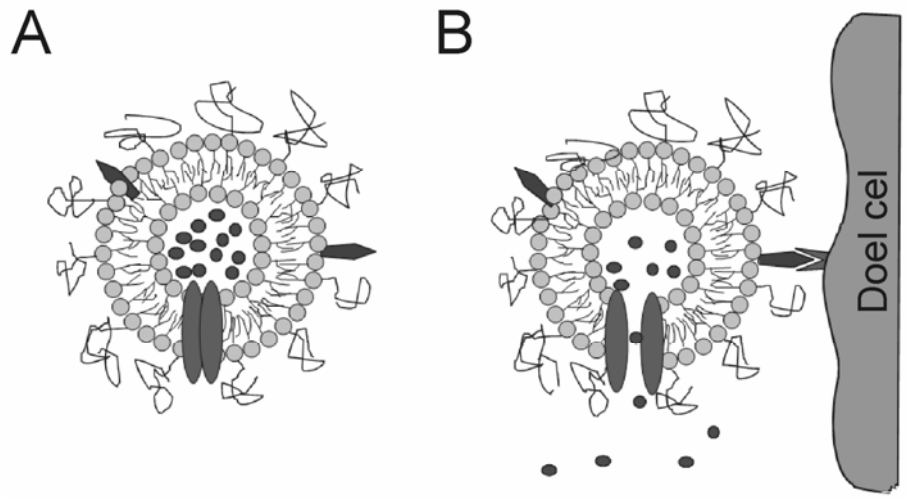

Figuur 6: Gecontroleerde afgifte van geneesmiddelen. De proteoliposoom in afbeelding A is gevuld met een geneesmiddel. Onder in de membraan is een gesloten MscL kanaal weergegeven. Aan de buitenkant van de proteoliposoom zitten eiwitten die helpen de proteoliposoom naar de doelcel te brengen. Ook zitten er staarten aan de buitenkant die de proteo-liposoom in het lichaam verborgen houden voor het imuunsysteem. In afbeelding B is de liposoom gearriveerd bij de doel cel en is het MscL kanaal geopend (bijvoorbeeld met behulp van licht). Het geneesmiddel verlaat de proteoliposoom en is succesvol afgeleverd.

Het is moeilijk om in het menselijk lichaam een osmotische verschuiving te veroorzaken, die gebruikt kan worden om het kanaal te activeren. Om deze reden richt het onderzoek zich op alternatieve procedures om het kanaal te activeren. Eén van die methodes wordt beschreven in hoofdstuk 4 van dit proefschrift. Door een aantal van de lipiden in een proteo-liposoom te vervangen door een lichtgevoelig lipide molecuul kon de activiteit

van het mechanosensitieve kanaal worden beïnvloed. Na bestraling met UV-licht met een golflengte van 365 nanometer werd de activiteit verviervoudigd. Bovendien was het proces volledig omkeerbaar en kon de activiteit worden teruggebracht naar het oorspronkelijke niveau door bestraling met licht met een golflengte van 436 nanometer.

Toekomstperspektief

Ondanks dat we in de afgelopen jaren veel hebben geleerd over MscL kanalen is er nog een hoop te doen. Op het gebied van de vorm en functie zouden we graag nog antwoorden willen hebben op vragen betreffende de vouwing van het kanaal in de open toestand en hoe het kanaal van de gesloten in de open toestand overgaat. De multimeer met vijf aan elkaar zittende eenheden van MscL zou hierbij een rol kunnen spelen.

De GUVs hebben laten zien dat ze erg goed toepasbaar zijn voor verschillende types onderzoek. De uitdagingen hier zitten vooral in het vinden van verdere onderzoekstypen en het nog beter combineren van patch-clamp met studies naar diffusie en verdeling in de membraan.

Momenteel is er veel belangstelling voor de verschillende mogelijkheden om de kanalen gericht te kunnen openen en sluiten. Met één van deze ”schakelbare” MscL kanalen hebben wij onderzocht welke stoffen wel en welke niet door de opening van het kanaal passen. Zo hebben wij bijvoorbeeld laten zien dat het eiwit insuline er doorheen kan. Deze resultaten zijn erg bemoedigend voor de toekomst van gecontroleerde afgifte systemen voor geneesmiddelen. De hier genoemde ideeën voor verder onderzoek komen voort uit dit proefschrift. Natuurlijk staan er ook nog vele andere vragen open, maar dat neemt niet weg dat ons begrip van de werking van mechanosensitieve kanalen met dit proefschrift verder is ontwikkeld.

Graag wil ik Marijke van der Vliet en Philomeen Duinisveld bedanken voor hun hulp bij het samenstellen van dit hoofdstuk.

List of publications

1. Poolman, B., Blount, P., Folgering, J.H.A., Friesen, R.H., Moe, P.C., and van der Heide, T. (2002) *Mol. Microbiol.* **44,** 889-902

2. Folgering, J.H.A., Kuiper, J.M., de Vries, A.H., Engberts, J.B.F.N., and Poolman, B. (2004) *Langmuir* **20,** 6985-7

3. Folgering, J.H.A., Moe, P.C., Schuurman-Wolters, G.K., Blount, P., and Poolman, B. (2005) *J. Biol. Chem.* **280,** 8784-92

4. Doeven, M.K., Folgering, J.H.A., Krasnikov, V., Geertsma, E.R., van den Bogaart, G., and Poolman, B. (2005) *Biophys. J.* **88,** 1134-42

5. Folgering, J.H.A., Wolters, J.C., and Poolman, B. (2005) Manuscript submitted for publication in *Prot. Sci.*

Eric Bleumink Fonds

Verdient meer dan uw aandacht alleen!!

Het Eric Bleumink Fonds van de Rijksuniversiteit Groningen verstrekt beurzen aan talentvolle studenten en jonge onderzoekers uit ontwikkelingslanden.

Ambitie
Met het Fonds geeft de RUG invulling aan de ambitie de reeds bestaande samenwerking met universiteiten uit te breiden en een bijdrage te leveren aan de groei van welvaart en welzijn in de ontwikkelingslanden. De RUG heeft al vele jaren goede contacten met zusterinstellingen in deze landen. Onderwijs en onderzoek zijn een motor voor maatschappelijke ontwikkeling. Dit komt zowel de mensen als hun land of regio ten goede. Ook voor de RUG zijn de internationale contacten en uitwisselingen belangrijk.

Kansen bieden
Veel studenten, jonge onderzoekers en universitaire stafleden in ontwikkelingslanden kunnen voor hun wetenschappelijke loopbaan baat hebben bij een kort of lang verblijf aan een universiteit in West-Europa. Zo kan de leeromgeving in de geïndustrialiseerde wereld een grote meerwaarde hebben voor de opleiding in het eigen land. Ook zijn persoonlijke contacten belangrijk. De ontmoeting tussen wetenschappers uit verschillende landen en culturen heeft voordelen voor alle partijen. Het kan leiden tot een hecht en blijvend wetenschappelijk netwerk.

Beurzen
Een beurs van het Eric Bleumink Fonds is afgestemd op de kosten van de opleiding en het is een vergoeding voor reiskosten, kosten van studiemateriaal en kosten van levensonderhoud. De bedragen zijn gebaseerd op de algemeen in gebruik zijnde regels van het Netherlands Fellowship Programme en voldoen aan nationaal en internationaal aanvaarde eisen.

De naamgeving
Het Fonds draagt de naam van prof.dr. Eric Bleumink, die ruim twaalf jaar de functie van Voorzitter van het College van Bestuur van de Rijksuniversiteit Groningen heeft bekleed. Eric Bleumink voelde zich zeer betrokken met de medemens en zette zich in om de universiteit in de maatschappij te

verankeren. Dat bleek in het bijzonder uit zijn inspanningen voor de samenwerking tussen de RUG en zusterinstellingen in ontwikkelingslanden. Het Eric Bleumink Fonds is in het leven geroepen ter gelegenheid van het afscheid van Eric Bleumink op 24 mei 2000.

De middelen en het beheer
Voor de inkomsten is het Fonds afhankelijk van periodieke of eenmalige bijdragen van alumni, studenten, medewerkers en relaties van de universiteit. Het Fonds heeft een bestuur onder leiding van de Rector Magnificus. Bijdragen worden volledig aan beurzen besteed. De kosten van bestuur, secretariaat, administratie en fondswerving worden niet doorberekend. Accountants van PriceWaterhouseCoopers controleren de financiën van het fonds. Alle donateurs en relaties van het fonds ontvangen tweemaal per jaar een Nieuwsbrief. In de Nieuwsbrief is aangegeven welke studenten en jonge onderzoekers een beurs hebben gekregen en hoe het met hen gaat.

Voor nadere informatie over donaties, schenkingen en legaten kunt u contact opnemen met:

Stichting Ubbo Emmius Fonds RUG
ubbo.emmius.fonds@bureau.rug.nl
tel 050-363 75 95

Bankrekening:
ABN AMRO Bank
rekeningnr. 56.30.98.961
t.n.v. Stichting Ubbo Emmius Fonds

Dankwoord

Dit is het dan, na vijf jaar en een beetje is dit het einde van mijn promotie en proefschrift. Ik heb in de afgelopen jaren veel geleerd, bijvoorbeeld dat ik soms nog een beetje meer geduld moet hebben. Daarnaast heb ik geleerd kort en bondig te formuleren, hoewel daar in de praktijk waarschijnlijk nog steeds weinig van is te merken. Vooral heb ik geleerd hoe te genieten van het bedrijven van wetenschap.

Voor ik mensen ga bedanken, wil ik graag nog even kort de aandacht vestigen op het Eric Bleumink Fonds. Dit fonds biedt studenten uit ontwikkelingslanden de mogelijkheid om dezelfde prettige en uitdagende ervaringen op te doen als ik in de afgelopen jaren. Wat mij betreft is dat een uitstekende reden om het fonds financieel bij te staan.

Hoewel ik verantwoordelijk ben voor de inhoud van dit proefschrift, is het beschreven werk niet alleen door mijn inzet tot stand gekomen, maar ook dankzij de hulp van een groot aantal anderen. Langs deze weg wil ik graag iedereen, die op zijn of haar manier een bijdrage heeft geleverd aan mijn proefschrift, heel hartelijk bedanken.

Een aantal mensen wil ik echter nog even persoonlijk bedanken. Allereerst mijn begeleider Bert Poolman. Bert, jij stond altijd klaar om mij een welgemeende ”schop onder mijn kont” te geven. Dit resulteerde meestal in een serie zeer succesvolle experimenten. Je was ook altijd bereid om mij bij te staan als het even wat moeizamer ging. Al met al, denk ik dat we het zo tot een prachtig einde hebben gebracht. Bedankt Bert!

Nadat het proefschrift klaar was, hebben Alan Mark, Arnold Driessen en Jan Engberts het werk nog eens grondig gecontroleerd en mij geholpen om ook de laatste foutjes er uit te halen; bedankt hiervoor. Jan, ik wil jou ook graag nog apart bedanken voor al je inzet bij de ”switch”-paper. Jouw vriendelijke en ondersteunende woorden hebben mij meerdere keren vooruit geholpen in lastige tijden.

Part of the scientific work presented in this thesis was performed in Dallas, at the University of Texas SouthWestern Medical Center, in the group of Paul Blount. Paul, thank you for your kindness and hospitality during my visits to Dallas. Also, I would like to thank all the Blount group-members who have helped making my visits very enjoyable both inside and outside the lab. A special word of thanks goes out to Paul Moe, he helped me during my first patch clamp experiments, and made life in the Blount-lab very lively and livable. Paul, thanks again for your help and for all the fun we had.

Naast de collega’s in Dallas, had ik in Nederland ook geweldige labgenoten, die het doen van experimenten tot een waar feest maakten. Tiemen, het was kort, maar krachtig en leerzaam. Mark, jouw hulp met de ”GUVs” was geweldig, je hebt het verhaal echt op een hoger plan getrokken. Ria, dank voor alle wijze woorden, die vaak op het juiste moment zijn gesproken. Gea, jouw hulp bij het maken van de Knock-Out en herrie in het lab was onmisbaar. Esther, dank voor al je dropjes en gezelligheid. Sytse, je

hulp en inzichten bij al mijn DNA en RNA werk zijn erg gewaardeerd. Jason, thank you for all the candy and cinnamon gum, hope to see you again soon.

Mijn dank gaat ook uit naar de mensen, met wie ik al die tijd mijn kamer heb mogen delen. Elisa, bedankt voor al je goede zorgen, je was een fijne room-mate. Jolanda, het was dan maar voor één jaar, maar wel erg gezellig. Gert, dank voor het eilandje van rust dat je altijd was in een woelig lab, je bent een echte vriend.

Er waren ook collega's van buiten het lab, die mij hebben geholpen. Alex en Marjon, bedankt voor jullie bijdrages aan de "switch"-paper. Ook al spraken we niet altijd dezelfde taal, door onze verschillende wetenschappelijke achtergronden, het was leerzaam om met jullie samen te werken. De BioMaDe "channel-protein group" was een andere makkelijk en prettig bereikbare bron van externe informatie. Bedankt voor het meedenken en de gezelligheid op woensdagochtend. Speciale dank ook voor Armağan, die samen met mij de patch-clamp in Groningen heeft opgestart.

De laatste collega's die ik wil bedanken, zijn mijn nieuwe collega's bij Brains-Online. Van Thomas Cremers kreeg ik de kans om bij jullie mijn technische vaardigheden uit te breiden. Ik voelde me vanaf de eerste dag prima bij jullie thuis en heb al veel nieuwe dingen geleerd.

Gelukkig heb ik niet alleen gewerkt in de afgelopen jaren. Ik heb op veel momenten met mijn vrienden kunnen genieten van weekendjes weg in het land. Ik hoop dat, nu het promoveren achter de rug is, er weer meer tijd is om jullie op te zoeken en om samen leuke dingen te doen. Vrienden van de sneak, jullie maakten iedere dinsdag tot een waarlijk feest, soms tot in de vroege uurtjes. Jullie waren er de "good" en de "bad times", veel dank voor jullie aanhoudende steun.

Tijdens mijn promotie heb ik ook kennis gemaakt met de vrienden en vriendinnen van Marijke. Jullie wil ik graag bedanken voor alle getoonde belangstelling in mijn promotie.

Tim, Erik, Marjolein, Pap en Mum: dank voor al jullie liefde, zorg en hulp in de afgelopen 30 jaar. Ik denk dat dit boekje een prachtig bewijs is van het feit dat we er iets moois van hebben gemaakt in die tijd. Nynke, Bernard en Maria, jullie hebben mij op een erg fijne manier opgenomen in jullie familie, hiervoor dank. Ondanks mijn gebrekkige Fries, voel ik me altijd prima thuis bij jullie in Gersloot. Ik hoop dat ik in de toekomst nog vaak langs mag komen.

Eric en Marieke, jullie zijn nog niet genoemd. Jullie bijdrage aan mijn proefschrift, geestelijke gezondheid en geluk in de afgelopen jaren is enorm geweest. Jullie hebben beiden op zowel wetenschappelijk gebied als persoonlijk gebied altijd voor mij klaar gestaan, wat mij betreft is jullie rol als paranimf een kleine weerspiegeling van deze bijdrage.

Marijke jouw liefde heeft mij ontzettend geholpen om dit proefschrift af te ronden. Je hebt je echt geweldig door de zware tijden geslagen, en mij altijd de juiste lichtpuntjes laten zien. Ik hoop dat je dat voor altijd wil blijven doen. LUVU.

Joost

Curriculum Vitae

Joost Folgering werd op 6 juli 1975 geboren in Nijmegen. Hij behaalde zijn VWO diploma aan het Canisius College Mater Dei in Nijmegen. In 1993 verbleef hij één jaar in Oxford, waar hij zijn A-levels voor wiskunde, biologie, scheikunde en natuurkunde behaalde aan het Oxford College of Further Education. In 1994 startte hij met de opleiding biologie aan de Rijksuniversiteit Groningen. Naast zijn studie was hij onder andere voorzitter van de Groninger Biologen Club en lid van de studentenfractie van de universiteitsraad. In januari 2000 is hij afgestudeerd na een afstudeerstage bij Nestlé in Zwitserland. In dat jaar begon hij ook aan zijn promotie-onderzoek aan mechanosensitieve kanalen van bacteriën. Gedurende zijn promotie was hij tevens lid van het bestuur van het Eric Bleumink fonds. Van januari tot juli 2005 was hij part-time werkzaam als post-doc aan de Rijksuniversiteit Groningen bij de afdeling biochemie. Sinds mei 2005 is hij werkzaam als electrofysioloog bij het bedrijf Brains on Line. Joost Folgering woont in Groningen samen met Marijke van der Vliet.